Cranfield University

KATHERINE KNIGHT

Numerical Methods for Vortical Flows

College of Aeronautics

PhD Thesis

Cranfield University

College of Aeronautics

PhD THESIS

Academic Year 2006-2007

Katherine Knight

Numerical Methods for Vortical Flows

Supervisors Dr Scott Shaw
Professor Kevin Garry

January 2007

Abstract

An investigation into the current methods employed to conserve vorticity in numerical calculations is undertaken. Osher's flux for the artificial compressibility equations is derived, implemented and validated in Cranfield University's second order finite volume compressible flow solver MERLIN. Characteristic Decomposition is applied as a method of vorticity conservation in both the compressible and artificial compressibility MERLIN solvers. The performance of this method for vorticity conservation in both these solvers is assessed. Following a discussion of the issues associated with application of limiter functions on unstructured grids three modified versions of the method of Characteristic Decomposition are proposed and tested in both the compressible and incompressible solvers. It is concluded that the method of Characteristic Decomposition is an effective method for improving vorticity conservation and compares favourably in terms of increased computational cost to vorticity conservation through grid refinement.

Contents

Nomenclature

a	speed of sound
c	artificial compressibility coefficient
x, y, z	components of cartesian coordiante system
$\mathbf{U}$	velcoity vector
u, v, w	x,y,z components of velocity
P	pressure
ρ	density
$\boldsymbol{\omega}$	vorticity vector
$\omega_x, \omega_y, \omega_z$	x,y,z components of vorticity
k	heat conduction coefficient
E	total energy
E_{ns}	enstrophy
t	time
T	temperature
$\mathbf{T}^{\mathbf{s}}$	stress tensor
τ	psuedo time
τ_{ij}	shear stress tensor
μ	dynamic viscosity
υ_{visc}	kinematic viscosity
δ_{ij}	kronecker's delta function

1. Introduction and General Objectives

Over the past three decades there has been significant progress in the understanding and development of numerical algorithms for the solution of the Navier-Stokes equations. The resulting schemes are widely used in commercial CFD software and research codes and have been demonstrated to be both accurate and robust for a wide range of flows. Unfortunately there is growing evidence that existing algorithms fail for flows in which the creation, development and interaction of vortical flow structures are important.

Existing algorithms suffer from the inability to preserve vorticity - dissipating it at an unphysical rate. Vortical structures, such as wing tip vortices, which should persist for a great length downstream from their point of origin are quickly dissipated often being overwhelmed by numerical viscosity within a couple of chord lengths. This problem is amplified when calculations are performed on unstructured and highly skewed and stretched structured grids. Although the problem is extensively documented in the literature the underlying causes for this failure are complex and are not well understood.

The importance of considering vorticity conservation in algorithm development, in order to provide numerical schemes which can accurately predict and maintain vortical structures, cannot be overstated. There is a broad spectrum of engineering applications in which vorticity is of key interest spanning aeronautical flows, in both the compressible and incompressible regimes, with applications including helicopter wakes, high-speed weapon and rocket aerodynamics, flows in the built environment, automotive flows and flow control.

The use of numerical analysis alongside wind tunnel testing is vital to aeronautical engineering providing a means of carrying out initial testing that can redirect, or narrow, the focus of a wind tunnel test campaign and allowing the simulation of aspects of flows which may be difficult, or impossible, to recreate and study effectively in wind tunnel experiments.

The development of unstructured grid generation techniques has provided a more time efficient method for generating grids for complex geometries compared to structured grid generation. Unfortunately the full potential for using unstructured grids in aeronautical flow calculations cannot currently be realised due to the failure of algorithms to achieve required levels of accuracy, without a prohibitively large number of cells, on unstructured grids in the presence of vorticity.

The desire to develop algorithms that can preserve vortices has spawned a great deal of research and varied approaches to overcoming this problem. Many of the approaches that have been explored have a limited field of application. Some of the methods rely on changes to the physics modelled by the algorithm, in order to conserve vorticity, which potentially causes undesirable changes to the structure of the vorticity and other flow features. While other algorithms are restricted to the incompressible flow regime or require some information regarding the distribution of vorticity to be known prior to the calculation.

The focus of this research is to explore the development of a consistent approach to vorticity conservation that can be applied in the compressible flow regime and the incompressible flow regime, by way of the artificial compressibility equations. In order to create an algorithm that can be applied to a wide range of real engineering problems an algorithm that retains the physics of the basic flow model is sought. Development of an algorithm that can better preserve vorticity on unstructured grids is also explored.

The thesis objectives are discussed and clarified following the literature review.

2. Literature Review - the Problem and Current Solutions

A comprehensive background on numerical methods in fluid dynamics can be found in the two volumes 'Numerical Computation of Internal and External Flows' by Hirsch[1,2] with a more detailed background on methods employed to solve non-linear hyperbolic conservation laws found in 'Riemann Solvers and Numerical Methods for Fluid Dynamics' by Toro[3].

When computing vortical flows current numerical schemes excessively dissipate vorticity in an unphysical manner. The precise cause of this problem is difficult to determine although several contributing factors have be identified.

Roe[4,5] states that the delicacy of the physical mechanisms by which vorticity is created and destroyed means that the vorticity distribution in a computed solution is particularly vulnerable to numerical error. In addition, the discrete equations for current algorithms have been developed without the need to enforce the equations governing the transport of vorticity in mind and it can be shown that these laws are often violated by the creation of vorticity due to physically irrelevant terms in the truncation error. The vulnerability of vorticity to numerical error along with the failure of current algorithms to enforce the equations governing conservation of vorticity in the discrete approximation leads to incorrect solutions for vorticity distribution including overly diffusive solutions with inaccurate generation, destruction and transport of vorticity.

In his work on Hyperbolic Systems of Conservation Laws Lax[6] identified problems with the computation of contact discontinuities, resulting in unphysical spreading, by difference schemes. Lax states that 'the reason for this is that contact discontinuities, in contrast to shocks, are very much like discontinuities of solutions of linear hyperbolic equations'. This is because they are associated with the linearly degenerate fields. He then goes on to say that difference schemes will spread these types of solutions so that after n time cycles the width of the contact discontinuity is

of order √n. Both contact discontinuities and vorticity are associated with the linearly degenerate fields and artificial spreading of vorticity by the same mechanism will also be a problem encountered by numerical schemes. Lax concludes that 'the spreading of contact discontinuities in difference calculations in Eulerian coordinates cannot be prevented unless one uses variable size spacing intervals which is tantamount to introducing Lagrange coordinates'.

An additional problem, when computing turbulent flows, is introduced due to the fact that almost all modern turbulence models employ moment of vorticity (algebraic models) or vorticity (multi-equation models) in modelling the near wall behaviour of boundary layers. As a consequence the behaviour of the models in the presence of vorticity or vortical structures, that are not associated with the near wall boundary layer, may be erroneous. For flows in which there is a clear distinction between the discrete vortical structures that are of interest and the boundary layer simple modifications can be made in order to prevent the incorrect application of turbulence models to predominantly laminar larger scale vortical structures. It is demonstrated in the work by Wik[7] that where this is not possible it is necessary to employ a more complex Reynolds Stress Model in order to avoid the unwanted application of the turbulence model in the presence of vortical structures.

High order schemes used in conjunction with grid refinement have been shown to provide greatly improved results for vortex dominated flows but carry a much increased computational cost. Work carried out by Wake and Choi[8] on structured grids demonstrated that use of a fifth order scheme, instead of a third order scheme, provided a factor 10 reduction in the number of points needed in each cross flow plane to convect a well aligned vortex. This improvement was even greater when dealing with a skewed vortex with a factor 30 reduction in the number of grid flow points needed. The work concluded that it is more efficient to move to using a higher order scheme than to increase the number of grid points for cases where a vortex needs to be convected over a long distance. Wake and Choi defined a vortex-convection skewness (VCS) parameter which indicates the necessary axial spacing required to resolve a vortex that is skewed relative to the grid. This was found to be very limiting in terms of the number of grid points required in the axial direction even for very small skew angles. Work by Hariharan and Sankar[9,10] using seventh

order schemes concludes that the problems encountered due to the much larger stencils needed to compute increasingly higher order schemes offset the advantages of using higher order schemes beyond a certain point. The importance of grid/vortex alignment using current algorithms, as demonstrated by Wake and Choi, and the limitations of using higher order schemes, especially for unstructured grids, highlights the need to further investigate alternative solutions for the false diffusion and excessive dissipation of vortical structures.

The method of vorticity confinement, developed predominantly by Steinhoff[11], for conserving vorticity in incompressible calculations uses the addition of an artificial term to the momentum equations of the Euler equations which has the effect of convecting vorticity towards its local extreme.

The momentum equations take the form

$$\partial_t \mathbf{U} = -(\mathbf{U}.\nabla)\mathbf{U} + \nabla(P/\rho) + \mu\nabla^2\mathbf{U} - \in \vec{s} \qquad (2.1)$$

with the addition of the confinement term $-\in \vec{s}$ where $\in$ is a numerical coefficient that decides the size of the convecting region.

$\vec{s} = -\mathbf{n} \times \boldsymbol{\omega}$ where $\boldsymbol{\omega}$ is the vorticity vector and $\mathbf{n}$ is a unit vector pointing away from the centroid of the vortical region.

$\mathbf{n} = \dfrac{\nabla\eta}{|\nabla\eta|}$ where η is a scalar field that has a local minimum on the centroid of the vortical region given by $\eta = -|\boldsymbol{\omega}|$

With the added term the flow equations admit solutions with concentrated vortices without spreading, even if the basic flow equations have diffusive terms. The added term acts as a velocity correction and is applied only in areas of relatively coarse grid where vortical structures are convecting and so can therefore be used in conjunction with conventional Euler/Navier-Stokes methods.

This method allows vorticity to be transported once generated but the modification of the equations is non-physical. The method is extremely useful for computing flow fields containing strong vorticity but where the details of the structure and behaviour

of vortical regions is not the primary interest. Steinhoff[11] compares his method in this way to shock capturing where 'the detailed internal dynamics of shocks are not computed, but rather a modified set of equations is solved which results in a shock spread over a few number of grid cells'. The numerical coefficient $\in$ effectively balances the diffusion and depends on grid size, grid aspect ratio and the chosen convection scheme in the basic solver. The use of the vorticity confinement method therefore needs to be tuned to each specific case in order to provide the best results. The method has more recently been extended for use in compressible flow simulation by interpreting the confinement term as a body force[12] in order to remain consistent with a conservation law framework, minimizing the adaptation needed to current compressible flow algorithms.

Vortex methods, including Vortex Lattice and Vortex Blob techniques, represent the vorticity distribution in a flow using markers carrying vorticity. The velocity field at a given time is calculated from the vorticity distribution via a Biot-Savart calculation which is then used to update the distribution of vorticity. These methods are restricted in application to incompressible flows; however the Vortex Embedding technique uses a Vortex Lattice method in conjunction with a compressible flow solver in order to extend vortex methods to compressible flows. These methods can be very effective for flows where the vorticity distribution is highly localised but are less suitable for more complex flows. All these methods require some initial information on the position of vortical regions in order to distribute the markers and encounter problems where there are interactions with surfaces or merging of vortices. An additional drawback of these methods is that the dimensions and details of the vortical structures are not rigorously dealt with by the computations, with the emphasis on the correct calculation of the location of the centroid surfaces of vortical structures and the total vorticity surrounding each point on the centroid surface. The internal structure of a vortex is dealt with by a user specified spreading function. Hybrid methods use a Navier-Stokes solver in areas of the flow where vorticity is generated and a vortex method in areas of the flow where vorticity is localised. A suitable model for the intermediate region also needs to be included. There are many possible approaches to the hybridization and it is possible that methods can be tailored to suit specific applications.

Roe's[4] approach to capturing vorticity is to seek a numerical scheme from which it is possible to obtain discrete equations for the transport of vorticity that are physically valid from the discrete equations that are used in the code. A discrete measure of vorticity conservation that can be applied to finite volume schemes on unstructured grids is developed - the requirement that a discrete version of the circulation around a closed surface remains invariant. In work looking for schemes with vorticity preserving properties, Roe concludes that schemes that are based, like most upwind schemes, on one-dimensional reconstructions and interpolation cannot preserve vorticity. The cell centred two dimensional finite volume Rotated Richtmyer scheme investigated by Roe[5] is one in which there is a unique flux through each interface but it is not evaluated with reference only to the two cells which it separates but by averaging the fluxes at its two end points and therefore involves four cell states. The method is shown to preserve vorticity by virtue of the fact that when contributions to the change in discrete vorticity from all cells meeting at a vertex are added together they all cancel, leading to a zero change in circulation around a vertex. This scheme is extended to three dimensional unstructured grids by a particular method of dissection of the control volume surrounding a vertex into sub cells. Roe also draws attention to the connection with the work carried out by Hyman and Shaskov[13,14] towards developing a discrete analogue of vector and tensor calculus that can be used for correct representation of continuum models. Hyman and Shaskov use the support-operator method in which a discrete approximation to a first order differential operator is constructed that satisfies the appropriate vector identity. This operator is then used in the construction of other discrete operators. Hyman and Shaskov go on to construct discrete analogues of second order differential operators. This work is developed in a finite difference framework but Roe observes that there is a link between the search for a correct discrete analogue for vector analysis and the search for an algorithm that correctly represents the identities relating to vorticity in the continuum model. Roe concludes that a close comparison of the two approaches could prove profitable.

More recent work carried out by Ismail and Roe[15] on developing a vorticity preserving scheme for the Euler equations has taken the approach of adding a correction term to the Roe solver which has the effect of removing spurious vorticity. This term is determined by using the vorticity transport equation to give an

independent estimate of the vorticity at each time step. This correction controls the curl of the momentum, or 'psuedo vorticity', and because the underlying scheme is consistent with the Euler equations it is concluded that the predicted vorticity will be close to the 'true vorticity'. It is found that the accuracy when computing rotational flow by this method is greatly dependent on the accuracy of the independent vorticity estimate. The divergence of momentum is discretized via a two step central scheme in which two options are possible for application of a limiter. In the first option, 'VP1', a limiter is applied only at the half-step and in the other, 'VP2', a limiter is applied on both the half and full steps. The slope limiter that is employed in both cases is Superbee. Results for both options are compared to a first order scheme and also a baseline second order scheme employing the Superbee slope limiter without the vorticity correction. It is found that the second order baseline Superbee scheme does not excessively diffuse vorticity due to its compressive nature however this scheme results in the generation of spurious enstrophy. The VP1 scheme lies between the first order and Superbee method with the VP2 scheme performing the best and producing negligible amounts of spurious enstrophy whilst conserving vorticity. This is attributed to vorticity physics being incorporated to the scheme in addition to conventional upwinding.

Work has been carried out by several different parties[16,17,18] to develop schemes to minimise dispersion, the spurious propagation of different frequency components of an acoustic wave at different speeds, in order that CFD algorithms can be utilised for aeroacoustic calculations. The low dispersion finite volume (LDFV) schemes developed have the property that in addition to minimizing the dispersion in the solution they provide a way of minimizing numerical dissipation. The LDFV scheme chooses an interpolation at cell faces, where the flux is calculated, that accurately represents the sinusoidal waves of short wavelengths and minimizes numerical dissipation. This method has been shown to improve the vortex capturing capabilities of a code.

Brown[19] suggests a method for rotor wake modelling based on the vorticity transport equations in conservative formulation using Toro's[20] weighted average flux (WAF) method extended to three dimensions to approximate the transport operator. The WAF method is a conservative Riemann problem based method that is modified in

order to use flux limiters. The production of vorticity is dealt with by the use of a source term. The use of the conservative formulation enables the total vorticity present in the computational domain to be conserved. An appropriate choice of flux limiter is shown to be necessary in order to maintain the compactness of the domains of vorticity. Figure 1 compares the results from an extremely compressive super-type limiter, which provides the best results, with min-type limiters proving to be excessively diffusive.

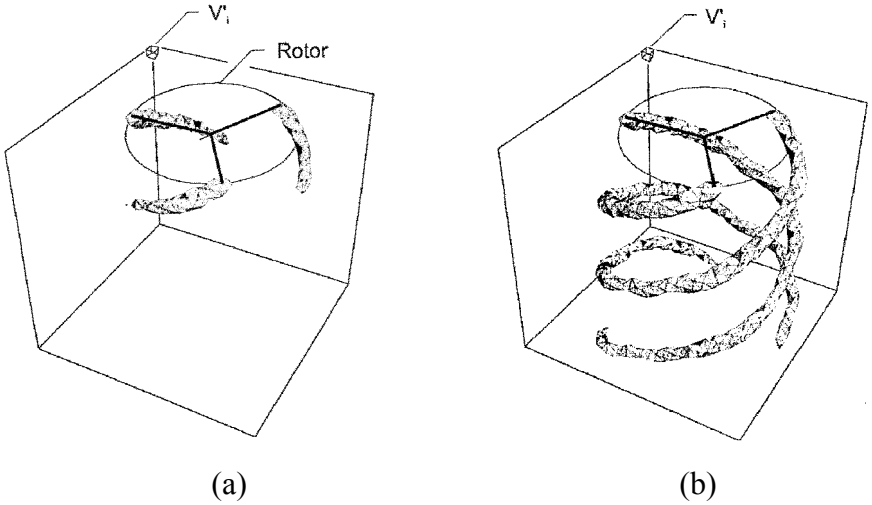

<u>Figure 1.</u> – Brown's rotor wake calculations (a) results with a min-type limiter, (b) results with a super-type limiter. The super-type limiter provides much greater vortex conservation with the vortex being convected to the edge of the computational domain as opposed to th min-type limter where the vortex is dissipated very quickly

Brown's work demonstrates that the use of the vorticity-velocity formulation in conservation form is not in itself enough to solve the problems encountered in computing vortical flows. Although the total vorticity contained in the computational domain may be conserved the vorticity is not confined. In combination with the application of an extremely compressive Super-type limiter this approach proves highly effective and the strength and definition of the tip vortices is maintained right the way to the edge of the computational domain. Although Brown identifies that application of a compressive limiter, to the vorticity field, is necessary in order to maintain the tip vortices he does not give an explanation as to why his scheme is so successful.

Employing Characteristic Decomposition in the solution of the Euler equations has been investigated by Kim, Williams and Lyrintzis[21] in order to preserve vorticity. The method of Characteristic Decomposition was first experimented with by Sweby[22] when he employed the Superbee flux limiter for the linear field and the Minmod or the Van Leer flux limiter for the non-linear fields for Sod's shock tube problem. He found that both these combinations provided improved resolution of the shock wave and contact discontinuity. When Superbee was applied across all fields the contact discontinuity was sharply resolved but the solution was not TVD in the region of the shock. When Minmod or Vanleer flux limiting was applied to all fields the solution was TVD in the region of the shock but the contact discontinuity was not sharply resolved.

Kim, Williams and Lyrintzis' method involves carrying out the interpolation of the right and left cell states via a transformation to the characteristic variables. The characteristic variables are defined by multiplication of the conservative variable vector by a set of the left eigenvectors of the flux Jacobian matrix[1]. MUSCL-type interpolation is then carried out via the use of characteristic variables and slope limiters are employed in the interpolation. The choice of slope limiter is varied to suit the nature of the characteristic variables under consideration. A compressive super-type limiter is applied to the linearly degenerate characteristic fields associated with the entropy and vorticity waves. A diffusive min-type limiter is applied to the non-linear fields associated with the acoustic pressure waves to suppress spurious numerical oscillations. The effect of the use of characteristic decomposition is shown in Figure 2.

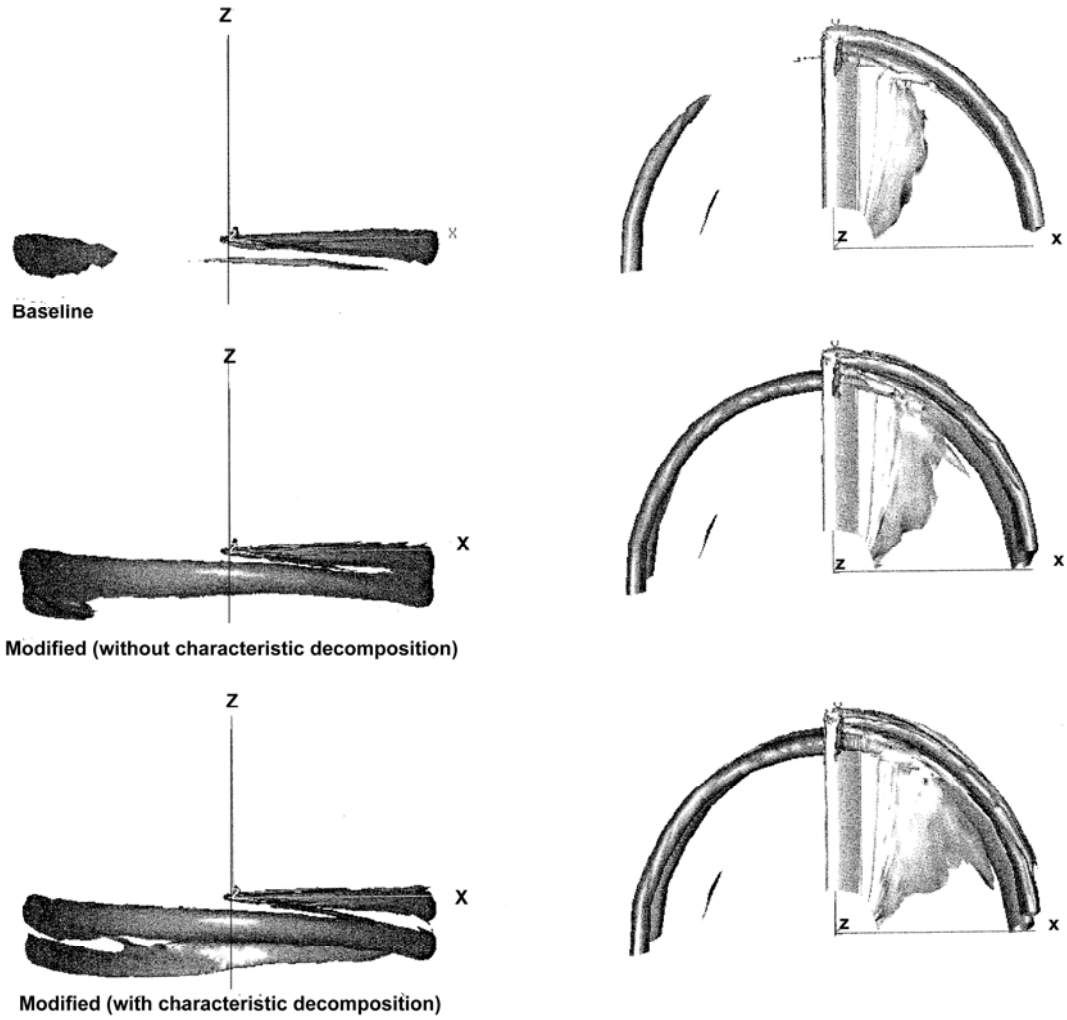

Figure 2. – Kim, Williams and Lyrintzis results using a baseline scheme and a higher order scheme with and without characteristic decomposition. It can be seen that moving to a higher order scheme provides greater vorticity conservation than the baseline scheme. Further improvement is gained by the introduction of characteristic decomposition.

The motivation behind this approach comes from the concept that linearly degenerate fields where wave speed is independent of amplitude, such as those associated with the entropy perturbation and vorticity wave, are prone to dissipate in the presence of numerical diffusion. The truly nonlinear fields such as those associated with acoustic pressure waves, where wave speed depends on amplitude, have a 'self stiffening mechanism' and a compressive limiter is not necessary[6].

Characteristic decomposition has been shown to provide improved results for rotor wake capturing and although this is computationally more expensive the additional cost is less than that required to use grid refinement to achieve the same level of tip

vortex conservation. The benefit of using a coordinate transform and varying choice of limiter to improve vorticity capturing capabilities is that adaption of existing codes to include this feature is relatively straight forward and the method can be used with whatever order of interpolation is chosen.

3. Discussion of Current Methods and Thesis Objectives.

The focus of this research is to explore the development of a consistent approach to vorticity conservation that can be applied in the compressible flow regime and the incompressible flow regime, by way of the artificial compressibility equations, in order to develop a method that can be applied to a wide range of real engineering problems for which vorticity is of paramount interest. The influence of the choice of turbulence model employed in a calculation on vorticity conservation is well understood and it has therefore been decided that an examination of turbulence models is outside the scope of this research.

The development and testing of vortex capturing methods is undertaken in Cranfield University's unsteady compressible viscous flow solver, MERLIN, which employs the Riemann solver of Osher in a three dimensional cell centred finite volume formulation with dual time stepping. The method of artificial compressibility is implemented in the same code in order to provide an incompressible solver.

The survey of current methods and research on the problem of vorticity capturing highlights several interesting areas of ongoing research, some of which are already providing practically applicable solutions and others which are still in their infancy. When seeking a numerical method that can be used across a broad range of applications, where there is a desire to understand the details of vortex behaviour for complex vortical flows, the use of vortex methods or vorticity confinement is not appropriate. The current work that seems the most promising is that undertaken by Brown using the vorticity transport equations and a compressive limiter, the work on characteristic decomposition undertaken by Kim, Williams and Lyrintzis and the work on development of a vorticity conserving scheme carried out by Ismail and Roe. The importance of the choice of limiter employed in these three methods seems to be a common thread. A more detailed look at the system of vorticity transport equations indicates why.

The three vorticity transport equations are given below. The terms in the first set of brackets are the advection terms with the terms in the second set of brackets being responsible for stretching of vorticity due to velocity gradients in the flow. When dealing with the advection terms Brown uses Toro's weighted average flux method extended to three dimensions using the standard Strang spatial splitting. Ismail and Roe use the vorticity transport equations to provide a correction to the Euler equations. They calculate the advection terms of the vorticity transport equation using an upwind method with a limiter applied to the linearly reconstructed data used in the flux function.

$$\frac{\partial \omega_x}{\partial t}+\left(u\frac{\partial \omega_x}{\partial x}+v\frac{\partial \omega_x}{\partial y}+w\frac{\partial \omega_x}{\partial z}\right)-\left(\omega_x\frac{\partial u}{\partial x}+\omega_y\frac{\partial u}{\partial y}+\omega_z\frac{\partial u}{\partial z}\right)=0$$

$$\frac{\partial \omega_y}{\partial t}+\left(u\frac{\partial \omega_y}{\partial x}+v\frac{\partial \omega_y}{\partial y}+w\frac{\partial \omega_y}{\partial z}\right)-\left(\omega_x\frac{\partial v}{\partial x}+\omega_y\frac{\partial v}{\partial y}+\omega_z\frac{\partial v}{\partial z}\right)=0 \qquad (3.1)$$

$$\frac{\partial \omega_z}{\partial t}+\left(u\frac{\partial \omega_z}{\partial x}+v\frac{\partial \omega_z}{\partial y}+w\frac{\partial \omega_z}{\partial z}\right)-\left(\omega_x\frac{\partial w}{\partial x}+\omega_y\frac{\partial w}{\partial y}+\omega_z\frac{\partial w}{\partial z}\right)=0$$

where

$$\omega_x=\frac{\partial w}{\partial y}-\frac{\partial v}{\partial z}$$

$$\omega_y=\frac{\partial u}{\partial z}-\frac{\partial w}{\partial x}$$

$$\omega_z=\frac{\partial v}{\partial x}-\frac{\partial u}{\partial y}$$

$$\omega=\omega_x\bar{i}+\omega_x\bar{j}+\omega_x\bar{k}$$

The advection terms can also be written as

$$\begin{pmatrix}u&0&0\\0&u&0\\0&0&u\end{pmatrix}\begin{pmatrix}\omega_x\\\omega_y\\\omega_z\end{pmatrix}_{,x}+\begin{pmatrix}v&0&0\\0&v&0\\0&0&v\end{pmatrix}\begin{pmatrix}\omega_x\\\omega_y\\\omega_z\end{pmatrix}_{,y}+\begin{pmatrix}w&0&0\\0&w&0\\0&0&w\end{pmatrix}\begin{pmatrix}\omega_x\\\omega_y\\\omega_z\end{pmatrix}_{,z} \qquad (3.2)$$

It can be seen that the advective terms are uncoupled with each spatial direction containing a diagonal matrix with repeated entries multiplied by the components of

vorticity. For each matrix the repeated values are the eigenvalues - this system is therefore not strictly hyperbolic as the eigenvalues are not distinct. The system has a three dimensional eigenspace in which every direction is an eigendirection. It is clear that the advection terms are in characteristic form with the components of vorticity being the characteristic variables. All the characteristic fields are linearly degenerate with repeated eigenvalues of $\lambda=u$ for the x spatial component $\lambda=v$ for the y spatial component and $\lambda=w$ for the z spatial component. Physically these fields represent the propagation of vorticity with the fluid velocity.

In the application of the WAF method to the advective terms Brown's method carries out interpolation on the components of vorticity which are the characteristic variables of the linearly degenerate characteristic fields of the system. He has success in conserving vorticity when a compressive limiter (Superbee) is applied - in fact it is found to be necessary for vorticity conservation. In Ismail and Roe's work it is found to be necessary to apply the Superbee limiter at both the half and full steps of the scheme applied to the advection terms of the vorticity conservation equation to achieve improved vorticity conservation, again this limiter is being applied to the characteristic variables related to the linearly degenerate fields.

This discussion has identified that the method of Characteristic Decomposition, Brown's work using the vorticity transport equation and Ismail and Roe's vorticity correction scheme all rely on the use of the compressive limiter Superbee when interpolating variables related to the linearly degenerate characteristic fields in order to conserve vorticity. The reason why the use of a compressive limiter for the linearly degenerate fields succeeds in improving the vorticity conservation capabilities of each method comes down to the nature of the linearly degenerate fields - which for the compressible Euler equations relate to propagation of contact discontinuities and vorticity. The linearly degenerate fields in nonlinear systems behave in a similar way to the solutions of linear hyperbolic equations. Valuable discussion on the nature of the differing characteristic fields of hyperbolic systems can be found in the text by Leveque[23] and the text by Toro[3]. The relevant points are summarised here.

A system of m non-linear hyperbolic conservation laws, in one spatial dimension, can be represented by the following equation

$$U_{,t} + F(U)_{,x} = 0 \qquad \text{where U=} \begin{pmatrix} u_1 \\ u_2 \\ \vdots \\ u_m \end{pmatrix} \tag{3.3}$$

Which in quasi-linear form is given by

$$U_{,t} + A(U)U_{,x} = 0 \quad \text{where} \quad A(U) = \frac{\partial F}{\partial U} \tag{3.4}$$

This system is hyperbolic if $A(U)$ has m real eigenvalues and is strictly hyperbolic if all these eigenvalues are distinct.

Each eigenvalue λ^p and corresponding eigenvector R^p corresponds to a characteristic family of waves. A hyperbolic system can be transformed to a system of equations where each equation represents the propagation of one of these families of waves – this is the characteristic form of the system and is obtained by multiplication of the dependent variables by the matrix of left eigenvectors. Transformed to this characteristic form the equations can be rewritten as a series of m equations

$$W^p(U)_{,t} + \lambda^p(U)W^p(U)_{,x} = 0 \tag{3.5}$$

where the characteristic curves satisfy

$$\frac{\partial x}{\partial t} = \lambda^p(U)$$

A characteristic field is genuinely nonlinear if it relates to a distinct eigenvalue and right eigenvector. For genuinely nonlinear fields the following relation holds

$$\nabla\lambda^p(U) \cdot R^p(U) \neq 0 \tag{3.6}$$

everywhere and $\nabla\lambda^p(U)$ is the gradient of $\lambda^p(U)$ with respect to U

For linearly degenerate fields relating to the repeated eigenvalues the opposite is true with

$$\nabla \lambda^p(U) \cdot R^p(U) = 0 \quad \text{everywhere} \tag{3.7}$$

The difference in these two types of fields can be explained by their effect on a simple wave, a smooth discontinuity associated with a single characteristic family, propagating in the field. Through a simple wave in a nonlinear field the characteristics are not parallel and are either converging or diverging on the wave leading to distortion. In the Riemann problem each wave will be either a single shock or a rarefaction wave. Linearly degenerate fields do not display this nonlinear behaviour and through a simple wave in a linearly degenerate field the characteristics are parallel, like in a linear system, leading to the wave propagating without distortion.

This pseudo-linear behaviour associated with the degenerate fields leads to the discontinuities associated with these fields being prone to experience the same type of numerical problems as noted by Lax[6] with the spreading of contact discontinuities of linear hyperbolic equations by numerical schemes. It is therefore necessary to apply a compressive limiter which sharpens the gradients of these fields in order to overcome the numerical error that leads to spreading of their associated discontinuities.

When looking for a method that is best suited for implementation in an existing finite volume solver and which is easily applied to a range of engineering applications the method of Characteristic Decomposition seems the most suitable option. Brown's work requires the generation of vorticity in the domain to be dealt with by a source term which significantly reduces the range of possible applications. The method suggested by Roe and Ismail has as yet only been implemented for two dimensional inviscid flow and extension to viscous flows has not been explored.

There are some issues in need of clarification with regards to the use of the method of Characteristic Decomposition.

- It is observed by Ismail and Roe that when the compressive limiter Superbee is applied to the conserved variables in a calculation although the conservation of vorticity is improved there is also spurious generation of vorticity due to the steepening nature of Superbee. It needs to be clarified if this same problem of the generation of spurious vorticity occurs, and if so to what extent, when the compression of Superbee is applied only to the fields where it is required to overcome numerical errors as in Characteristic Decomposition.

- The implementation and demonstration of the effectiveness of the method of Characteristic Decomposition in an artificial compressibility scheme has not been demonstrated.

- The work on using Characteristic Decomposition for vorticity conservation has concentrated on application along with high order schemes. The effectiveness of the method of Characteristic Decomposition with second order schemes has not been demonstrated.

- The work on using Characteristic Decomposition for vorticity conservation has concentrated on calculations using structured grids. The effectiveness of the method of Characteristic Decomposition on unstructured grids has not been assessed. It is however well known that the performance of one dimensional limiting schemes, such as Superbee, on unstructured grids causes problems and it may be possible to improve the performance of Characteristic Decomposition on unstructured grids by modifying the application of the limiters to make their behaviour more compatible with an unstructured grid formulation.

4. Thesis Objectives

Validation of an artificial compressibility scheme in Cranfield's compressible solver MERLIN

Assessment of the method of Characteristic Decomposition applied in both the Compressible and Artificial Compressibility Schemes.

Assessment of the performance of the method of Characteristic Decomposition on unstructured grids

Development and assessment of a variation of the method of Characteristic Decomposition for improved performance on Unstructured Grids

5. Implementation of Baseline Incompressible Scheme

In order to provide a scheme in which to test the method of characteristic decomposition for incompressible flows the method of Artificial Compressibility has been implemented in the framework of the existing compressible solver MERLIN. MERLIN is a three dimensional second order finite volume flow solver, for the unsteady compressible viscous flow equations, which employs dual time stepping. The equations solved by the compressible MERLIN solver are given below.

$$\int_V \frac{\partial Q}{\partial \tau} dV + \int_V \frac{\partial Q}{\partial t} dV + \int_S F dS - \int_S G dS = 0 \qquad (5.1)$$

$$Q = \begin{bmatrix} \rho \\ \rho \mathbf{U} \\ E \end{bmatrix} \qquad F = \begin{bmatrix} \rho(\mathbf{U}\cdot\mathbf{n}) \\ \rho\mathbf{U}(\mathbf{U}\cdot\mathbf{n}) + P\mathbf{n} \\ (E+P)(\mathbf{U}\cdot\mathbf{n}) \end{bmatrix} \qquad G = \begin{bmatrix} 0 \\ \mathbf{T}^S \\ \mathbf{T}^S\cdot\mathbf{U} + q^S \end{bmatrix}$$

$$\mathbf{T}^S = \begin{bmatrix} \tau_{xx} & \tau_{xy} & \tau_{xz} \\ \tau_{yx} & \tau_{yy} & \tau_{yz} \\ \tau_{zx} & \tau_{zy} & \tau_{zz} \end{bmatrix} \cdot \mathbf{n} \qquad \tau_{ij} = \mu\left(\frac{\partial u_i}{\partial x_j} + \frac{\partial u_j}{\partial x_i} - \frac{2}{3}\frac{\partial u_k}{\partial x_k}\delta_{ij}\right)$$

$$q^S = \begin{bmatrix} q_i \\ q_j \\ q_k \end{bmatrix} \cdot \mathbf{n} \qquad q_i = -k\frac{\partial T}{\partial x_i}$$

Where V denotes the volume of a cell and S the cell surface.
Q is the vector of conserved variables, F the inviscid flux vector and G the viscous flux vector. $\mathbf{n}$ is the surface normal outward facing unit vector and $\mathbf{U}$ the complete velocity.

These equations are solved by the dual timestepping method where by they are marched to a steady state in pseudo time, τ, at each physical time step via a 2nd order

explicit method. As an explicit method is used the pseudo time steps are restricted by the cfl condition. The flux evaluations are carried out by applying the Riemann solver of Osher, with a MUSCL interpolation to provide second order accuray, to the locally one dimensional Riemann problems at the cell faces. The physical time step is updated via the implicit 2nd order backward in time Euler method.

The background of the method of Artificial Compressibility is discussed below.

The research and development of methods applied to the compressible flow equations has consistently outstripped efforts directed at the solution of incompressible flows. The method of artificial compressibility allows the wealth of knowledge from this research to be applied to the solution of incompressible flows. The Compressible Navier-Stokes equations describe flows of all Mach numbers but when it comes to numerical solution of these equations for low Mach numbers the methods applied to higher Mach number flows run into problems with convergence and stability. In fact testing carried out in Cranfield's compressible flow solver, MERLIN, showed problems with convergence appearing for $M \approx 0.1$ and a failure of the code for $M < 0.01$. This is because as Mach number reduces the speed of acoustic waves increases, tending to infinity in the limit, leading to a large disparity in acoustic wave and convection speeds. An approach to overcoming this is to instead solve the incompressible equations but these offer some challenges themselves due to the lack of coupling of the pressure and velocity fields. The Method of Artificial Compressibility was first introduced by Chorin[24] in 1967 as a way of overcoming this problem. This method transforms the left hand side of these equations into a hyperbolic type, mathematically similar to the compressible equations but with a pseudo acoustic wave speed, by introduction of an artificial derivative of pressure into the continuity equations thus opening them up to solution by the many Riemann Solvers available. This method was extended for application to unsteady viscous flows by Merkle[25] in 1987 via the application of dual time stepping. Another useful discussion of dual time stepping applied to the artificial compressibility equations can be found in the work by Breuer and Hanel[26].

Governing System of Equations – Artificial Compressibility

$$\int_V \frac{\partial Q_\tau}{\partial \tau} dV + \int_V \frac{\partial Q_t}{\partial t} dV + \int_S F dS - \int_S G dS = 0 \qquad (5.2)$$

$$Q_\tau = \begin{bmatrix} P \\ \mathbf{U} \end{bmatrix} \quad Q_t = \begin{bmatrix} 0 \\ \mathbf{U} \end{bmatrix} \quad F = \begin{bmatrix} (\mathbf{U}\cdot\mathbf{n})c^2 \\ \mathbf{U}(\mathbf{U}\cdot\mathbf{n}) + \frac{P}{\rho}\mathbf{n} \end{bmatrix} \quad G = \begin{bmatrix} 0 \\ \mathbf{T}^S \end{bmatrix}$$

$$\mathbf{T}^S = \begin{bmatrix} \tau_{xx} & \tau_{xy} & \tau_{xz} \\ \tau_{yx} & \tau_{yy} & \tau_{yz} \\ \tau_{zx} & \tau_{zy} & \tau_{zz} \end{bmatrix} \cdot \mathbf{n} \qquad \tau_{ij} = \mu\left(\frac{\partial u_i}{\partial x_j} + \frac{\partial u_j}{\partial x_i} - \frac{2}{3}\frac{\partial u_k}{\partial x_k}\delta_{ij} \right)$$

Where V denotes the volume of a cell and S the cell surface.
Q is the vector of conserved variables, F the inviscid flux vector and G the viscous flux vector. **n** is the surface normal outward facing unit vector and **U** the complete velocity. c is the artificial compressibility coefficient

In converting the compressible solver to solve the artificial compressibility equations original solver is modified as follows. The variables solved for are altered for the artificial compressibility scheme. The Energy equation is no longer solved. The boundary conditions and Oshers Flux for the inviscid terms are replaced by those for the artificial compressibility scheme. The viscous fluxes for the momentum equations remain unchanged and the viscous algorithms of the compressible code are retained. The calculation of the CFL condition for the pseudo time steps is altered to depend on the pseudo speed of sound.

In the method of artificial compressibility the unsteady incompressible equations are recovered at each physical time step. When the solution is marched to a steady state in pseudo-time, and the pseudo-time derivative $\partial Q_\tau / \partial \tau$ tends to zero, the artificial

compressibility term vanishes form the equations leaving the unsteady incompressible equations.

The Riemann Solver of Osher for the Artificial Compressibility Equations

The locally one dimensional problem solved at the cell faces by the reimann solver for the artificial compressibility equations is given below.

$$\frac{\partial \overline{Q}_\tau}{\partial \tau} + \frac{\partial H}{\partial \overline{x}} = 0 \qquad (5.3)$$

where

$$\overline{Q}_\tau = \begin{pmatrix} P \\ \overline{u} \\ \overline{v} \\ \overline{w} \end{pmatrix} \qquad H = \begin{pmatrix} \overline{u}c^2 \\ \overline{u}^2 + P \\ \overline{v}\overline{u} \\ \overline{w}\overline{u} \end{pmatrix}$$

$\overline{u} = \mathbf{U} \cdot \mathbf{n}$ $\quad U = \begin{pmatrix} u \\ v \\ w \end{pmatrix}$ $\quad n = \begin{pmatrix} n_x \\ n_y \\ n_z \end{pmatrix}$ is the local surface normal, outward pointing, unit vector c is the artificial compressibility coefficient

The Riemann solver of Osher was first presented in the papers by Engquist and Osher [27] and Osher and Soloman[28]. A good account of this method is also given in Toro[3] in which the application of the method for any non-linear system of hyperbolic conservation laws is given. Toro states that 'one of the attractions of Osher's scheme is the smoothness of the numerical flux; the scheme has also been proved to be entropy satisfying'. The derivation of Osher's flux depends on integration in phase space. The integration paths are integral curves associated with the set of right eigenvectors of the system. For the artificial compressibility equations these curves along with their intersection points need to be determined. The generalised Riemann invariants are used to determine the intersection points. The Osher flux for a general system of hyperbolic equations with variable vector U is defined by the following equation.

$$F_{i+1/2} = F(U_0) + \int_{U_0}^{U_1} A^{-}(U)\,dU \tag{5.4}$$

where the integral *is taken in phase space along*

$$I(U) = I_1(U) \cup I_{2,3}(U) \cup I_4(U)$$

giving

$$F_{i+1/2} = F_0 + \int_{U_0}^{U_{1/3}} A^{-}(U)dU + \int_{U_{1/3}}^{U_{2/3}} A^{-}(U)dU + \int_{U_{2/3}}^{U_1} A^{-}(U)dU \tag{5.5}$$

The full derivation of the Osher Flux for the Artificial Compressibility Equations is given in Appendix A.

Choice of Value for the Artificial Compressibility Coefficient.

There have been many different approaches to determining the appropriate value of the Artificial Compressibility coefficient, c. Some people choose a constant value for c normally in the range $1 \rightarrow 3$ and then use an empirical approach to alter this value, if found necessary, for a particular calculation. There has also been work to determine the ideal value of c dependent on flow velocity, most notably that by Turkel[29,30]. It seems sensible to take the approach of defining c in this way as c has dimensions of velocity and so there can be no universal appropriate value for c as this will depend on the non-dimensionalization.

There are several things to consider when choosing a value of the artificial compressibility coefficient. The speed of propagation of the pseudo acoustic waves is determined by c and so this choice effects the convergence characteristics of a code. For a low value of c the acoustic wave speeds will be smaller, for a given convection speed, and so the ratio of pseudo acoustic to convection speeds will be smaller leading to better convergence characteristics. On the other hand for small c the influence of the artificial time derivative on the continuity equation will be greater

leading to a possible loss of accuracy for a given level of convergence. Marx[31] concluded that c 'appears to have more influence on the convergence rate of a method than on the accuracy of the results' and so it is the convergence characteristics that should be of greatest concern when making a choice of c value.

For those who choose a value for c dependent on the flow velocity there is then the decision of whether to keep this value a constant, dependent on the farfield velocity, or to allow this value to vary with the maximum flow velocity. There is also a need to consider a lower limit on the value of c in order to avoid problems close to stagnation points.

In [30] Turkel derives a variable value of c which would minimize the largest possible ratio of wave speeds which is given by

$$c^2 = \max(3(u^2 + v^2), \varepsilon) \tag{5.6}$$

where ε is a fraction of $(u^2 + v^2)_{max}$ to avoid problems near to stagnation points.

Rizzi[32] shows that a value of

$$c^2 > (u^2+v^2) \tag{5.7}$$

provides better conditioning preventing problems near stagnation points putting a lower acceptable limit on the value of c. In the later paper Turkel[30] observes that a constant value for c in fact provides better convergence but concludes that 'the reasons for this are not clear'. The issue of whether a constant value of c is preferable has not been clarified with several papers coming to contradictory conclusions, for example Marx[31] and Elsworth and Toro[33] both find a variable c preferable with Marx stating that 'a variable – in time – c^2, linked to maximum velocity can also stabilize an otherwise diverging calculation'. It seems sensible to experiment with both variable and constant values of c when implementing artificial compressibility in a code for the first time, starting with a value close to that predicted as ideal by Turkel[29].

6. Testing of the Artificial Compressibility Scheme

Initial validation of the artificial compressibility scheme concentrates on calculation of an inviscid steady flow. This test case is used in order to test the most appropriate choice of artificial compressibility coefficient and to validate the artificial compressibility scheme. It is useful to apply several levels of testing to the code – firstly to validate the core of the artificial compressibility method embedded in the unsteady viscous flow solver and then to validate the viscous terms by calculating a laminar flow over a flat plate and comparing to the Blausius similarity solutions. The dual time stepping scheme can then be tested against a suitable test case in this case the laminar flow over a circular cylinder. All calculations performed in the testing of the artificial compressibility scheme employ the Barth and Jespersen limiter[35]. This limiter has been chosen as a baseline for comparison throught out this work due to it's popularity and strong performance. The Barth and Jespersen limiter is applied so that the reconstructed values in a cell are bounded by the maximum and minimum values that can be found by considering the cell and it's neigbours.

For unstructured cell B the Barth and Jespersen limiter function $\Psi_{BJ}(r)$ takes values such that the following condition is enforced

$$\min(q_N, q_B) \le q_B + \Psi_{BJ}(r)\vec{r} \bullet \nabla q_B \le \max(q_N, q_B) \forall N \in Neighbour(B) \tag{6.1}$$

Here $\vec{r}$ is the vector connecting the cell centre to the face centre- making $\vec{r} \bullet \nabla q_B$ the interpolated difference, which is to be limited, in q from the cell centre to the face.

$$r = \frac{\frac{1}{2}(q_A - q_B)}{\vec{r} \bullet \nabla q_B} \tag{6.2}$$

Inviscid Flow around a slotted flap aerofoil

This test case is the calculation of the flow around a two dimensional slotted-flap aerofoil at a nondimensionalised velocity = 0.2. In the MERLIN solvers all velocities

are nondimensionalised by the freestream speed of sound of a compressible flow at the velocity under consideration. The exact solution for the pressure distribution is given in Williams[35] and the calculation of the exact solution was carried out as follows. “The Inviscid flow about two lifting circles was calculated by the method of images and then the two circles were mapped conformally onto two aerofoils by applying the Karman-Trefftz transformation twice.” This test case is towards the top range of the speeds for which the artificial compressibility scheme is appropriate and so provides a challenging case and also the opportunity to compare its performance to a compressible flow solver at Mach 0.2.

The calculation is carried out on an unstructured grid consisting of 15000 cells with 501 cells around the main element and 201 around the flap. These points are distributed such that the grid spacing and the leading and trailing edges of both the main element and flap is 0.0001m. The leading edge of the main element is placed at (0, 0) and the boundary of the computational domain is circular with radius 20m. Figures 3 and 4 show the computational domain. All calculations are run with a cfl=0.1.

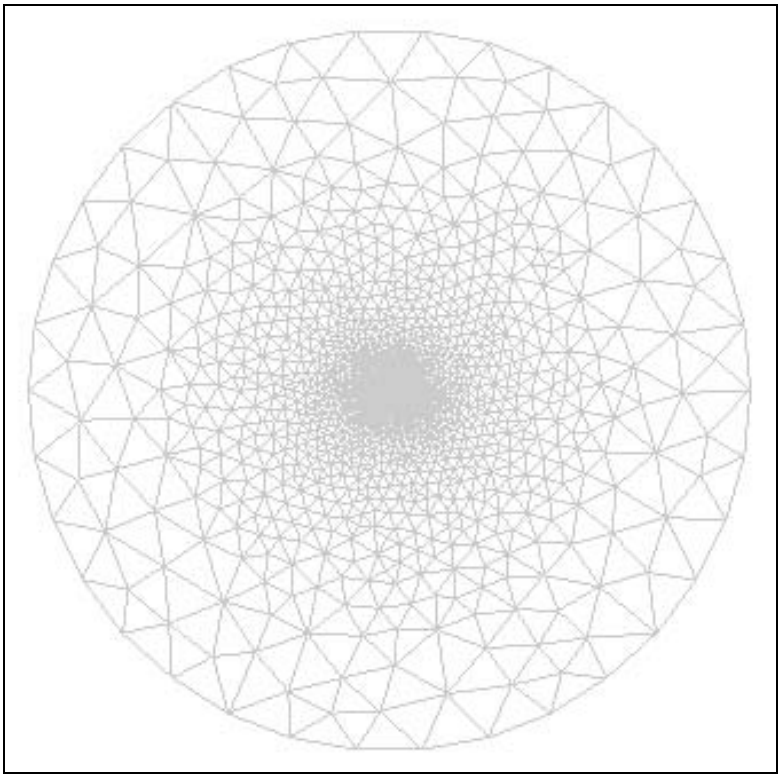

Figure 3 – The computational domain for the Slotted Flap Calculation

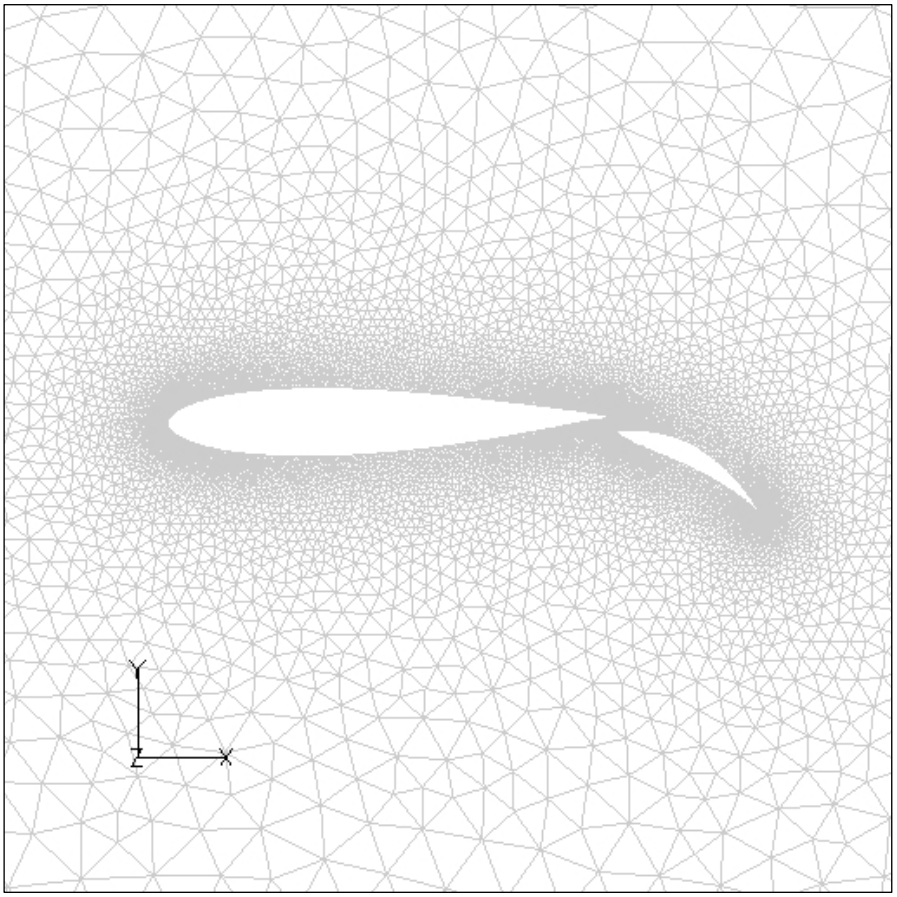

Figure 4 – Close up of the distribution of cells in the region of the aerofoil for the slotted flap calculation

Initial tests centred around the choice of artificial compressibility coefficient. It was confirmed that the lower bound of $c^2 > (u^2+v^2)$ is valid and in fact it was not possible to achieve a converged solution if this relationship was violated. Following this finding constant values of c determined by the relationship

$$c = \alpha \sqrt{(u^2+v^2)_{farfield}} \tag{6.3}$$

and variable values of c with

$$c = \alpha \sqrt{(u^2+v^2)_{max}} \tag{6.4}$$

at each time step were tested. The parameter α taking values in the range (1.1, 5)

It was found, as suggested by Turkel[29], that a constant value of c consistently gives the best convergence rates across a range of c values. This is demonstrated in the following figures.

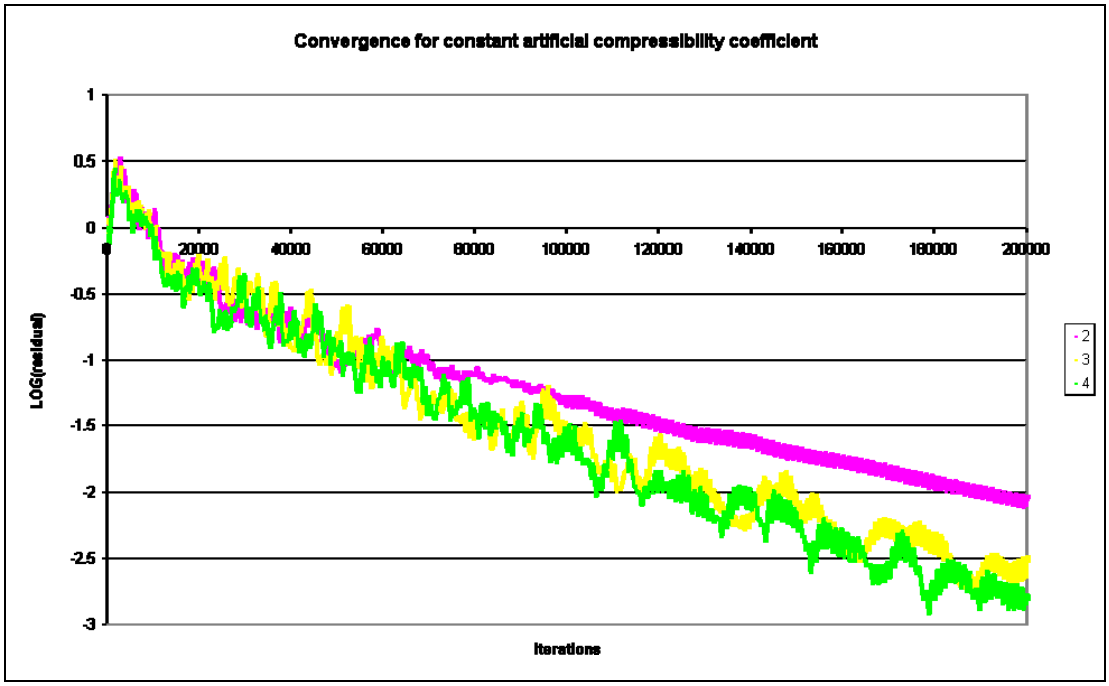

Figure 5

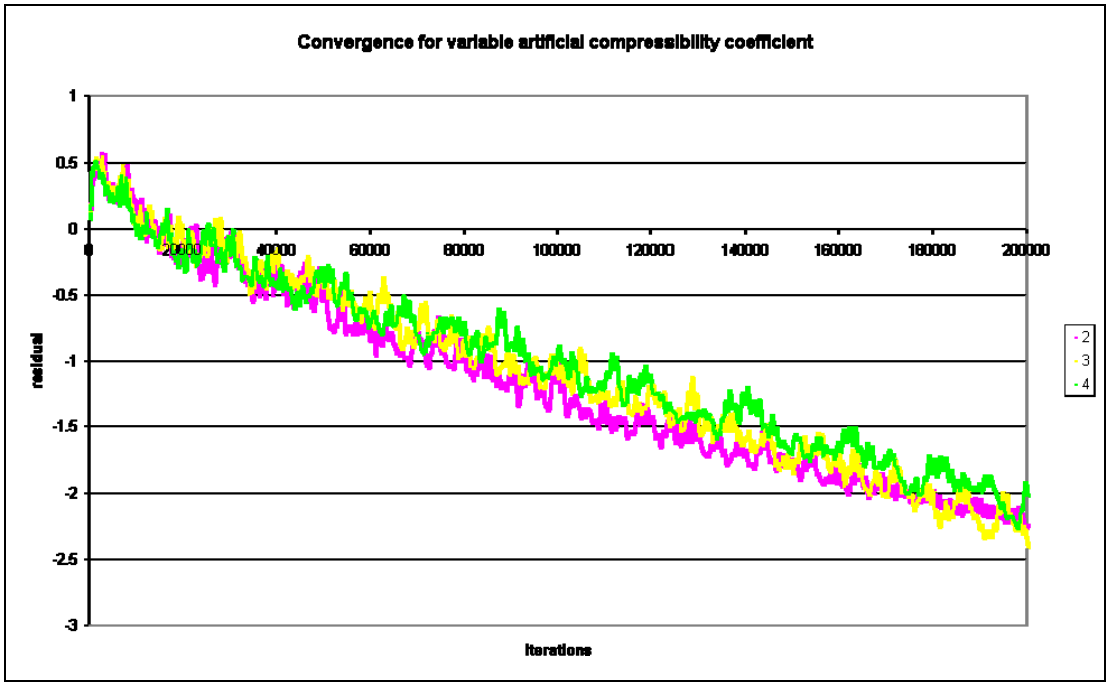

Figure 6

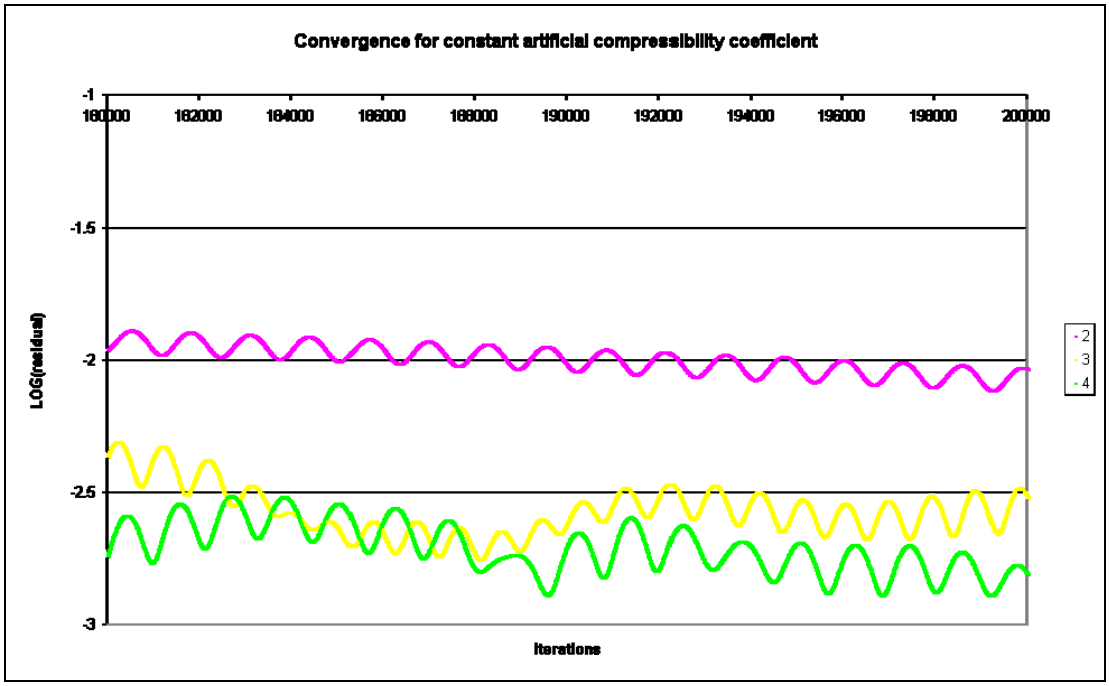

Figure 7

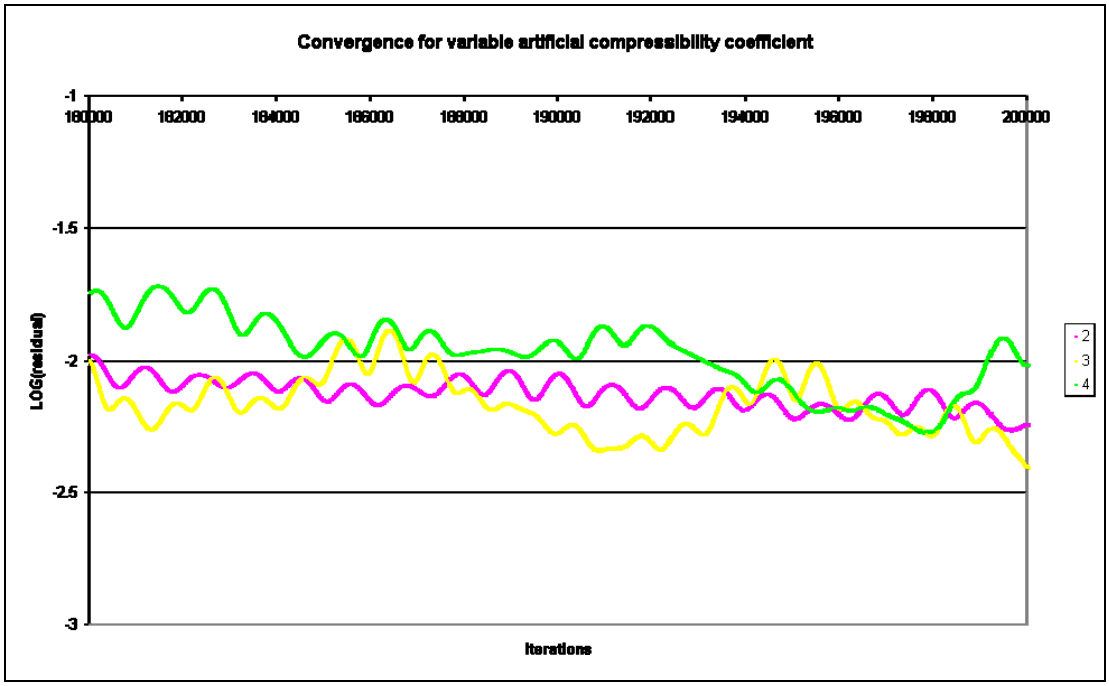

Figure 8

The accuracy of the calculation is not greatly affected by the choice of c value but testing in the region of the value c=3, suggested by Turkel, found that c=3.5 gave a slightly more accurate value at the leading edge if the aerofoil as is shown in figures 9 and 10.

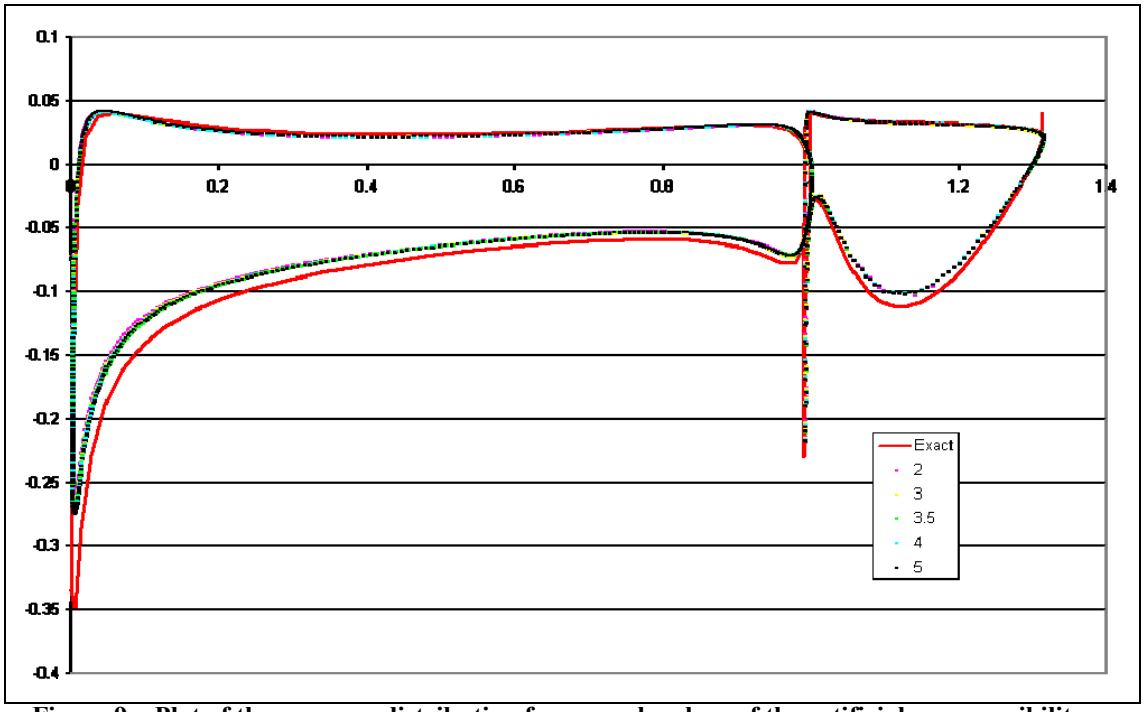

Figure 9 – Plot of the pressure distribution for several values of the artificial compressibility coefficient

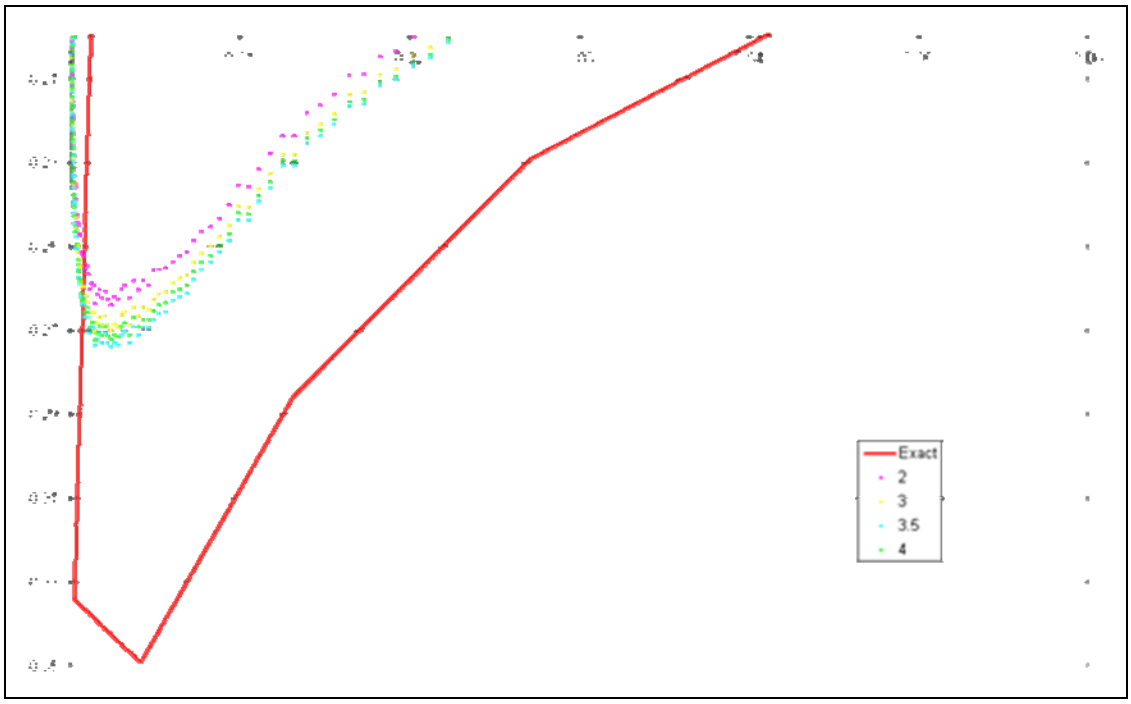

Figure 10 – Close up of the peak region in Figure 9 – it can be seen that an artificial compressibility coefficient = 3.5 provides the most accurate solution in this area.

Comparing the artificial compressibility formulation to results achieved with the compressible flow solver the artificial compressibility scheme is slightly less accurate around the leading edge as can be seen from Figure 11.

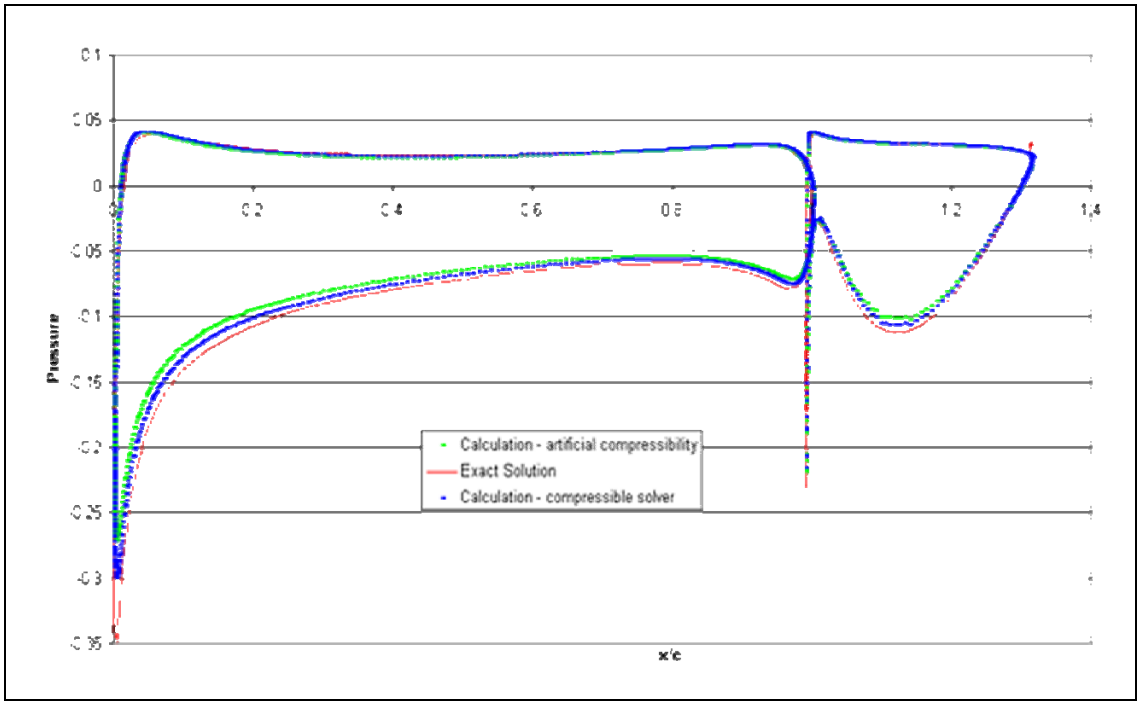

Figure 11– Plot of the pressure distribution for the artificial compressibility and compressible solvers. It can be seen that the compressible solver provides the slightly better solution

Both codes have problems with resolving the flow accurately in this area and this is thought to be due to having an insufficiently fine grid around the leading edge. The performance of the artificial compressibility algorithm for this case is sufficiently accurate to conclude that the scheme is working as intended and that it is suitable for calculation of steady incompressible flows at nondimensionalised velocity = 0.2 and below.

The results of grid convergence studies for both the artificial compressibility and compressible schemes are shown in Figures 12 and 13. The two coarser grids have 13000 and 8000 cells.

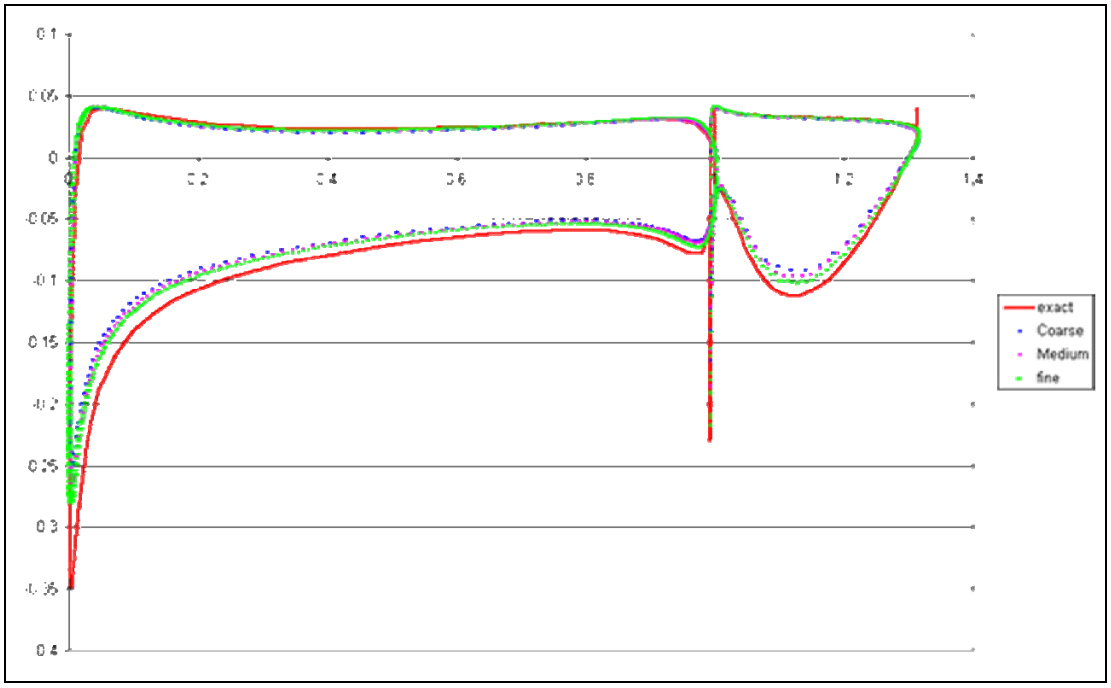

Figure 12 -Plot of the pressure distribution for the artificial compressibility solver on three grid densities

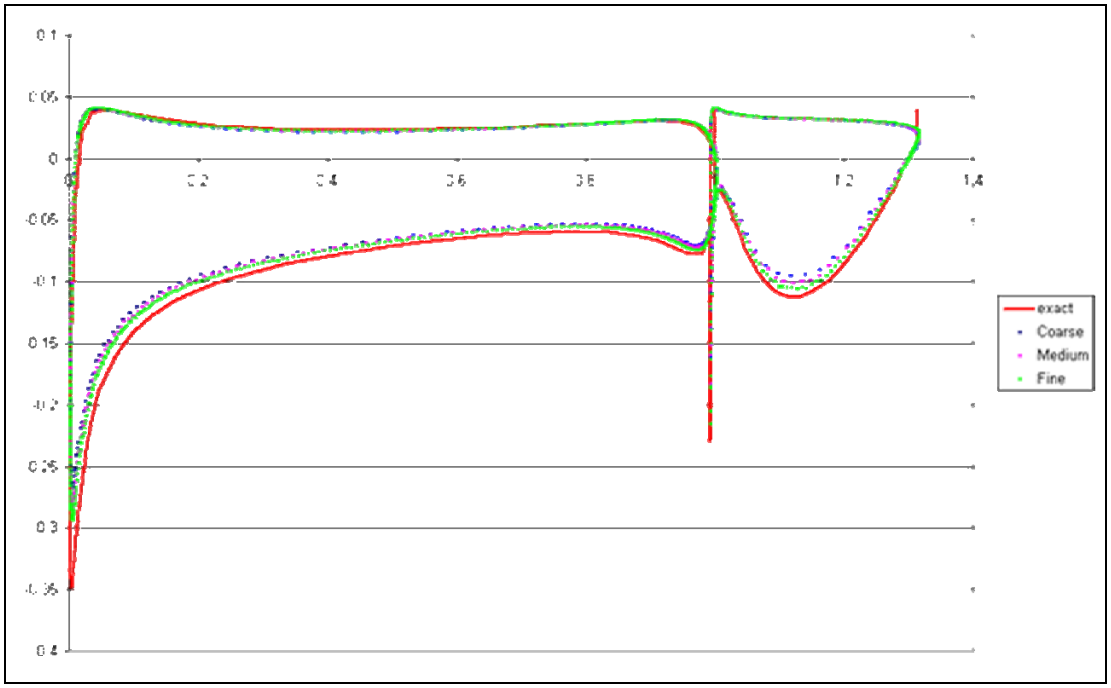

Figure 13 - Plot of the pressure distribution for the compressibe solver on three grid densities

The behaviour of both the artificial compressibility and incompressible codes as the grids are refined are similar and it can be seen that as the grid resolution improves the calculated solutions for both schemes are approaching the exact solution.

Calculation of the Laminar flow over a Flat Plate

The laminar flow past a flat plate at zero angle of incidence, at Mach = 0.1 is calculated. The flow is calculated at a Reynolds number of 250000 based on the length of the flat plate and the temperature is 388.89K. A laminar boundary layer forms along the plate which can be compared with the Blasius similarity solutions given below

the similarity similarity variable is given by

$$\eta = y\sqrt{\frac{U_{fs}}{2\nu_{visc}x}} \tag{6.5}$$

with the velocity profiles given by

$$u = U_{fs} f'(\eta) \tag{6.6}$$

for comparison purposes η is plotted against $\frac{u}{U_{fs}}$ and $f'(\eta)$

and

$$v = \sqrt{\frac{\nu_{visc} U_{fs}}{2x}}(\eta f'(\eta) - f(\eta)) \tag{6.7}$$

for comparison purposes η is plotted against $\frac{v}{\sqrt{\frac{\nu_{visc} U_{fs}}{2x}}}$ and $(\eta f'(\eta) - f(\eta))$

The values of the functions f' and f, along with a comprehensive discussion of similarity solutions, can be found in the text by White[36].

The two dimensional computational domain has its inflow boundary at x=-0.25 and outflow boundary at x=1. The flat plate is at y=0 and the farfield boundary is placed at y=1. The streamwise grid density is Δx=0.02 with 63 grid points. In the transverse

direction there are 69 grid points with an initial $\Delta y=0.0005$ with the first 40 points in the transverse direction below $y=0.1$ giving a fine distribution in the region of the boundary layer as is shown in figures 14 and 15. All calculations are carried out with cfl=0.3

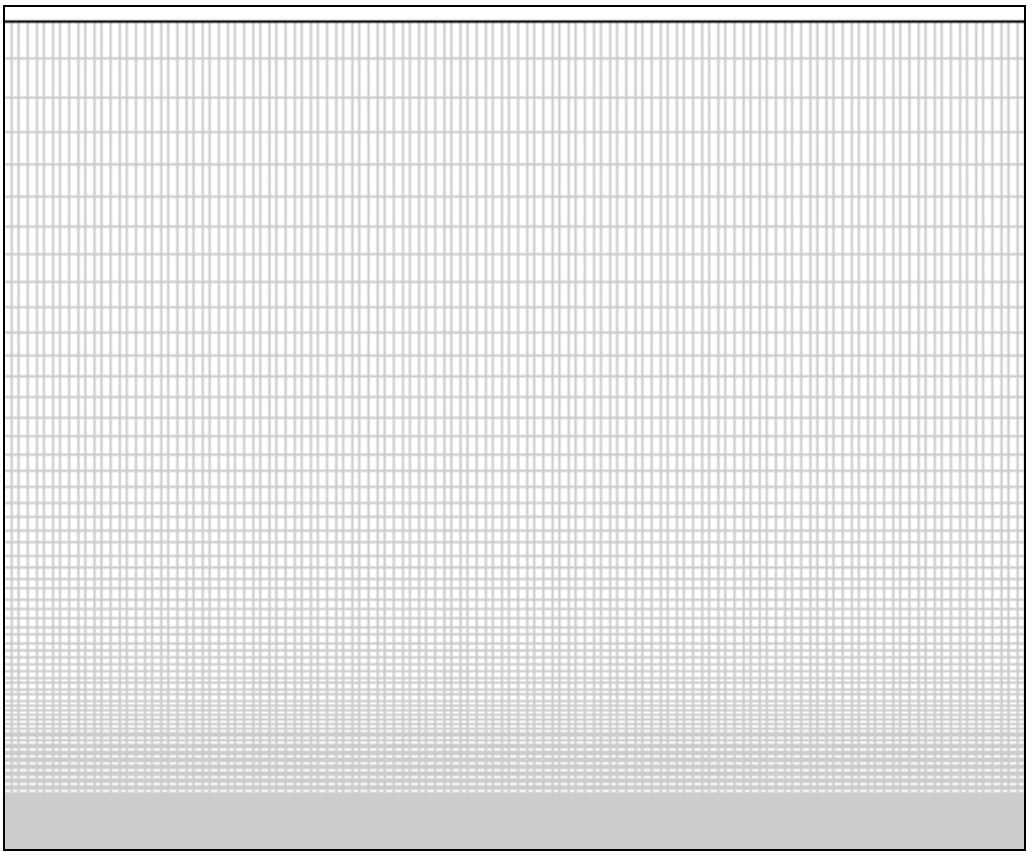

Figure 14 – Computation domain for the laminar flat plate calculation

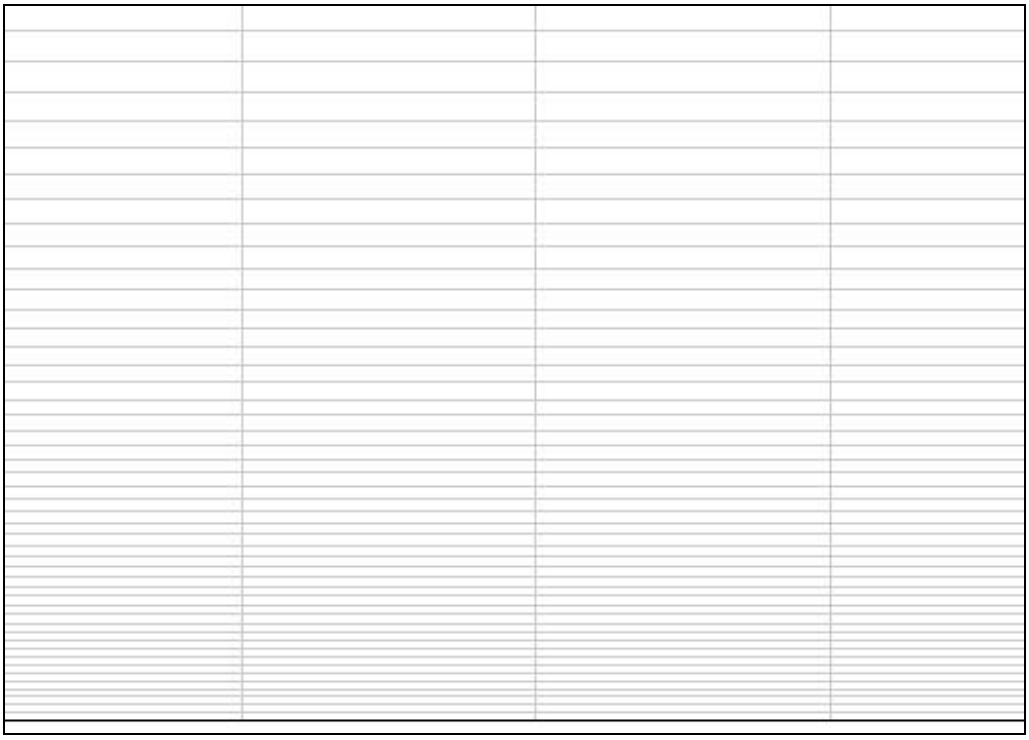

Figure 15 – close up of the grid distribution for the first 48 transverse points in the area of the wall boundary for the laminar flat plate calculation

The solutions obtained for the flat plate calculation for the artificial compressibility code are compared to the Blausis solutions in figures 16 and 17.

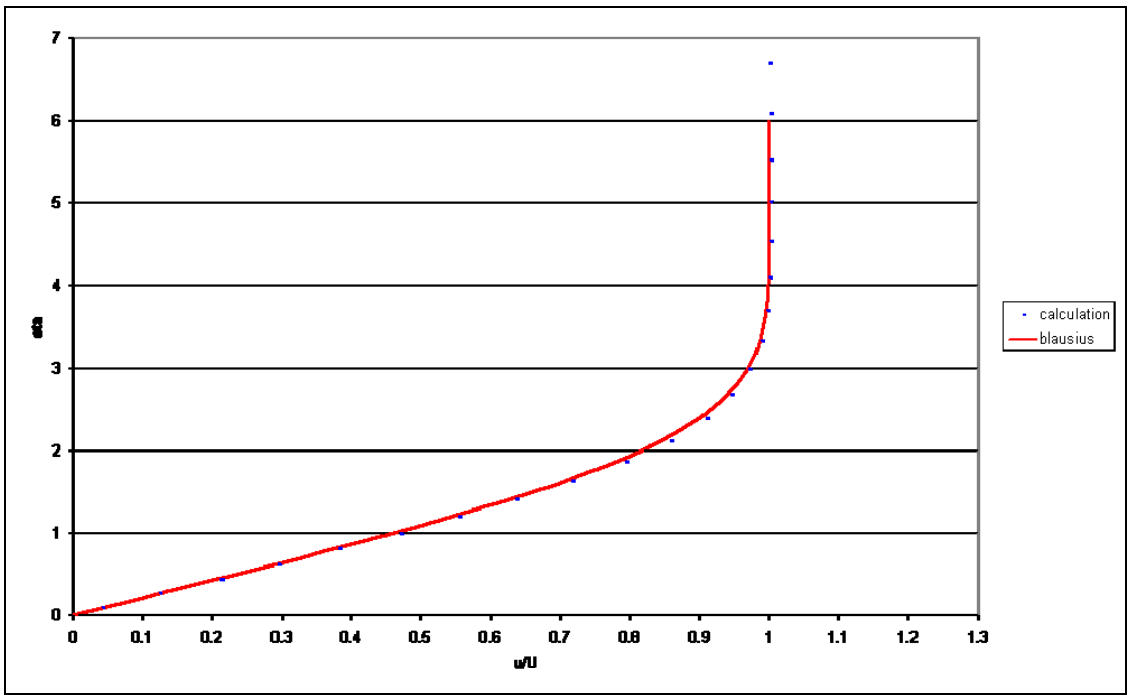

Figure 16 – Comparison of the Artificial Compressibility Scheme to the Blausius solution for the streamwise components of velocity, the calculation comes close to the analytic solution

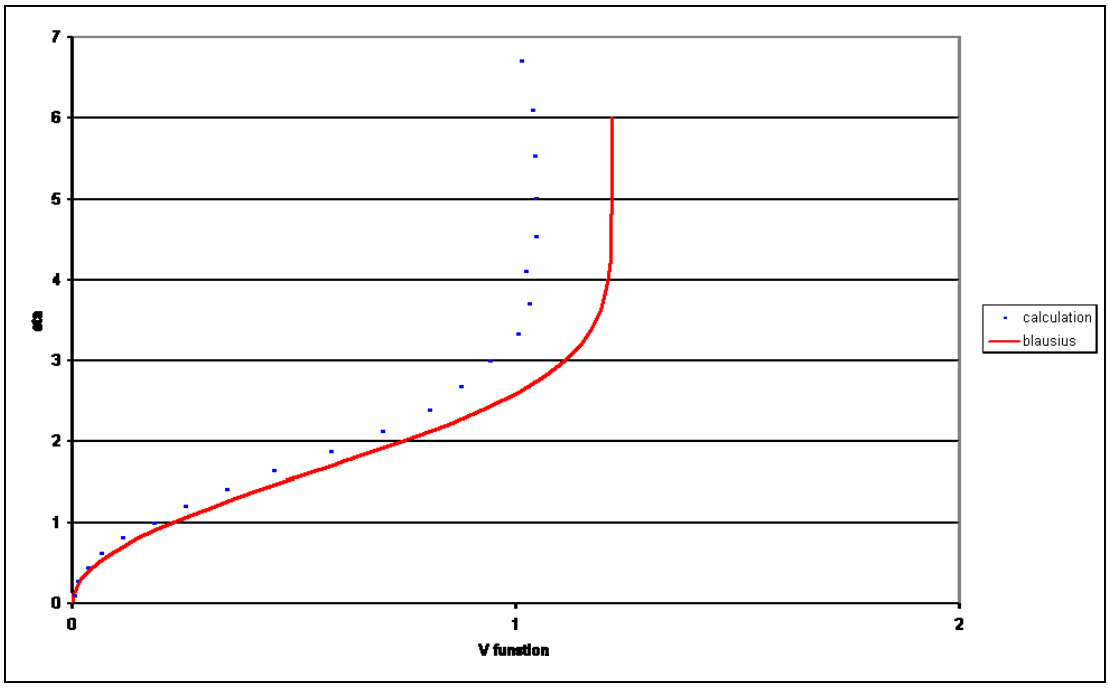

Figure 17 - Comparison of the Artificial Compressibility Scheme to the Blausius solution for the transverse components of velocity

The solution for function for the v component of velocity appears to be less accurate than the solution the u velocity component but when it is taken into consideration that the components of velocity in the transverse direction are many orders of magnitude smaller than those in the streamwise direction the solutions seem reasonable. The calculated velocity profiles compare favourably with the analytic solutions and it can be concluded the viscous terms in the code are working as intended.

The Laminar Flow Over a Circular Cylinder at Mach=0.2

The two dimensional flow over a laminar circular cylinder at Reynolds number 150, based on the cylinder diameter, is calculated. The freestream flow is Mach=0.2 and the temperature is 278K. The results can be compared to experimental date obtained for the Strouhal number which is the dimensionless vortex shedding frequency given by

$$S_t = f\frac{D}{U} \qquad (6.8)$$

where D is the diameter of the cylinder, U is the freestream velocity and f is the frequency of vortex shedding.

For a Reynolds number of 150 the Strouhal number can be expected to be in the region of 0.16 – 0.18.

The computational domain is circular with a radius of 200m and is centred on the cylinder. The structured grid has 401 points around the cylinder and 201 points in the radial direction with an initial wall spacing of $1x10^{-3}$. The hybrid grid has the same distribution of structured mesh surrounding the cylinder to a distance 0.1m normal to the cylinder surface. The remainder of the domain is unstructured with the farfield boundary having an even distribution of 401 cells. Figure 18 and 19 show the computational domains of both grids in the region of the cylinder. It can be noted that in both grids the quality of the grid reduces dramatically down stream of the cylinder and the vortex capturing capabilities of the calculations will be affected by this.

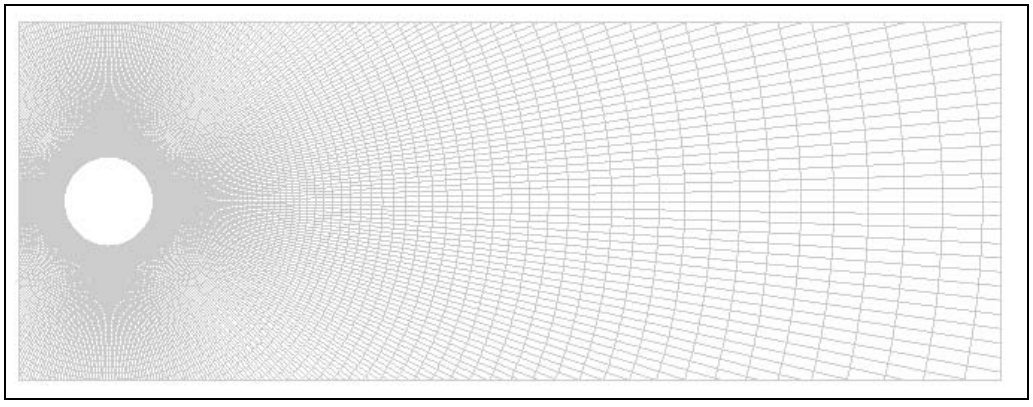

Figure 18 – Structured grid in the region of the cylinder

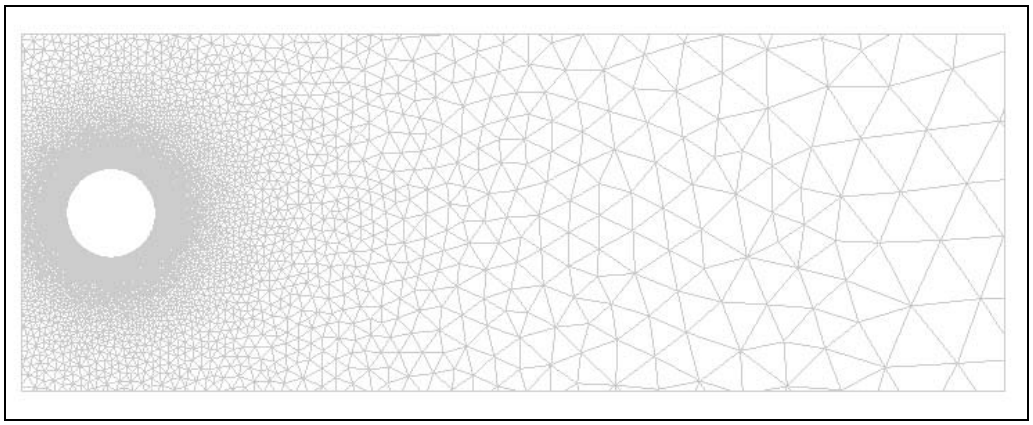

Figure 19– Unstructured grid in the region of the cylinder

All calculations are carried out with a cfl=0.3 and run for a total physical time of 3s with a time step of dt=0.01s.

The Strouhal numbers calculated from the frequency of variations in pressure at a monitor position below the vortex shedding path are S_t=0.146 for both the structured and unstructured cases. Tests were carried out to find the number of subiterations at which the calculated Strouhal number stopped changing with additional iterations and it was found to be 2500 sub iterations for each physical time step. A test on the time step convergence was carried out in which the physical time steps were halved to see the change in the calculated Strouhal number in the structured case the Strouhal number was higher at S_t=0.15 but remained unchanged for the unstructured case. All these predicted values are less than the magnitude of the Strouhal number predicted by experiment. The Strouhal number increases with Reynolds number for Reynolds numbers in the region of 150. The under prediction of the Strouhal number may be due to numerical dissipation in the code increasing the effective viscosity and so dropping the effective Reynolds number. The physical time step chosen may also influence the predicted values which may improve with further reduction of the physical timesteps but the amount of reduction possible is restricted by computational costs and there was little change for a 50% reduction in physical timestep. It must also be considered that the freestream Mach number =0.2 is towards the top end of the appropriate range for application of the artificial compressibility scheme and this may have some influence on the accuracy of the predicted Strouhal number.

The following figures show the vorticity shed from the cylinder for both the structured and unstructured calculations at 300 physical timesteps.

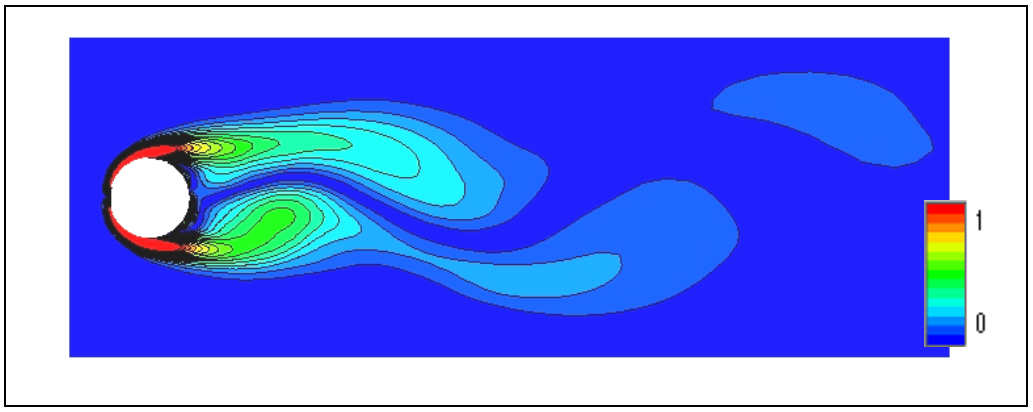

Figure 20 Structured Calculation, Vorticity Magnitude non-dimensionalised by the physical freestream speed of sound

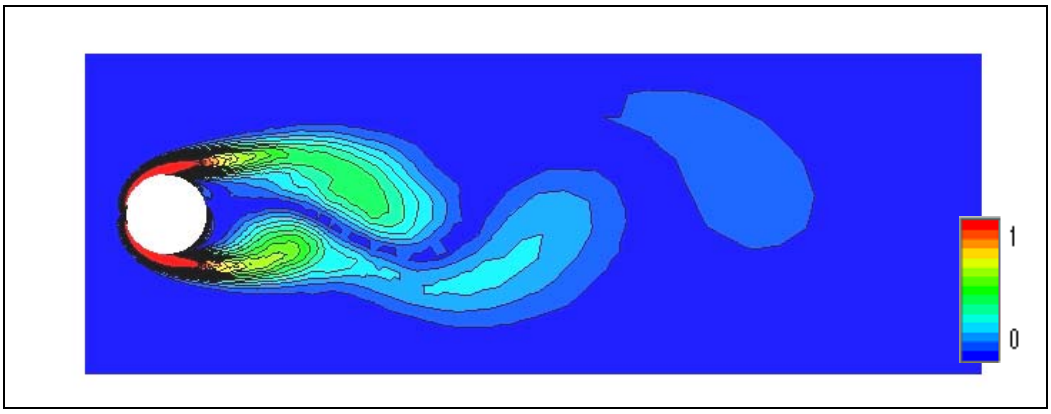

Figure 21 Unstructured Calculation, Vorticity Magnitude non-dimensionalised by the physical freestream speed of sound

Taking into consideration the factors possibly affecting the performance of the artificial compressibility scheme in this calculation it can be concluded that implementation of dual time stepping in the scheme is performing as expected.

7. Implementation of Characteristic Decomposition

The method of characteristic decomposition applies different limiter functions to different variables during the reconstruction of the slopes in a higher order calculation of a system of hyperbolic conservation laws. A compressive limiter, Superbee, is used for variables associated with the linearly degenerate fields whilst the more diffusive limiter, Minmod, is applied to those associated with the genuinely nonlinear fields. The method of application of characteristic decomposition, for a system of three dimensional equations, follows.

In order to apply a Riemann Solver in conjunction with a Godunov type scheme to a three dimensional system of hyperbolic conservation laws the x-split Riemann problem is solved.

The equations in use will therefore be in the form

$$U_t + F(U)_x = 0 \qquad \text{where U=} \begin{pmatrix} u_1 \\ u_2 \\ \vdots \\ u_m \end{pmatrix} \tag{7.1}$$

Where U is the vector of local conserved variables

In quasi-linear form this is given by

$$U_t + A(U)U_x = 0 \quad \text{where} \quad A(U) = \frac{\partial F}{\partial U}$$

The matrix A(U) has m eigenvalues λ^p and left and right eigenvector L^p and R^p. The linearly degenerate fields are associated with repeated eigenvalues whilst the genuinely non-linear fields have distinct eigenvalues and linearly independent eigenvectors.

The local characteristic variables, W, of the system can be obtained via the transformation

$$W = LU \tag{7.2}$$

It is assumed the following relationship is valid

$$\overline{\Delta W} = L\overline{\Delta U} \tag{7.3}$$

The gradients of the local conserved variables are obtained via the chain rule from the gradients of the global variables and are used to calculate the limited differences $\overline{\Delta U_{compressive}}$ and $\overline{\Delta U_{dissusive}}$

The interpolation function is then given by

$$W_{i+1/2} = L_i U_i + L_{1i}\overline{\Delta U_{compressive}} + L_{2i}\overline{\Delta U_{dissusive}} \tag{7.4}$$

Where L_i is the matrix of left eigenvectors and L_{1i} and L_{2i} are matricies of the eigenvectors of the linearly degenerate fields and genuinely nonlinear fields respectively such that

$$L_i = L_{1i} + L_{2i} \tag{7.5}$$

the interpolated local conserved variables are recoved via

$$U_{i+1/2} = \mathrm{R}_i W_{i+1/2} \tag{7.6}$$

and the global variables recovered from the local conserved variables

The details of the implementation of characteristic decomposition for the artificial compressibility and compressible Euler equations can be found in Appendices B and C respectively.

8. Testing of the Method of Characteristic Decomposition

The Effect of Characteristic Decomposition on the Slotted Flap Aerofoil Test Case

Compressible Solver –

Figure 22 shows the effect of the application of Characteristic Decomposition in the compressible flow solver on the slotted flap aerofoil test case.

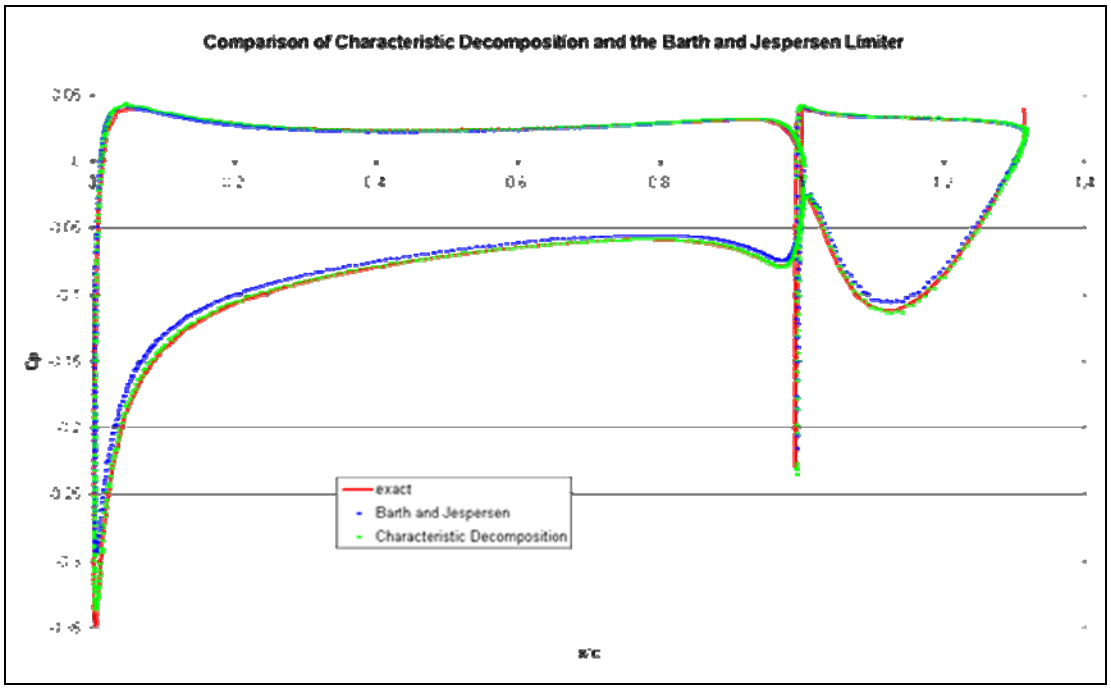

Figure 22 – Comparison of the pressure distributions obtained with the Barth and Jespersen Limiter and Characteristic Decomposition – Characteristic Decomposition shows a great improvement over the Barth and Jespersen limiter

The application of Characteristic Decomposition greatly improves the performance of the compressible code for this test case. The additional computational cost of this scheme over the base line scheme is an additional 25% per iteration. The effect on convergence also needs to be taken into account when considering the benefit of the additional accuracy of the Characteristic Decomposition scheme. Figure 23 Shows a comparison of the convergence histories of the baseline and Characteristic Decomposition Schemes. The baseline scheme shows better convergence

characteristics than the Characteristic Decomposition Scheme although the convergence is similar until the point at which the residual levels out for the Characteristic Decomposition scheme. This behaviour is expected as the method of Characteristic Decomposition employs non-differentiable limiters which are known to suffer from convergence stall to a greater degree than three dimensional limiters such as Barth and Jespersens. The Characteristic Decomposition scheme can then be considered to give a considerable improvement in accuracy over the baseline scheme at 25% additional computational cost.

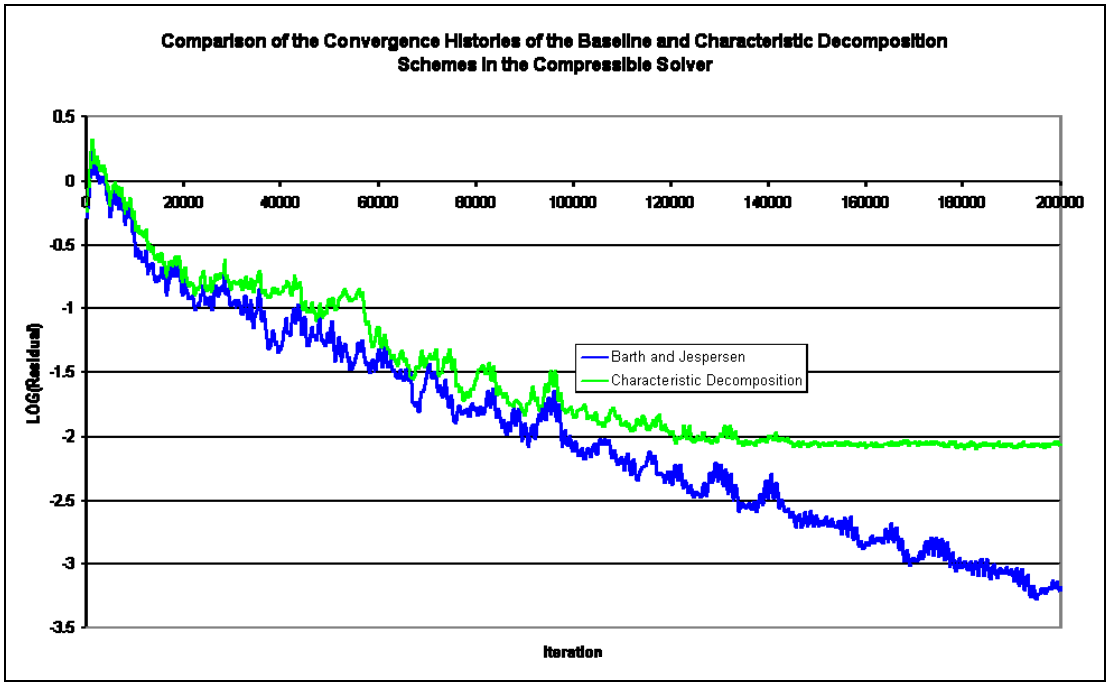

Figure 23 – Convergence histories for Barth and Jespersen and Characteristic Decomposition Schemes – the onset of convergence stall is evident for the Characteristic scheme

Artificial Compressibility Solver –

Figure 24 shows the effect of the application of Characteristic Decomposition in the artificial compressibility flow solver.

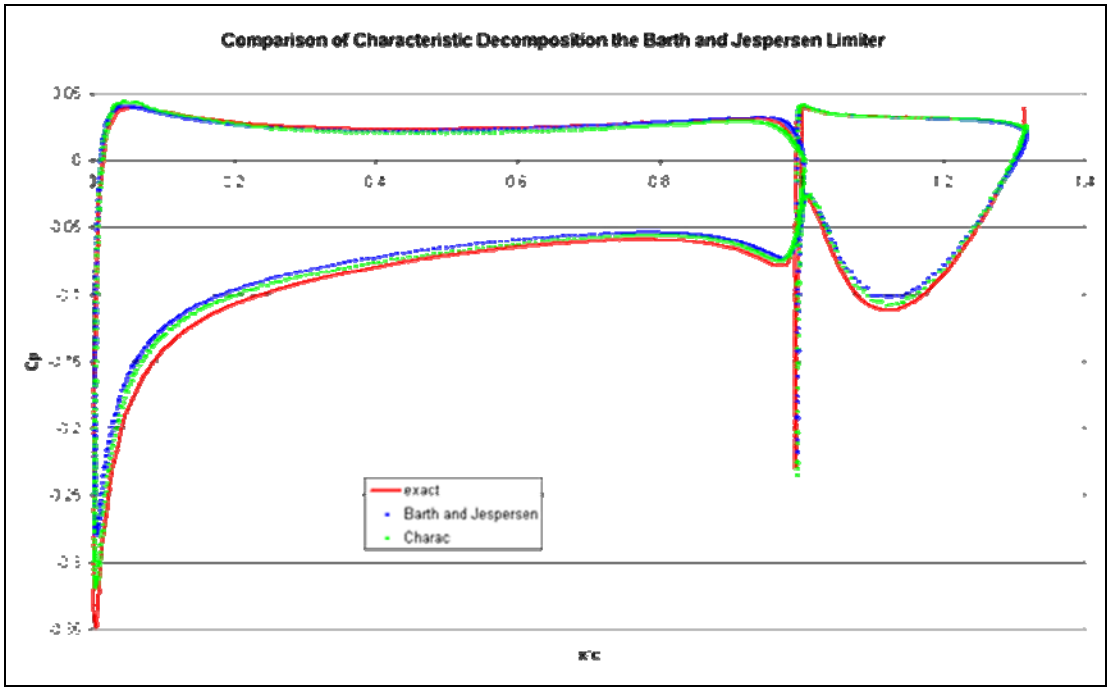

Figure 24– Comparison of the pressure distributions obtained with the Barth and Jespersen Limiter and Characteristic Decomposition – Characteristic Decomposition shows a great improvement over the Barth and Jespersen limiter

As with the compressible code the implementation of Characteristic Decomposition in the artificial compressibility scheme provides an improvement in the calculated pressure distribution on the aerofoil and flap. Figure 25 shows the convergence histories of both the baseline and Characteristic schemes for this test case. For both the baseline and Characteristic Decomposition schemes the convergence is slower for the artificial compressibility scheme than the compressible solver. Again the baseline scheme shows better convergence behaviour. In this case the convergence of the Characteristic Decomposition scheme remains approximately one order of magnitude greater than the baseline scheme.

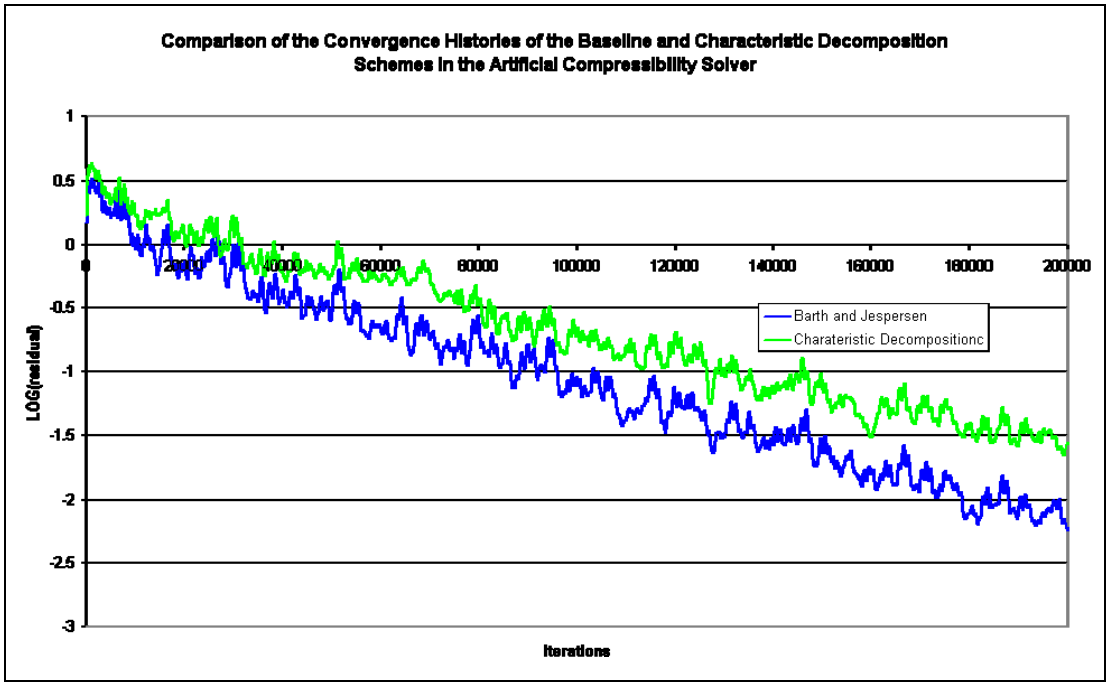

Figure 25– Convergence histories for Barth and Jespersen and Characteristic Decomposition Schemes – the onset of convergence stall is evident for the Characteristic scheme

Appendix D contains the results obtained for the baseline and characteristic decomposition scheme for various levels of grid refinement. It is noted that the implementation of Characteristic Decomposition has little effect on the behaviour of the calculated solution as the grid is refined as compared to the baseline scheme.

For both the compressible and artificial compressibility schemes the Superbee limiter was tested and failed to achieve a converged solution.

Calculation of Flow over a Supersonic Wedge.

The two dimensional inviscid flow over a supersonic wedge with half angle 15^o and freestream Mach number 2.5 is calculated. The freestream temperature is 288.89K. An oblique shock is formed at the leading edge of the wedge and the calculated change in conditions across the shock can be compared to the analytic solution. Details of the analytic solution for this flow can be found in Anderson[37] and the relations across the shock are summarised in the following table (figure 26).

Angle of oblique shock	36.94490^o
Mach number behind the oblique shock	1.873526
Pressure ratio (p2/p1)	2.467500
Density ratio (rho2/rho1)	1.866549
Temperature ratio (T2/T1)	1.321958

Figure 26 Analytic solution of the Inviscid Flow of a wedge of half angle 15^o with freestream Mach number 2.5

The flow is calculated on a two dimensional grid with grid density 155 in the streamwise direction and 101 points in the transverse direction. This gives a nearly even grid spacing of approximately 0.01 in each direction, Figure 27 shows the computational grid. The leading edge of the wedge is located at (0, 0) with the inflow boundary of the domain located at x=-0.5m, the outflow boundary at x=1m and the farfield boundary at y=1m. All calculations are carried out with cfl=0.1

This test case is used to assess the effect of the implementation of Characteristic Decomposition on the ability of the compressible code to capture the shock and provide a monotone solution.

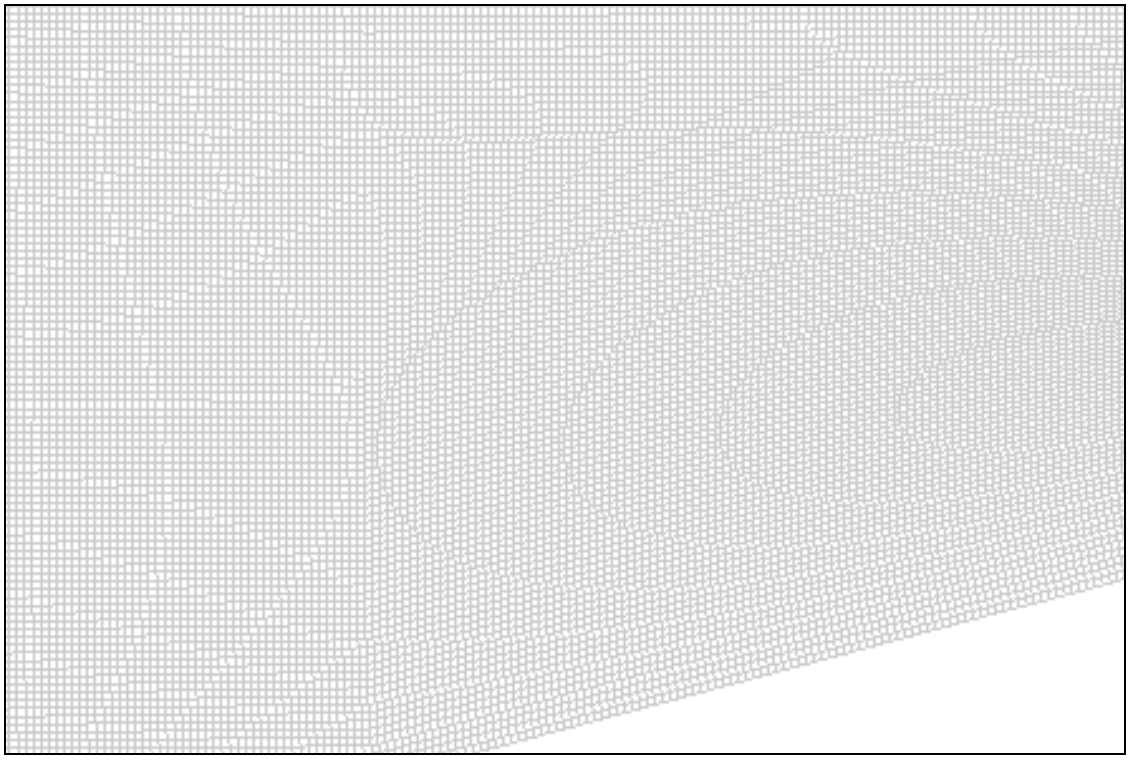

Figure 27 – The computational domain for the Supersonic Wedge Calculation

Figure 28 shows the behaviour of the Barth and Jespersen limiter, the Superbee limiter and Characteristic Decomposition on the change in pressure across the shock.

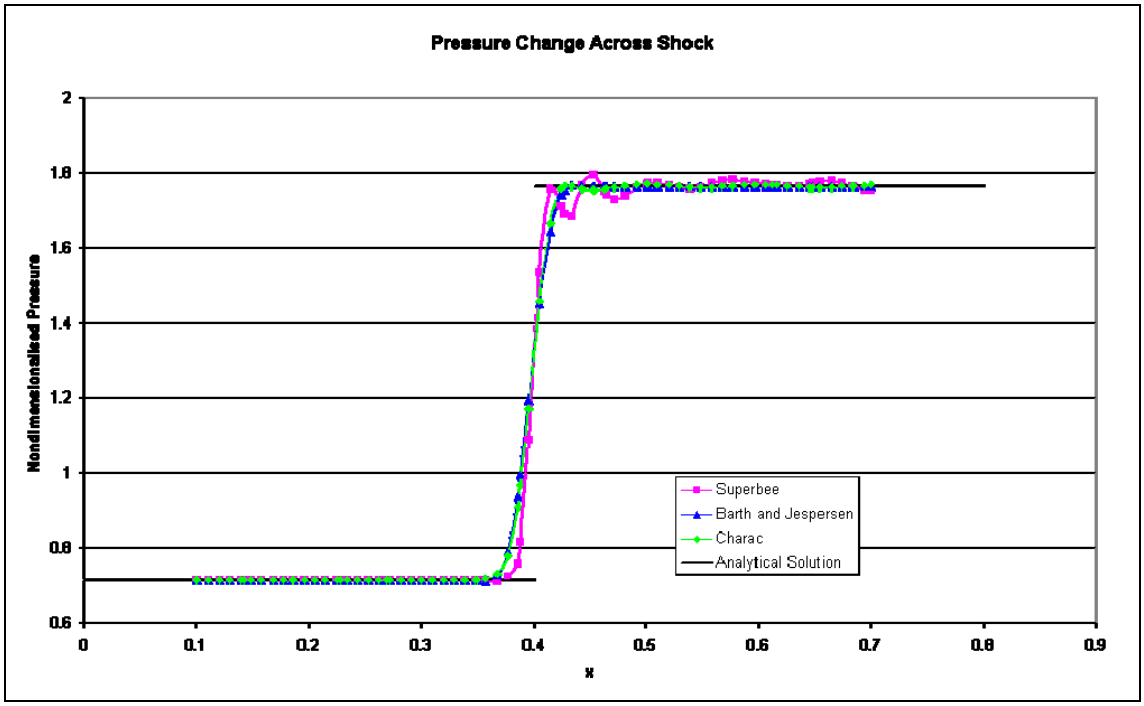

Figure 28 – Pressure change across the shock for the supersonic wedge case – the Superbee limiter fails to provide a monotone solution.

The Characteristic Decomposition and Barth and Jespersen limiters both provide a monotone solution resolving the shock in the same number of grid points where as the Superbee limiter fails to provide a monotone solution for this test case although it resolves the shock in fewer grid points.

Calculations were also carried out on coarser grids in order to provide a grid convergence study. Calculations were performed on grids with densities of 117x77 and 77x51. The range of variation in the coarsness of the grids used for this study were limited by the ability of the scheme to achieve a converged solution for this test case – it was therefore necessary to use varying non integer refinement ratios. The integral average of the Mach number behind the shock was used in order to calculate the GCI index for this grid convergence study the results of which are summarised in the following table. Here r is the grid refinement ratio and epsilon the relative error. The GCI is the Grid Convergence Index and is a measure of the percentage the computed value is away from the value of the asymptotic numerical value.

Grid	r	Average Mach	% error Av Mach	epsilon	GCI
77x51	1.3	1.866843	0.356684672	0.062858	0.242453
117x77	1.5	1.868018	0.294011402	0.27395	0.657481
151x101		1.873149	0.020116081		-

Figure 29 Superbee

Grid	r	Average Mach	% error Av Mach	epsilon	GCI
77x51	1.3	1.866643	0.367359731	0.117282	0.452372
117x77	1.5	1.868835	0.250371762	0.216867	0.520481
151x101		1.872897	0.03357733		-

Figure 30 Barth and Jespersen

Grid	r	Average Mach	% error Av Mach	epsilon	GCI
77x51	1.3	1.865269	0.44070806	0.035891	0.138436
117x77	1.5	1.865939	0.404962626	0.240404	0.576969
151x101		1.870436	0.164955279		-

Figure 31 Characteristic Decomposition

For all schemes the GCI values are low and this indicates that the grids are within the asymptotic range. For the calculation of the average Mach the scheme that provides the most accurate solution is the Superbee scheme followed by the Barth and Jespersen and then Characteristic Decomposition although the percentage errors for all schemes are low.

The effects of the differing schemes on convergence histories are shown in Figure 32.

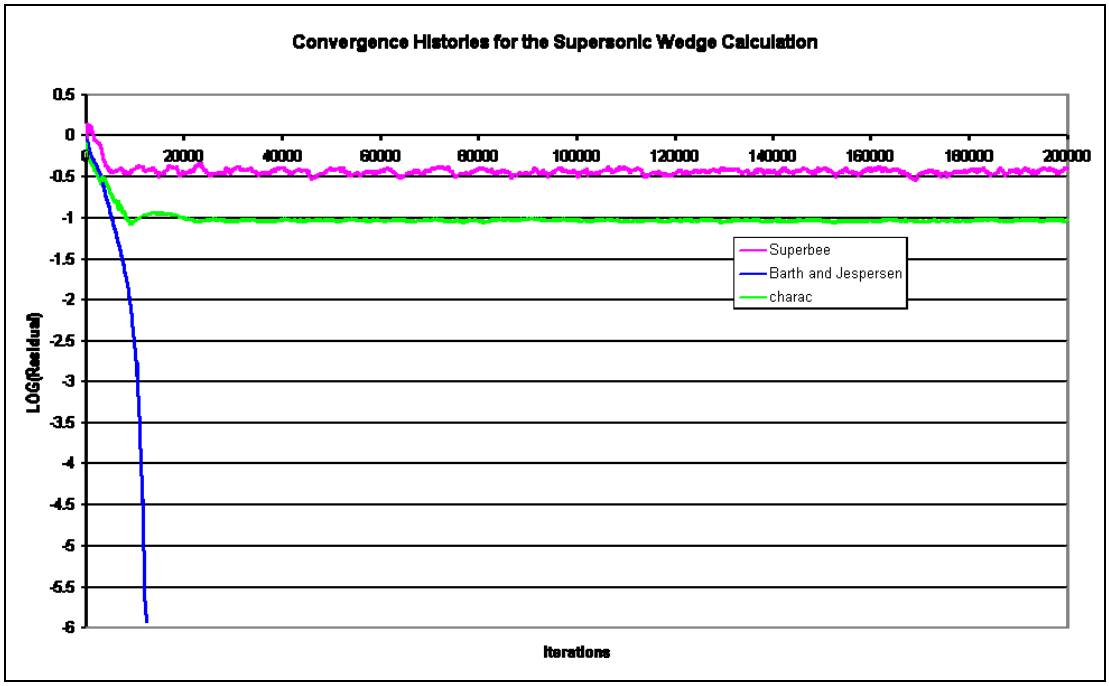

Figure 32 – Convergence histories for the Supersonic Wedge case – convergence stall is evident for both the Superbee and Characteristic Decomposition schemes

The issue of convergence stall is very apparent for both the Superbee limiter and Characteristic Decomposition Schemes for this test case. This is likely to be due to

the activation of the limiters due to small numerical oscillations in the smooth regions of the flow. The Superbee limiter's convergence stalls without achieving even one order reduction in magnitude of the residual and continues to show large oscillations about its final average value whilst Characteristic Decomposition stalls at one order of magnitude reduction.

It can be concluded that although the application of Characteristic Decomposition affects the convergence behaviour of a code as compared to the Barth and Jespersen scheme due to the use of the non-differentiable limiters Minmod and Superbee it does not suffer from the problems achieving a monotone solution in the same way as the Superbee limiter. The effect of the application of Characteristic Decomposition on the Grid Convergence behaviour of the code is such it can be assumed that if grids are in the Asymptotic range for the Barth and Jespersen scheme they will also be likely to be for the Characteristic Decomposition Scheme.

Calculation of the flow over a laminar flat plate

The following Figures 33 and 34 compare the performance of Characteristic Decomposition and the Barth and Jespersen and Superbee limiters for the laminar flat plate test case.

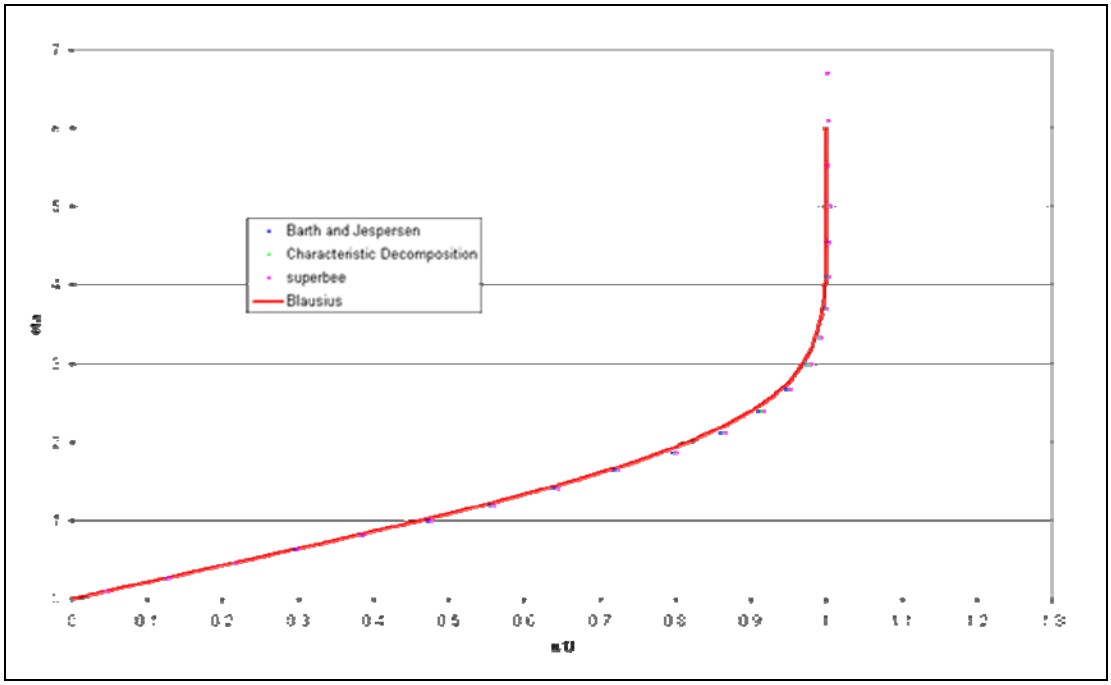

Figure 33– Comparison of the Barth and Jespersen, Superbee and Characteristic Decomposition schemes to the Blausius solution for the streamwise components of velocity, all the calculations come close to the analytic solution

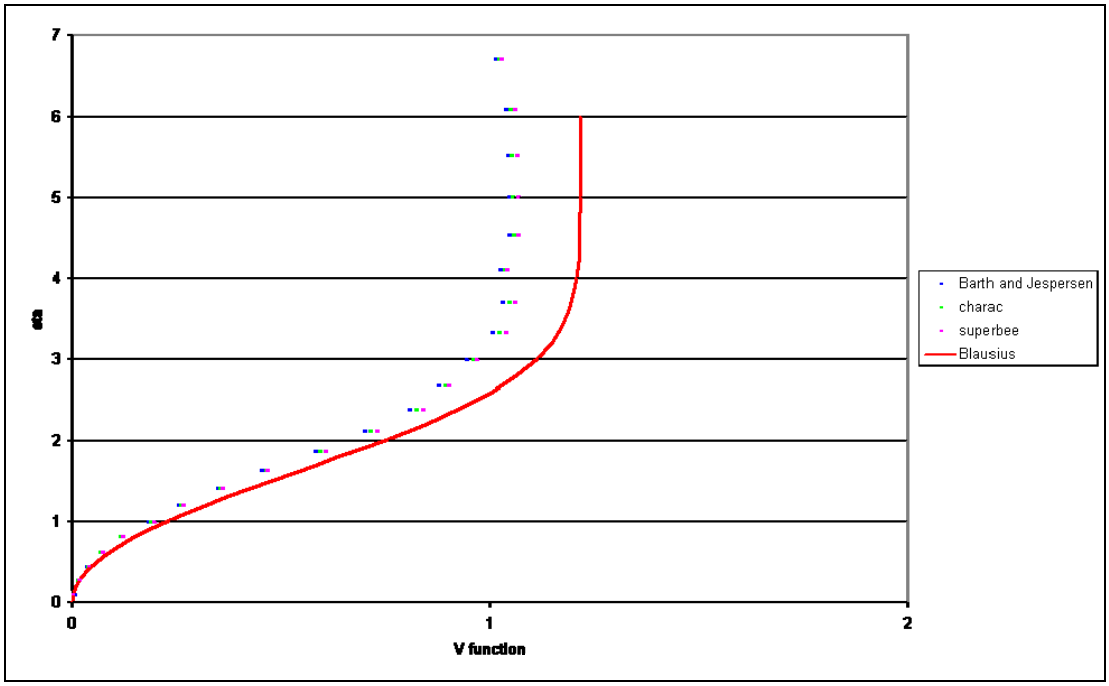

Figure 34- Comparison of the Barth and Jespersen, Superbee and Characteristic Decomposition schemes to the Blausius solution for the transverse components of velocity

There is very little variation between the solutions obtained using each of these methods and it can be concluded that the application of Characteristic Decomposition has little effect on the accuracy of the viscous terms in the code.

Figure 35 shows the convergence histories for these calculations and it can be seen that the convergence behaviour is very similar in all three cases but the Barth and Jespersen limiter levels out at one order of magnitude less than the Superbee limiter and Characteristic Decomposition.

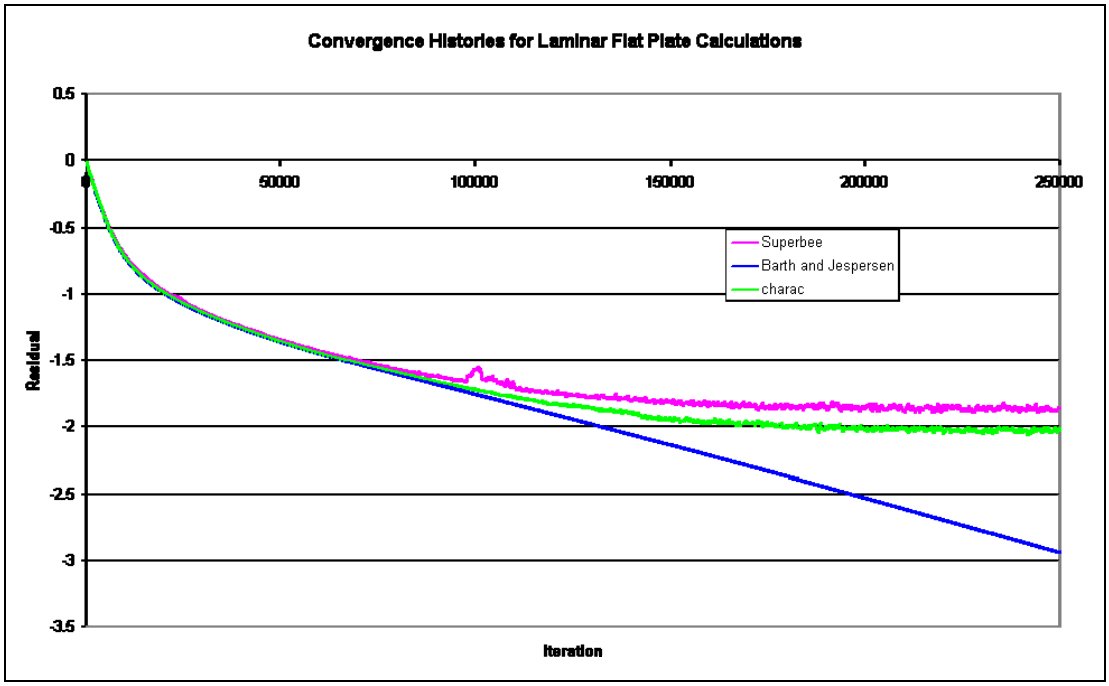

Figure 35– Convergence histories for the Laminar Flat Plate case – convergence stall is evident for both the Superbee and Characteristic Decomposition schemes

Calculation of the Laminar Unsteady flow over a Circular Cylinder –

The results obtained for the calculation of the Strouhal number for the laminar flow over a circular cylinder test case were unchanged at S_t=0.146 for both the unstructured and structured Characteristic Decomposition calculations and the unstructured Superbee calculation. For the Structured Superbee calculation the calculated Strouhal number rose to S_t=0.15 indicating that the compressive nature of the Superbee limiter is lowering the effective viscosity of the numerical scheme and therefore raising the effective Reynolds number.

The following figures show the vorticity shed form the laminar cylinder at 300 timesteps for the Barth and Jespersen, Superbee and Characteristic Decomposition schemes for the unstructured and structured grids.

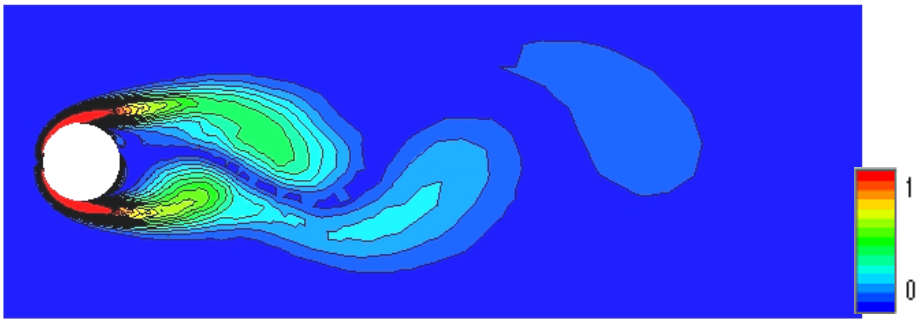

a.

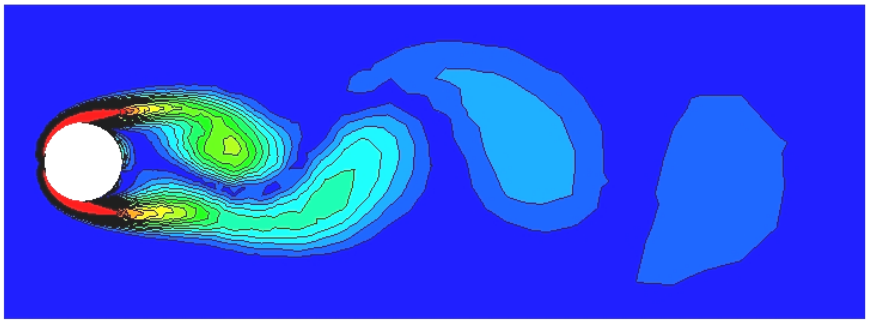

b

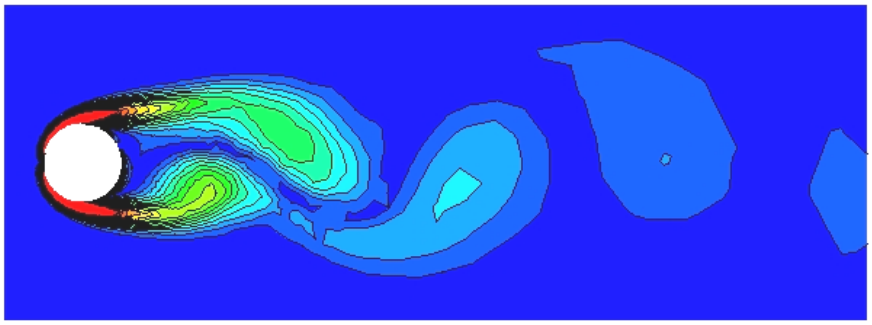

c

Figure 36- Plots for Unstructured Grids of Vorticity Magnitude non-dimensionalised by the physical freestream speed of sound. a=Barth and Jespersen b=Superbee c=Characteristic Decomposition

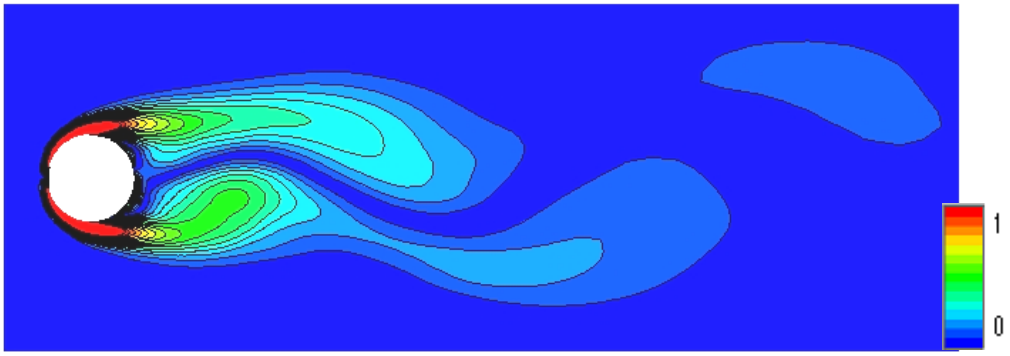

a

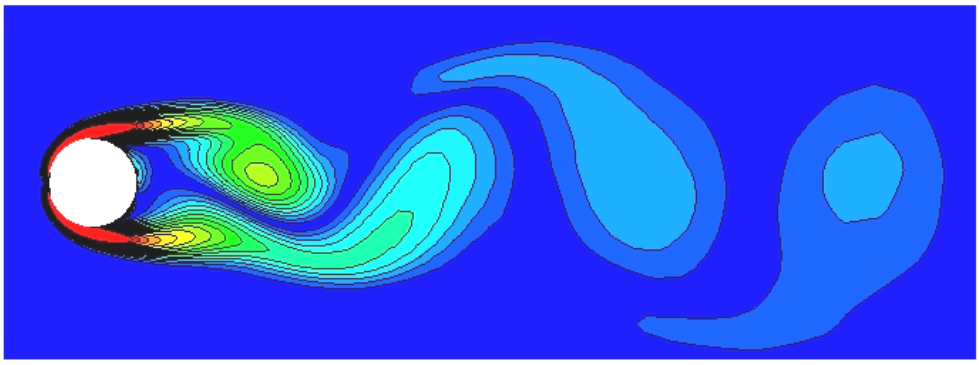

b

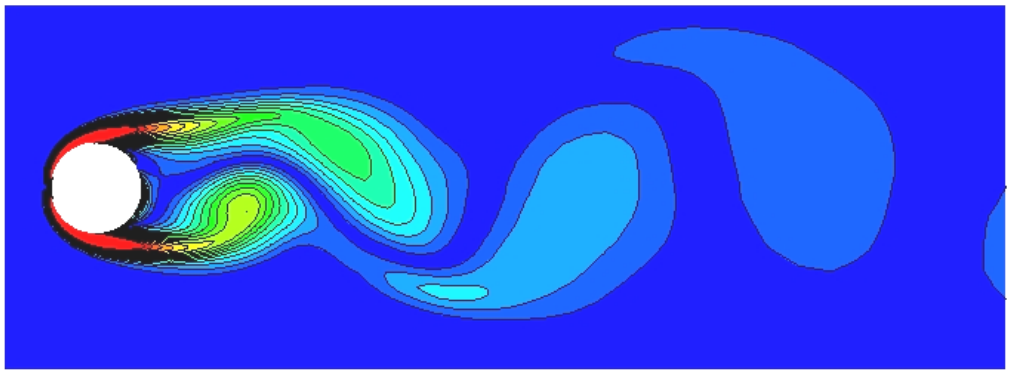

c

Figure 37 - Plots for Structured Grids of Vorticity Magnitude non-dimensionalised by the physical freestream speed of sound. a=Barth and Jespersen b=Superbee c=Characteristic Decomposition

For both the structured and unstructured grid calculations the Superbee and Characteristic Decomposition schemes are visibly convecting the shed vortices further down stream than the Barth and Jespersen scheme. It appears that Characteristic Decomposition performs best for vorticity magnitude conservation for the unstructured grid and that Superbee performs best for the structured grid. It is difficult to draw a definite conclusion about the vorticity conserving nature of the different schemes from this test case as the onset of vortex shedding happens at different times in the physical time steps of the calculations for different cases and so the positions of the shed vortices at any one physical time are not in synch across the different calculations.

Calculation of an Inviscid Convecting Vortex

This test case involves the calculation of a two dimensional inviscid convecting vortex. An exact solution derived assuming a Gaussian pressure distribution and periodic boundary conditions is given in reference[15] by the following equations.

$$u = M\cos\alpha + c_1[y - y_0 - Mt\sin\alpha]\exp[-c_2([x - x_0 - Mt\cos\alpha]^2 + [y - y_0 - Mt\sin\alpha]^2)] \quad (8.1)$$

$$v = M\sin\alpha - c_1[x - x_0 - Mt\cos\alpha]\exp[-c_2([x - x_0 - Mt\cos\alpha]^2 + [y - y_0 - Mt\sin\alpha]^2)]$$

$$P = P_{\inf} - 0.25\rho\frac{c_1^{\,2}}{c_2}(\exp[-2c_2([x - x_0 - Mt\cos\alpha]^2 + [y - y_0 - Mt\sin\alpha]^2)] - 1)$$

where α is the flow angle M the mach number and c_1 and c_2 are perturbation coefficients

The computational domain for all calculations extends from x=(-40,40)m y=(-40,40)m and the centre of the vorticity perturbation is at x_0=-20m y_0=0m. A structured grid with grid density in 80x80 and an unstructured grid with boundary density 40x40 giving 1500 cells are used as the baseline grids. These grids are shown in figures 38 and 39. All computations are run with cfl=0.3.

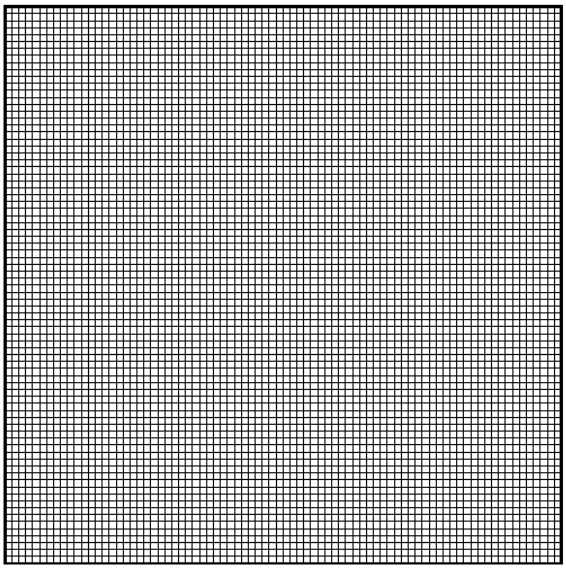

Figure 38 – Computational Domain for Structured Grid Calculation

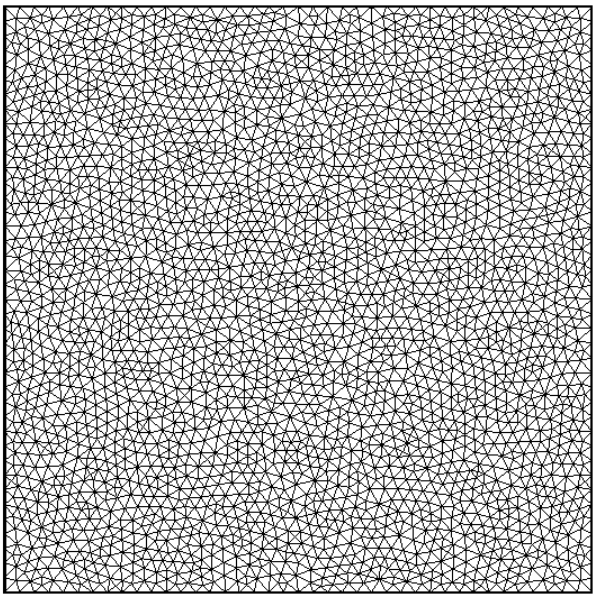

Figure 39- Computational Domain for Unstructured Grid Calculation

A compressible test case is set up with M=0.5, c_1=-0.04 and c_2=0.02 the timestep is dt=0.0004703 and the calculation is run for 500 physical time steps in order to convect the vortex 40m.

A test case for the incompressible code is set up with M=0.2, with a weaker vortex given by c_1=-0.0375 and c_2=0.016 the timestep is dt=0.001758 and the calculation is run for 500 physical time steps in order to convect the vortex 40m. Due to the slower speed of propagation of the vortex and it's weaker strength this test is a greater challenge in terms of vorticity conservation for a code.

The initial vorticity distribution should convect unchanged with the freestream velocity. The results of these calculations are analysed by looking at several measures of vorticity conservation in the domain. Firstly the distribution of vorticity magnitude is considered to indicate change in the vortex shape and magnitude. The decline in maximum vorticity magnitude is plotted against the time step to give an indication of the rate of dissipation of the vorticity within the vortex. The enstrophy given by

$$E_{ns}(U) = \int_S \left|\nabla U\right|^2 dS \qquad (8.2)$$

is integrated over the whole domain and plotted against time step. This is a quantity related to the kinetic energy of the flow and gives an indication of the rate of

dissipation within the computational domain. For an inviscid calculation the enstrophy should remain constant due to the dissipationless nature of inviscid flow. It is therefore a useful measure of the numerical dissipation as it indicates whether a particular numerical scheme is dissipating or is raising the total kinetic energy contained within the domain.

Results for the compressible convecting vortex case.

Structured Grid –

The decline in peak vorticity for the structured vortex case for Characteristic Decomposition, the Barth and Jespersen and Superbee limiter is shown in the figure 40.

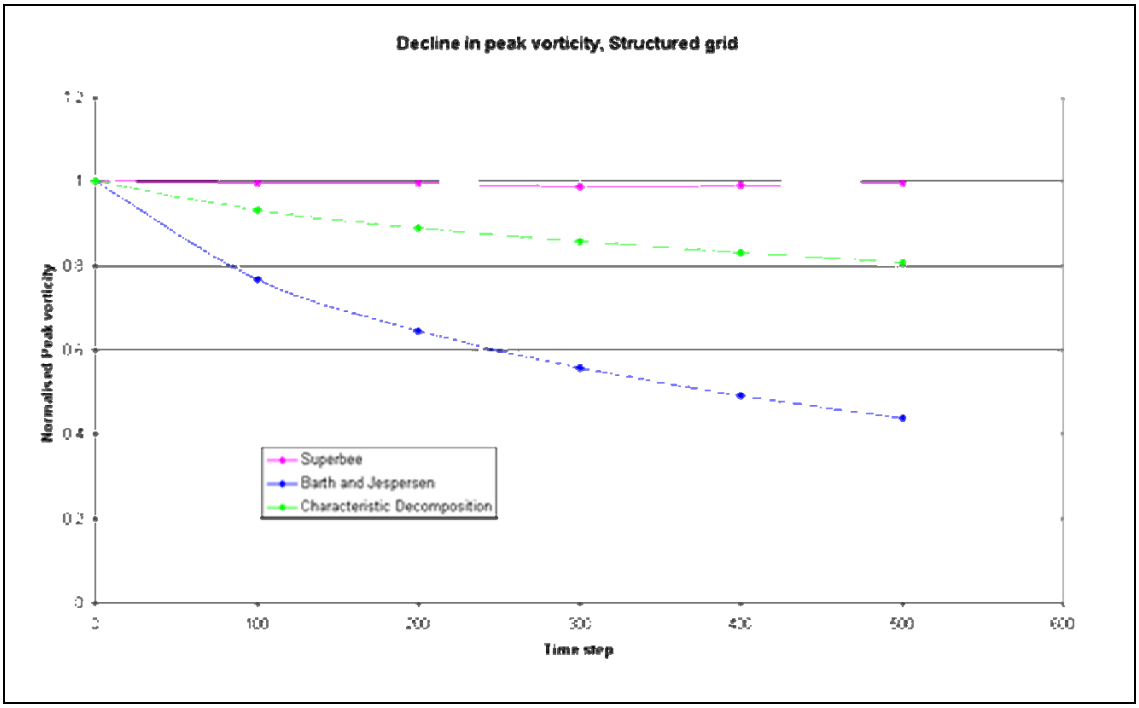

Figure 40 – Decline in Peak Vorticity for Structured Grid calculation. Characteristic decomposition shows a marked improvement over the Barth and Jespersen limiter and Superbee maintaines peak vorticity close to unity.

It can be seen that the peak vorticity is conserved for the Superbee scheme and that the Characteristic Decomposition scheme maintains approximately twice the vorticity magnitude of the Barth and Jespersen scheme.

Figure 41 shows the change in Enstrophy in the computational domain for each of the above calculations.

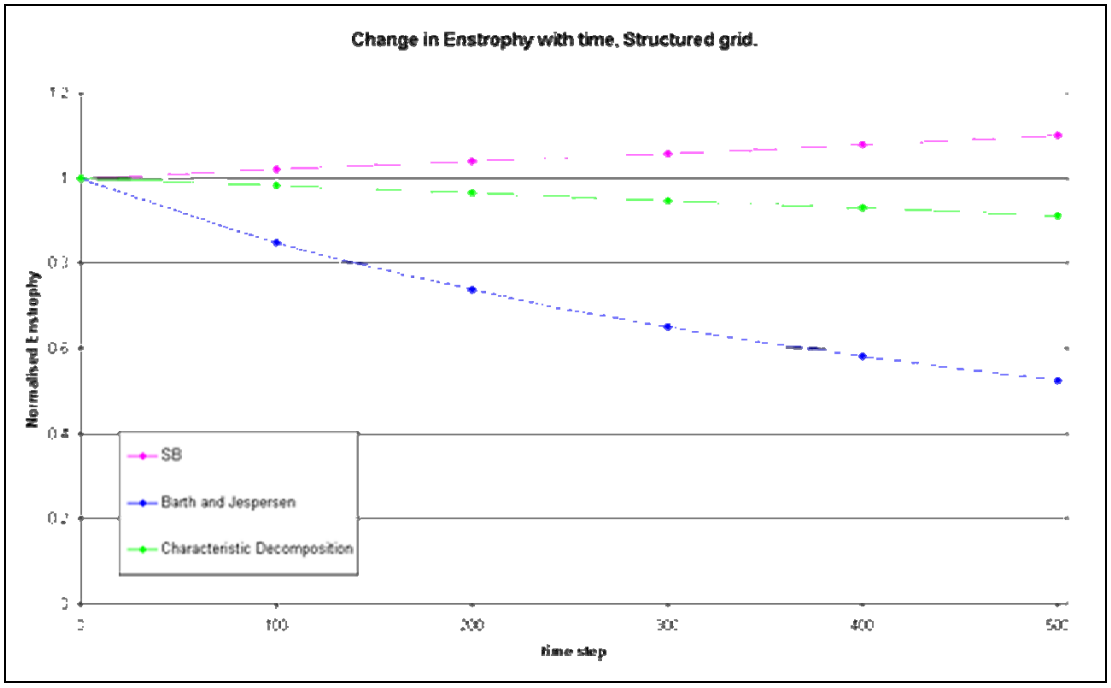

Figure 41– Change in Enstrophy for Structured Grid calculation. Characteristic decomposition shows a marked improvement over the Barth and Jespersen limiter when maintaining Enstrophy. Superbee is generating spurious enstrophy with the value rising above unity.

It can be seen that although the Superbee limiter preserves the peak vorticity of the vortex the scheme is increasing the Enstrophy within the computational domain with time. This is evident from looking at the following figure 42 which depicts vorticity magnitude at 500 timesteps compared to the initial vortex which should convect unchanged. It can be seen that the Superbee scheme is creating spurious vorticity and that the shape of the vortex has become distorted. Vorticity conservation for Characteristic Decomposition is much improved over the baseline Barth and Jespersen scheme and does not suffer from the generation of spurious vorticity and vortex distortion in the same way as the Superbee scheme.

The calculation was also run with the timestep reduced by 50% and the difference in the computed values of peak vorticity differed by 0.11482% from the original calculation indicating the calculation is run with a sufficiently small time step.

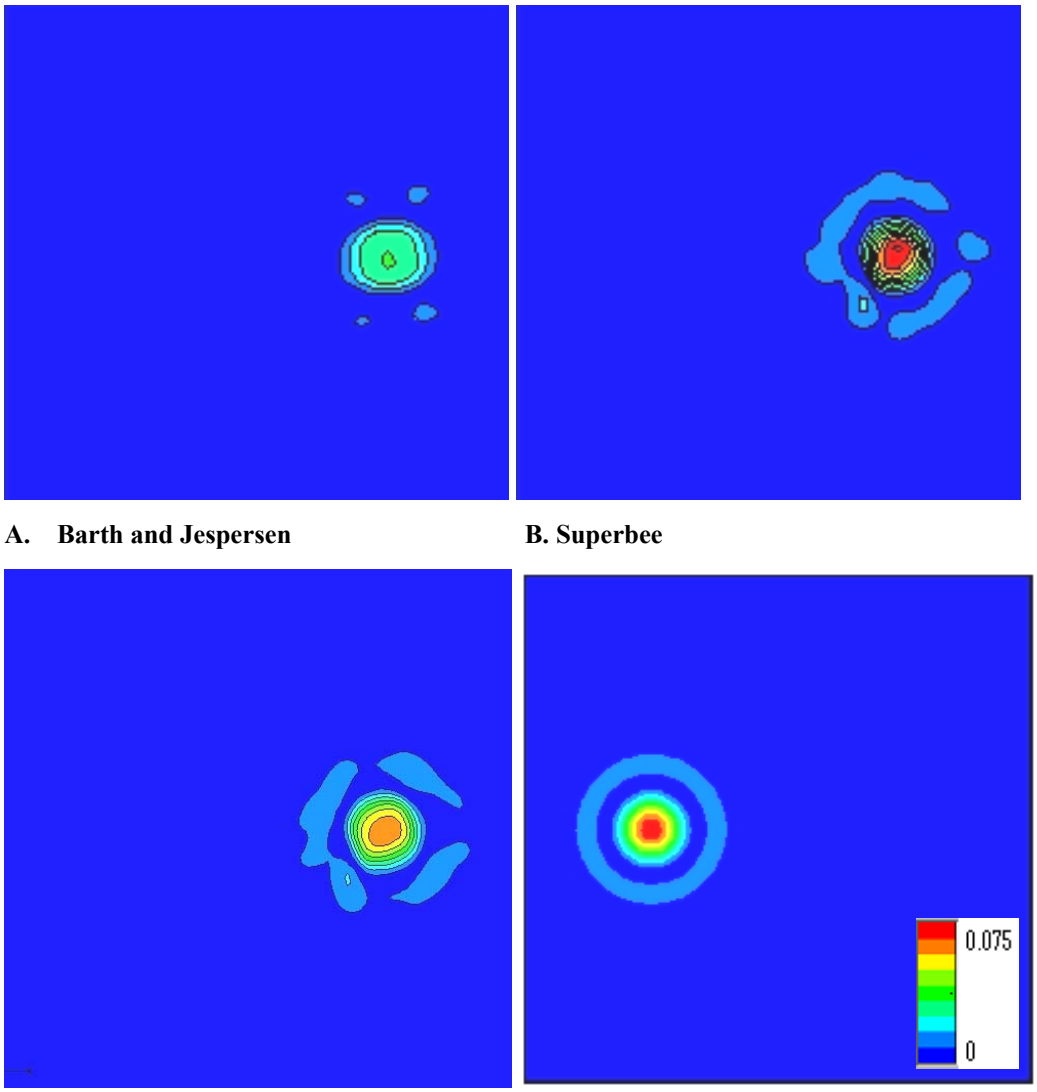

A. Barth and Jespersen **B. Superbee**

C. Characteristic Decomposition **D, initial vorticity distribution**

Figure 42 - Plots of vorticity magnitude calculated from nondimensionalised velocity distribution for the structured grid calculation. The generation of spurious vorticity by the Superbee limiter is evident whilst the Charateristic Decomposition scheme improves vorticity conservation without suffering from this problem.

Unstructured Grid –

The decline in peak vorticity for the unstructured vortex case for Characteristic Decomposition, the Barth and Jespersen and Superbee limiter is shown in the figure 43.

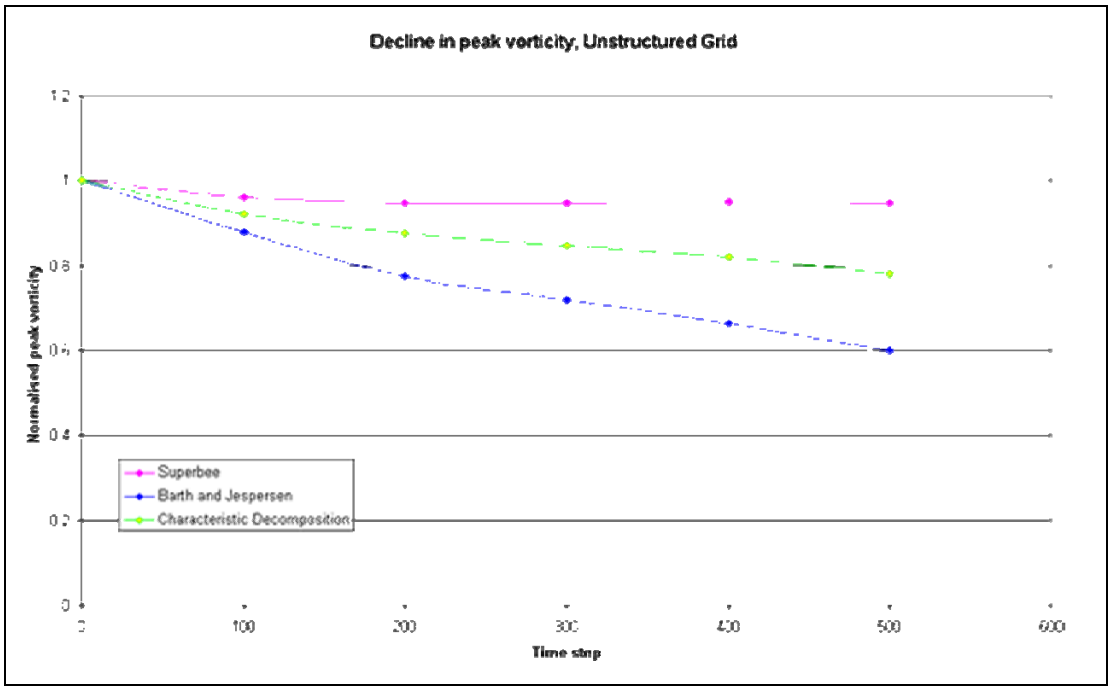

Figure 43– Decline in Peak Vorticity for Unstructured Grid calculation. Characteristic decomposition shows a marked improvement over the Barth and Jespersen limiter with Superbee showing the greatest conservation of peak vorticity

As with the structured case Superbee maintains the peak vorticity magnitude the best and Characteristic Decomposition provides an improvement over Barth and Jespersen. Figure 44 shows the change in Enstrophy in the computational domain for each of the above calculations.

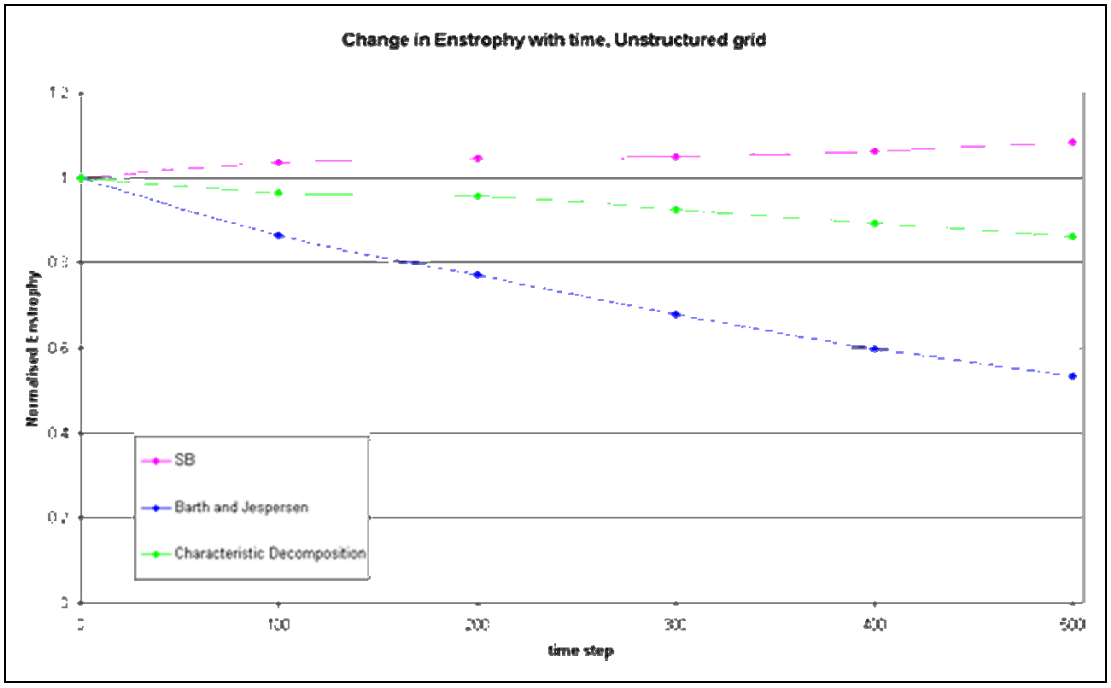

Figure 44– Change in Enstrophy for Unstructured Grid calculation. Characteristic decomposition shows a marked improvement over the Barth and Jespersen limiter when maintaining Enstrophy. Superbee is generating spurious enstrophy with the value rising above unity.

Again it can be seen that Superbee is increasing the enstrophy in the domain with time. The effect of this is less evident in the distribution of vorticity magnitude than in the structured grid calculation. The following figure 45 depicts vorticity magnitude at 500 time steps compared to the initial vortex which should convect unchanged. Vorticity conservation for Characteristic Decomposition is much improved over the baseline Barth and Jespersen scheme and does not suffer problem of increasing enstrophy in the domain.

The calculation was also run with the timestep reduced by 50% and the difference in the computed values of peak vorticity differed by 0.079859% from the original calculation indicating the calculation is run with a sufficiently small time step.

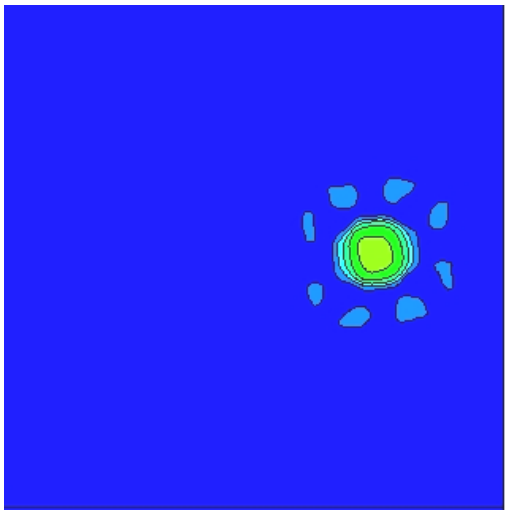

A. Barth and Jespersen

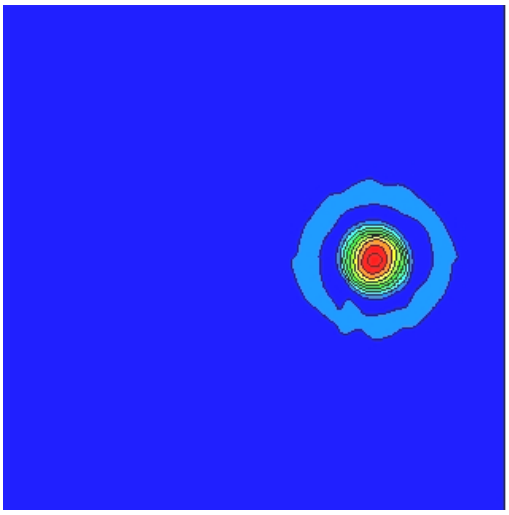

B. Superbee

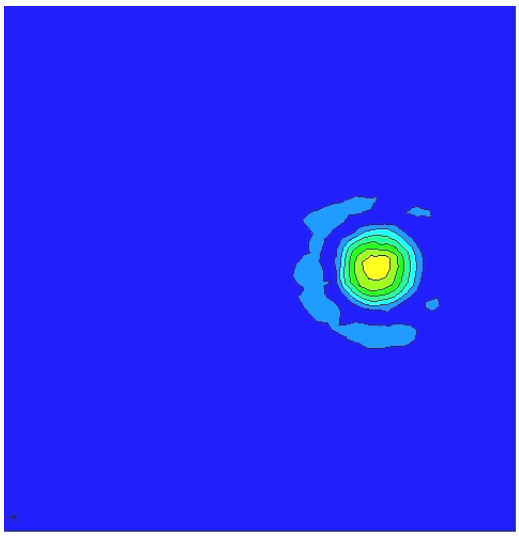

C. Characteristic Decomposition

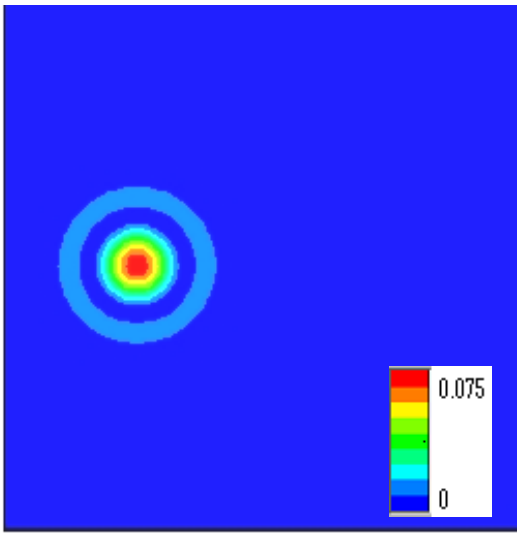

D, initial vorticity distribution

Figure 45- Plots of vorticity magnitude calculated from nondimensionalised velocity distribution for the unstructured grid calculation. The generation of spurious vorticity by the Superbee limiter is evident whilst the Charateristic Decomposition scheme improves vorticity conservation without suffering from this problem.

Results for the artificial compressibility convecting vortex case.

Structured Grid –

The decline in peak vorticity for the structured vortex case for Characteristic Decomposition, the Barth and Jespersen and Superbee limiter is shown in Figure 46.

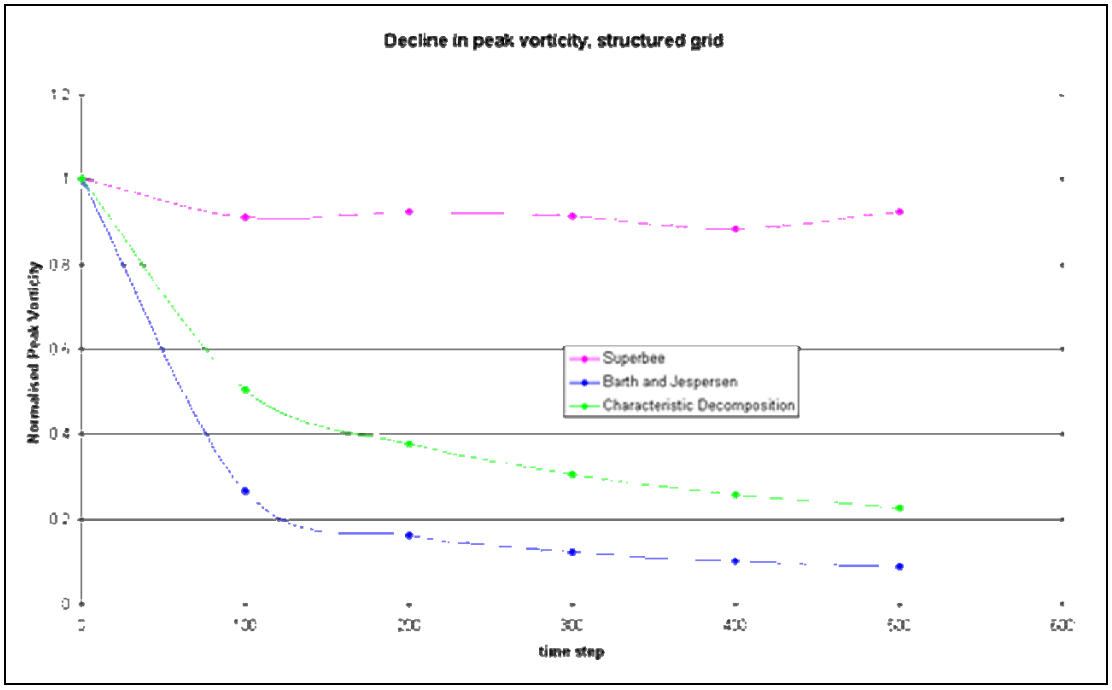

Figure 46 – Decline in Peak Vorticity for Structured Grid calculation. Characteristic decomposition shows an improvement over the Barth and Jespersen limiter with Superbee showing the greatest conservation of peak vorticity

Here the Superbee limiter again conserves the peak vorticity the best with the Characteristic Decomposition providing a significant improvement over the baseline Barth and Jespersen limiter. Figure 47 shows the change in enstrophy in the domain with this calculation.

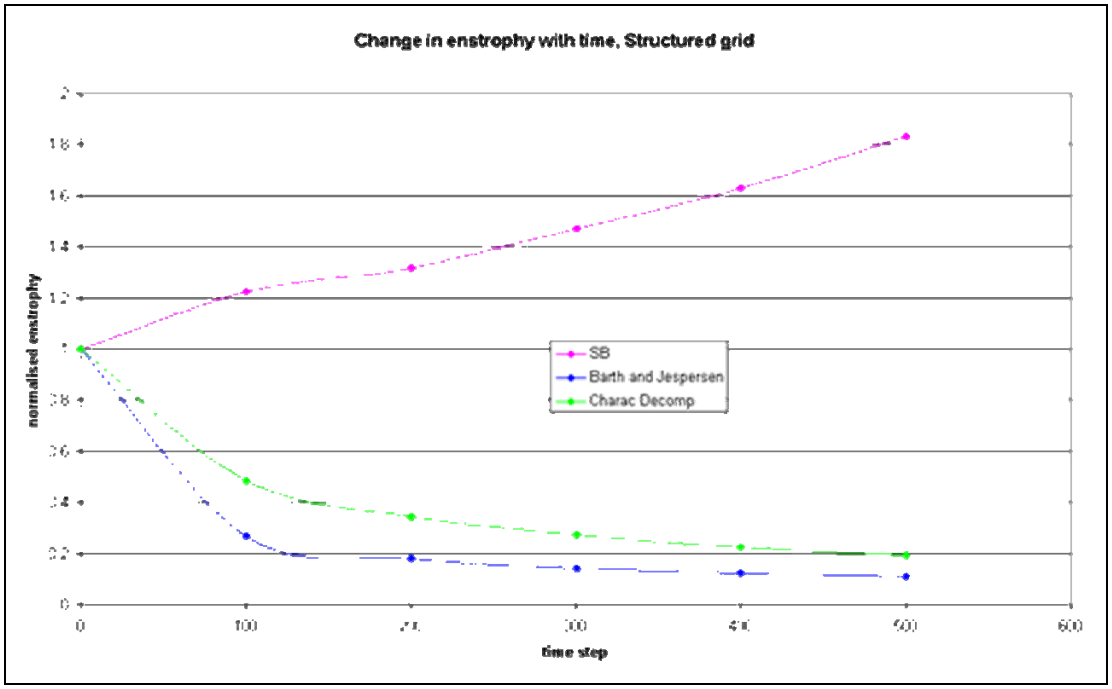

Figure 47 – Change in Enstrophy for Structured Grid calculation. Characteristic decomposition shows an improvement over the Barth and Jespersen limiter when maintaining Enstrophy. Superbee is generating spurious enstrophy with the value rising above unity.

Again in this case it can be seen that the Superbee limiter increases the enstrophy in the domain with time. Figure 48 shows the distribution of vorticity magnitude for this case. Here the problem associated with generation of spurious vorticity and vortex distortion associated with the raise in enstrophy in the domain is very evident for the Superbee calculation. Characteristic Decomposition again provides an improvement over the Barth and Jespersen Limiter.

The calculation was also run with the timestep reduced by 50% and the difference in the computed values of peak vorticity differed by 0.130571% from the original calculation indicating the calculation is run with a sufficiently small time step.

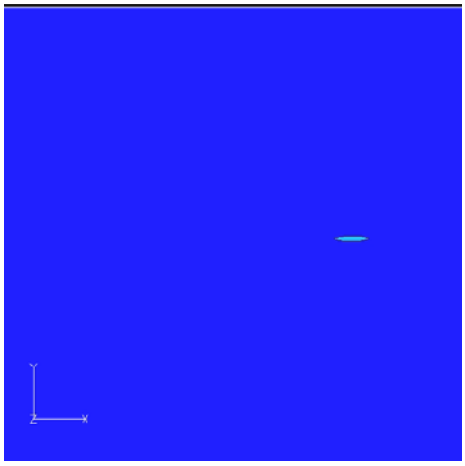

A. Barth and Jespersen

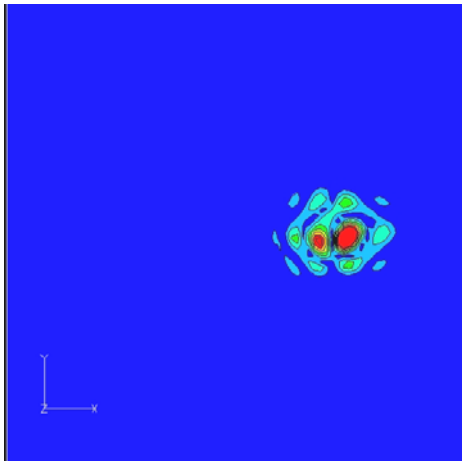

B. Superbee

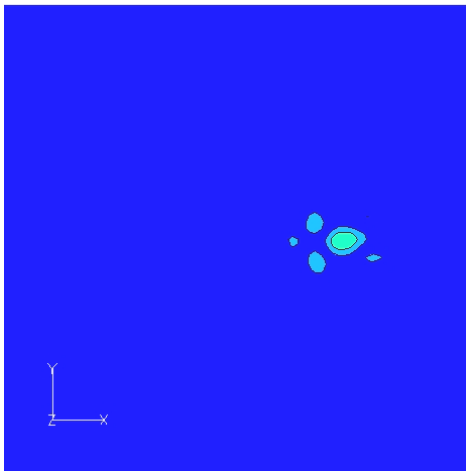

C. Characteristic Decomposition

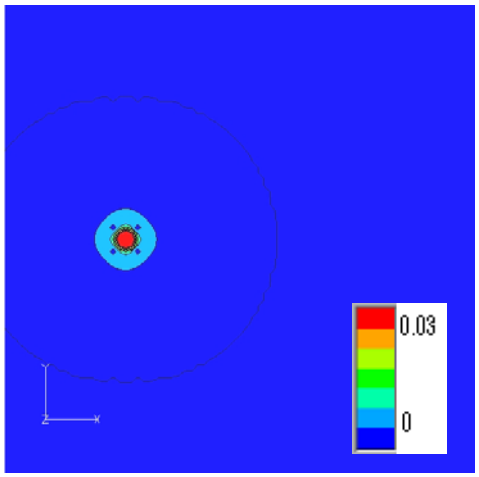

D, initial vorticity distribution

Figure 48 - Plots of vorticity magnitude calculated from nondimensionalised velocity distribution for the structured grid calculation. The generation of spurious vorticity by the Superbee limiter is evident whilst the Charateristic Decomposition scheme improves vorticity conservation without suffering from this problem.

Unstructured Grid –

The decline in peak vorticity for the unstructured vortex case for Characteristic Decomposition, the Barth and Jespersen and Superbee limiter is shown in Figure 49.

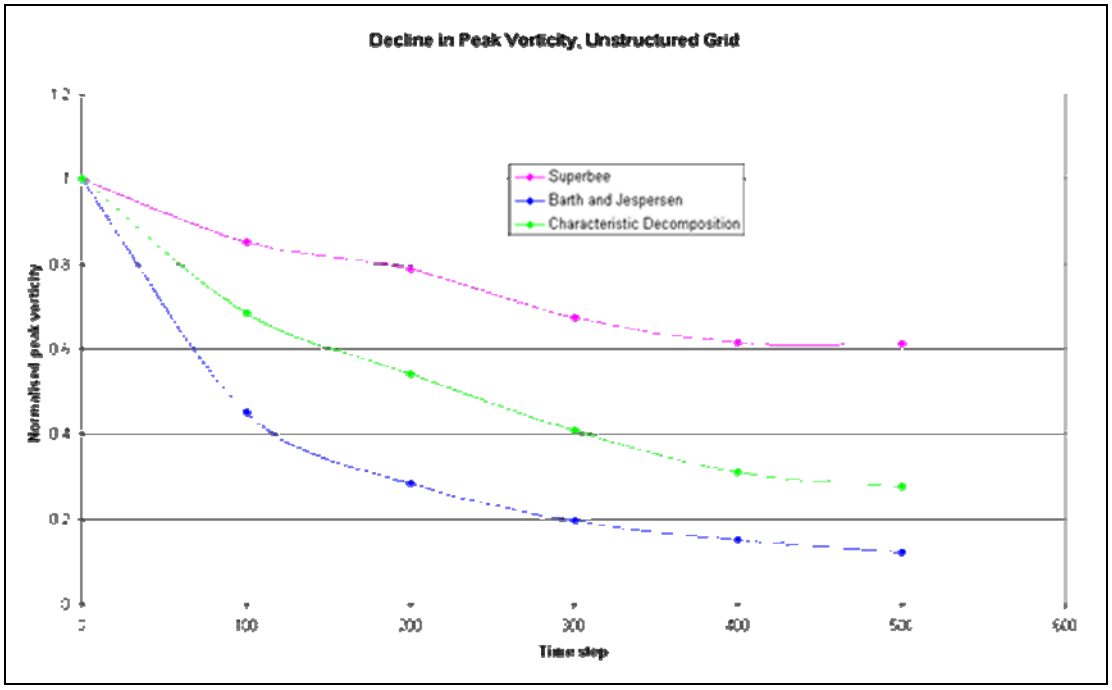

Figure 49 – Decline in Peak Vorticity for Unstructured Grid calculation. Characteristic decomposition shows an improvement over the Barth and Jespersen limiter with Superbee showing the greatest conservation of peak vorticity

Here the Superbee limiter again conserves the peak vorticity the best with the Characteristic Decomposition providing a significant improvement over the baseline Barth and Jespersen limiter. Figure 50 shows the change in enstrophy in the domain with this calculation.

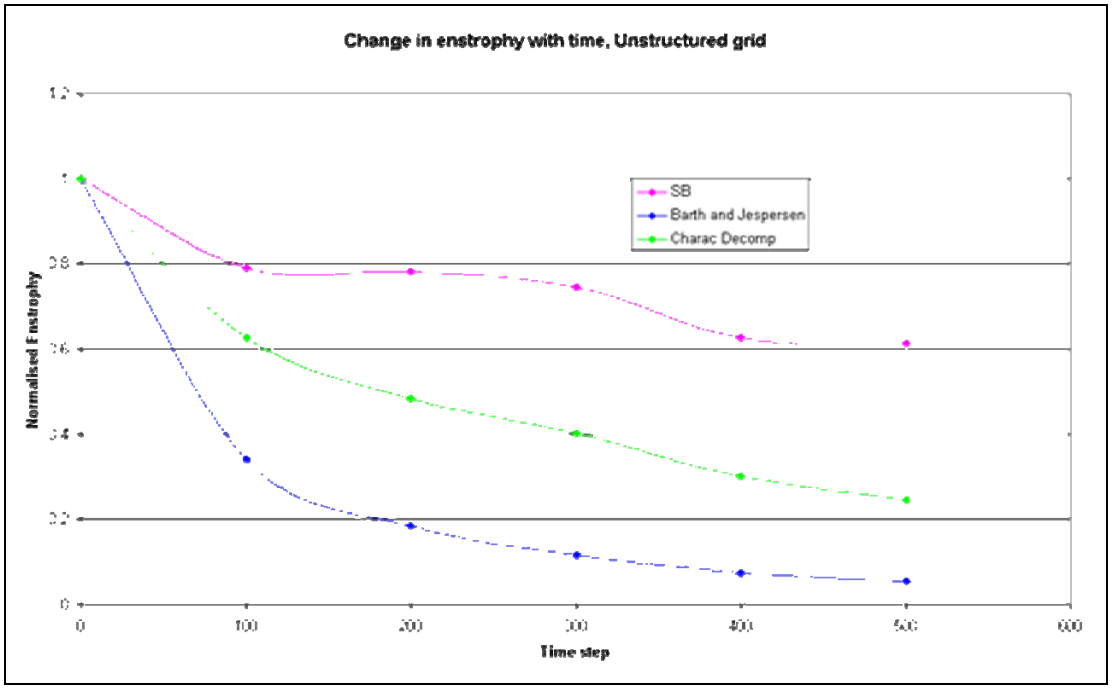

Figure 50– Change in Enstrophy for Unstructured Grid calculation. Characteristic decomposition shows an improvement over the Barth and Jespersen limiter with Superbee showing the greatest conservation of enstrophy.

Here none of the calculations are increasing the enstrophy with time. Figure 51 shows the distribution of vorticity magnitude for this case. In this case the vorticity dissipation is so strong in the Barth and Jespersen case that timestep = 500 the vortex is no longer visible in the domain. The Superbee limiter provides the greatest vorticity conservation and in this case where the numerical dissipation is strong the Superbee limiter does not seem to be affected by the same problem of generation of spurious vorticity and gain in enstrophy in the computational domain.

The calculation was also run with the timestep reduced by 50% and the difference in the computed values of peak vorticity differed by 0.120108% from the original calculation indicating the calculation is run with a sufficiently small time step.

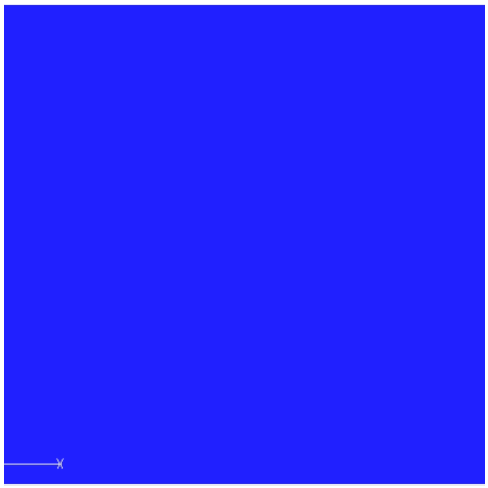

A. Barth and Jespersen

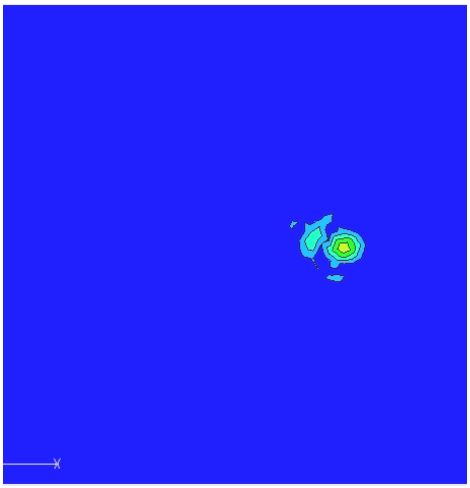

B. Superbee

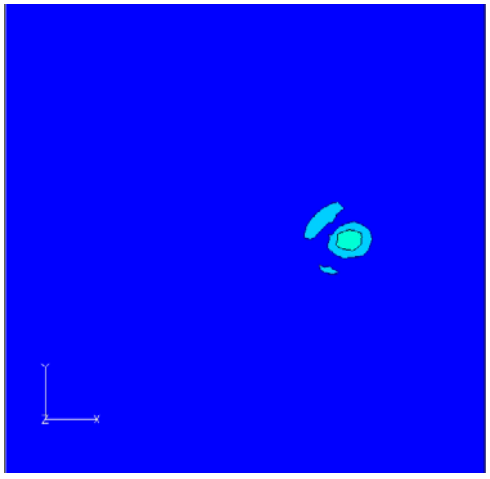

C. Characteristic Decomposition

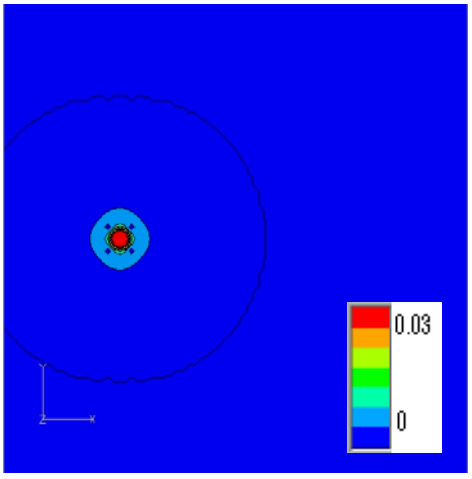

D, initial vorticity distribution

Figure 51- Plots of vorticity magnitude calculated from nondimensionalised velocity distribution for the unstructured grid calculation. The generation of spurious vorticity is not seen in any of the schemes .

9. The Trouble with Slope Limiters Applied to Irregular and Unstructured Grids

The method of Characteristic Decomposition shows improvements over the baseline schemes for both structured and unstructured grids. However there are a number of known issues associated with the use of slope limiters on irregular and unstructured grids which should be addressed in order to gain maximum benefit from this method when applied to these grids.

In the MUSCL approach to creating higher order methods the piece-wise constant data in first order Godunov type methods is replaced by interpolated values of the data computed using approximations of the gradients in a cell. According to Godunov's theorem monotone schemes are at most first-order accurate which means that for all higher order methods spurious oscillations will occur in the solution variables in the vicinity of high gradients of these variables. Slope limiter methods overcome this problem by using some measure of the gradients in the solution to revert to first order methods in regions of high gradients therefore removing the spurious oscillations.

A comprehensive discussion of the theory of slope limiter methods can be found in Toro[3]. The relevant points as regards to slope limiter methods are summarised here.

In Van Leer's series of papers 'Towards the Ultimate Conservative Difference Scheme'[38] he stated three rules of slope limiting that are necessary in order to prevent the onset of spurious oscillations

1. The interpolated variables will not take values beyond the average values in neighbouring cells.
2. If the cell average is an extremum with respect to neighbouring cell averages the slope must be set to zero in that cell.
3. If the sign of the slope differs from that in neighbouring cells the slope must be set to zero.

These rules will not guarantee the complete suppression of spurious oscillations when applied to nonlinear equations but give an upper bound on the gradients that may produce monotone solutions. The ability of these upper bounds to be sufficient to produce monotone solutions also has some dependence on the cfl number. Larger cfl numbers provide less numerical damping and can thus require stronger limiting. When applying characteristic decomposition the genuinely non-linear fields are associated with the λ=u-a and λ=u+a eigenvalues and so for some values of the cfl number, cfl=(Δt/Δx)a, stronger limiting may be necessary with these fields in order to produce monotone solutions. The linearly degenerate fields are associated with the λ=u eigenvalues of the system and so the upper bounds given by the above rules are less likely to need further restriction to achieve monotone solutions.

The formulation of slope limiters, such as Superbee and Minmod, is based in a scalar one dimensional regular structured grid framework. Toro[3] section 13.8.4 gives a description of how the Superbee and Minmod slope limiters are obtained giving

$$q_{i+\frac{1}{2}} = q_i + \tfrac{1}{2}\overline{\Delta_i} \qquad (9.1)$$
$$q_{i-\frac{1}{2}} = q_i - \tfrac{1}{2}\overline{\Delta_i}$$

$$\overline{\Delta_i} = \begin{cases} \max[0, \min(\beta\Delta_{i-\frac{1}{2}}, \Delta_{i+\frac{1}{2}}), \min(\Delta_{i-\frac{1}{2}}, \beta\Delta_{i+\frac{1}{2}})], & \Delta_{i+\frac{1}{2}} \rangle 0 \\ \min[0, \max(\beta\Delta_{i-\frac{1}{2}}, \Delta_{i+\frac{1}{2}}), \max(\Delta_{i-\frac{1}{2}}, \beta\Delta_{i+\frac{1}{2}})], & \Delta_{i+\frac{1}{2}} \langle 0 \end{cases}$$

Where $\beta = 1$ gives Minmod and $\beta = 2$ gives Superbee

and

$\Delta_{i-\frac{1}{2}} = q_i - q_{i-1}$ and $\Delta_{i+\frac{1}{2}} = q_{i+1} - q_i$

The slope limiting can also be written in terms of a function r given by

$$r = \Delta_{i+\frac{1}{2}} / \Delta_{i-\frac{1}{2}} \tag{9.2}$$

$$q_{i+\frac{1}{2}} = q_i + \tfrac{1}{2}\Psi(r)\Delta_{i-\frac{1}{2}}$$

$$q_{i-\frac{1}{2}} = q_i - \tfrac{1}{2}\Psi(\frac{1}{r})\Delta_{i+\frac{1}{2}}$$

$$\Psi(r) = \max[0, \min(\beta r, 1), \min(r, \beta)] \tag{9.4}$$

here the function obeys a symmetry condition such that

$$\frac{\Psi(r)}{r} = \Psi(\frac{1}{r}) \tag{9.5}$$

For one dimensional structured grid formulations it is usual to write the expressions for $q_{i+\frac{1}{2}}$ and $q_{i-\frac{1}{2}}$ in terms of a different function $\Phi(r)$ and a single limited gradient Δ_i
such that

$$q_{i+\frac{1}{2}} = q_i + \tfrac{1}{2}\Phi(r)\Delta_i \tag{9.6}$$

$$q_{i-\frac{1}{2}} = q_i - \tfrac{1}{2}\Phi(\frac{1}{r})\Delta_i$$

where $\Delta_i = (q_{i+1} - q_{i-1})/2$

$\Phi(r)$ then obeys a different symmetry condition such that $\Phi(r) = \Phi(\frac{1}{r})$ (9.7)

For multidimensional structured grids additional space dimensions can be treated seperately in the same manner. This formulation is less useful when dealing with an unstructured multidimensional grid where the cells representing i+1 and i-1 are not easily identified.

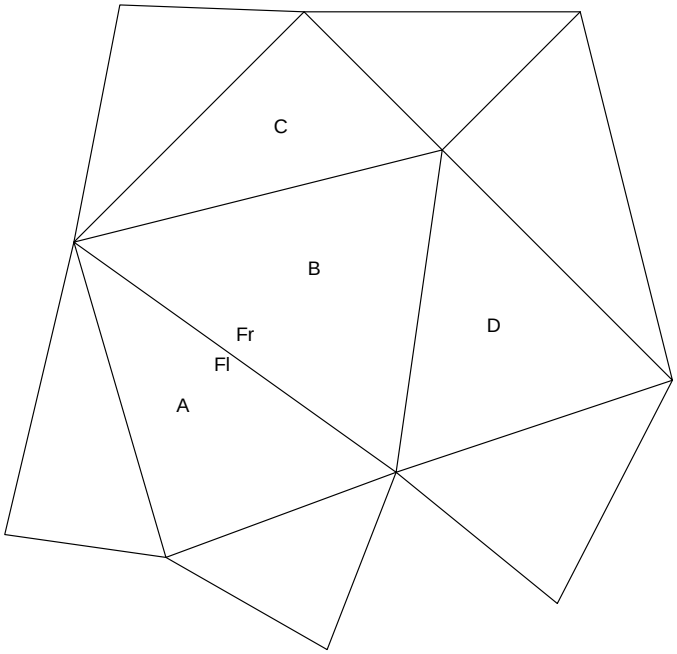

Figure 52 – A typical unstructured cell (B) and it's neighbours (A,Cand D)

Figure 52 shows an unstructured grid with cell B surrounded by three neighbours A,C and D. Fr and Fl are the left and right sides of the face connecting cells A and B to which the data will be interpolated. Typically for an unstructured grid as shown above cell B will have available the information relating to its surrounding cells. The gradient of the variables in each cell is calculated using a least square or Green-Gauss approximation. The Green-Gauss method is used in the MERLIN solvers. For cell centered schemes the Green-Gauss method integrates around the boundary of the cell and uses Green theorem to estimate the average gradient over that control volume. The least square method solves the values of the gradients which minimise the sum of the differences between neighbouring values and values extrapolated from the point under consideration to the neighbouring locations. The least squares method is not dependent on grid topology and although the neighbouring cells are usually used the stencil can be expanded to include further cells. Unlike the Green-Gauss method the least squares method represents a linear function exactly.

The interpolation from the centre of cell B to the face Fr will therefore be carried out using the following formula.

$$q_{Fr} = q_B + \Psi(r)\vec{r} \bullet \nabla q_B \qquad (9.8)$$

Here $\vec{r}$ is the vector connecting the cell centre to the face centre- making $\vec{r} \bullet \nabla q_B$ the interpolated difference, which is to be limited, in q from the cell centre to the face. This is equivalent to the $\frac{1}{2}\Delta_{i-\frac{1}{2}}$ term in the structured grid formulation. The function $\Psi(r)$ has the same formulation as in the structured grid formulation with r being defined in terms of the information available giving

$$r = \frac{\frac{1}{2}(q_A - q_B)}{\vec{r} \bullet \nabla q_B} \qquad (9.9)$$

In this formulation the data will be interpolated to all three faces in cell B using the same equation with the relevant r and $\vec{r}$ terms for each face.

Problems with slope limiters.

Slope limiting is found to perform well on regular structured grids however when slope limiters are applied to irregular and unstructured grids problems are encountered with both accuracy and convergence.

The work by Venkatakrishnan[39] demonstrates that the problems encountered when trying to achieve converged solutions on irregular grids are due to limiter chatter where the limiter is being activated by small oscillations in the variables in smooth regions of the flow. Limiter chatter prevents the solution from converging, often stalling convergence after a few orders of magnitude reduction in the residual, and also degrades the accuracy of the solution by activating the limiter and so reverting to a first order solution in smooth regions of the flow. The problem of limiter chatter is found to be worse for non-differentiable limiters which utilise the Max and Min functions such as the Superbee and Minmod limiters used in the method of characteristic decomposition. One method used to overcome this problem is to implement a threshold for oscillations within the flow below which the limiter will not activate. This type of modification can alleviate the convergence problems associated with limiter chatter but at the cost of achieving completely monotone solutions in some cases. If the threshold is set at too high a level the calculation can

also become unstable. This type of method for overcoming the convergence issues associated with limiter application is not considered for use along with characteristic decomposition due to the need for the limiter to be applied to the 'smoother' discontinuities associated with the linearly degenerate fields.

The work by Aftosmis[40] also concludes that the limiter chatter is the cause for the convergence stall problem and finds that this problem can cause a complete failure to converge for some triangular meshes. Aftosmis finds that improvements in convergence can be gained by using a less harsh directional limiting procedure in which only the face normal component of the gradient is limited. This type of limiting is sufficient to achieve monotone solutions but leads to the limiter being activated less frequently and improves the convergence of the calculation by approximately an order of magnitude. He also observes that in calculations in which convergence appears to stall there are only small amplitude fluctuations in the solution about the steady state and so monitoring the solution variables as opposed to the convergence histories can indicate when an acceptable level of convergence has been reached.

The work by Berger, Aftosmis and Murman[41] examining the behaviour of limiters on irregular grids finds that preservation of monotonicity and the ability of slope limiters to exactly reproduce linear solutions is necessary for both solution accuracy and convergence. When limiters are applied to irregular grids the limiters need to take into account mesh irregularities. The two main sources of the problems encountered when using limiters on irregular grids are failure to take account of mesh stretching and mesh skewing. This leads to limiter chatter, reduced accuracy and excessively dissipative solutions.

The effects of mesh skewing are demonstrated in figure 53.

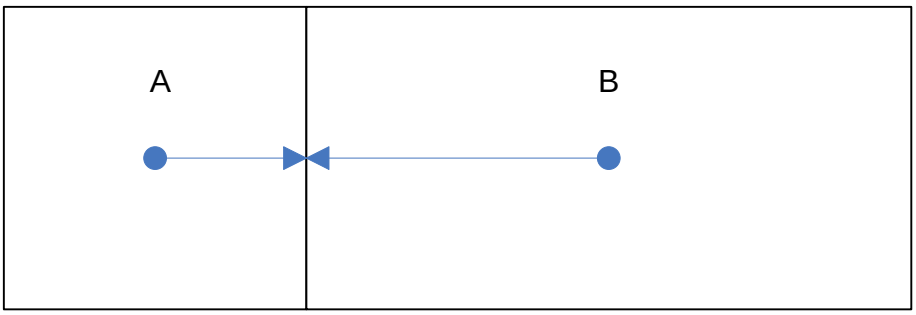

Figure 53 – it is clear that standard limiters will fail to preserve linear data for cases where there is mesh stretching as they assume a regular grid spacing in their formulation. For example in this case a 2:1 streching factor would mean that linear data interpolated in cell B to the face separating cells A and B would be interpreted as an over shoot by a factor of 2 and would be limited by all but the most compressive limiters leading to the degredation of linear data and solution accuracy.

In their work Berger, Aftosmis and Murman demonstrate the effects of mesh skewing with the following figure

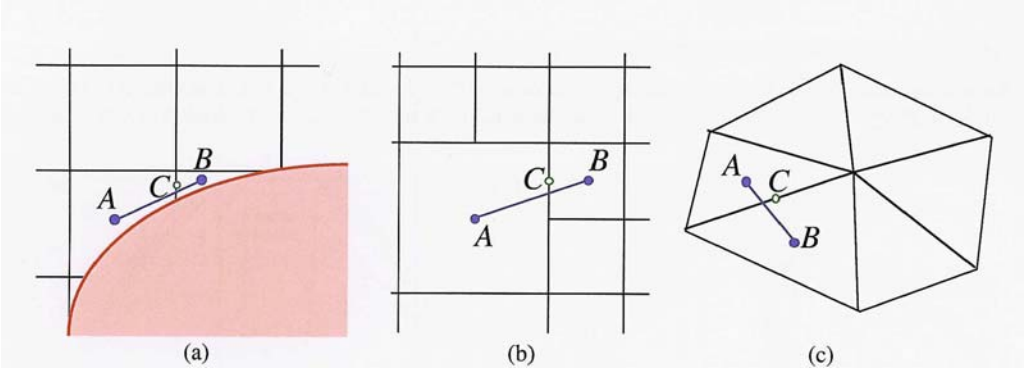

Figure 54 - In all three examples linear data will not be preserved by standard limiters. Let the line between cell centres A and B be a level line of the solution. The flux evaluation and solution limiting occur at point C, which is not on the line. Point C will look like an overshoot, and the *exact* gradient which was reconstructed at A and B will be limited.

It is observed that taking account of mesh stretching by simply rewriting existing limiter formulations in terms of scaled differences, in order that linear data will not be limited, results in the limiter not adhering to the monotonicity conditions. Overcoming the issue of mesh skewing at the same time as mesh stretching by limiting the gradients as opposed to the differences also encounters the same problem.

In order for the reconstruction at the face to obey the monotonicity conditions it is necessary that

if $q_B \le q_A$

$$q_B \le q_B + \Psi(r)\vec{r} \bullet \nabla q_B \le q_A \tag{9.10}$$

which gives

$$\Psi(r) \le \frac{q_A - q_B}{\vec{r} \bullet \nabla q_B} = 2r \tag{9.11}$$

Which defines the upper limit of allowable gradients - which is obeyed by limiter functions dependent on r

If $\Psi(r)$ is rewritten in terms of scaled differences

$$r_s = r\frac{2\vec{r}}{\overrightarrow{r_{BA}}} \quad \text{where } \overrightarrow{r_{BA}} \text{ is the vector from the centre of cell B to cell A} \tag{9.12}$$

$\Psi(r_s)$ will not always obey the condition

$$\Psi(r_s) \le 2r \tag{9.13}$$

There have been a number of approaches to developing limiters for application to unstructured grids that take into account the nature of unstructured grids in multiple dimensions. Notably the work by Barth and Jespersen[34], Batten, Lambert and Causon[42], Hubbard[43] and Jawahar and Kamath[44]. Although a number of these approaches have shown great improvements over limiter developed from a one dimensional framework their use is not compatible with the implementation of characteristic decomposition which relies on a face by face limiting of the local face normal characteristic variables.

Another issue that affects the accuracy of unstructured grid schemes is the accuracy of the calculated gradient which is used in the interpolation. Triangular or tetrahedral cells in unstructured grids have less nearest neighbours from which to calculate gradients than quadrilateral and hexahedral cells in structured grids which contributes to the poorer performance of unstructured grids when compared to comparable structured grids. Work by Peric[45] using polyhedral unstructured meshes has shown that it is possible to use these unstructured meshes to achieve solutions that are comparable to those from structured grid calculations whilst maintaining the ease of mesh generation of tetrahedral cells. Calculations on the meshes also have much improved convergence behaviour when compared to tetrahedral meshes. This is attributed to the greater number of neighbours available for each gradient calculation.

Approaches to improving Characteristic Decomposition on Unstructured Grids –

In order to improve the application of characteristic decomposition on irregular and unstructured grids there are a number of alternations that have been explored.

In the work by Berger, Aftosmis and Murman it is concluded that it is not possible to rewrite the limiter functions in terms of scaled differences or to limit the gradients directly as although this will improve the treatment of linear data it will not preserve the monotonicity of the solution.

It is possible to rewrite limiters in terms of the scaled differences or to limit the gradients directly if a second limiting is performed in order to enforce the monotonicity condition. In order to achieve this the limiter functions can be rewritten as follows

$$\Psi(r, r_s) = \begin{cases} \min\{\max[0, \min(\beta r_s, 1), \min(r_s, \beta)], 2r\} & r > 0 \\ 0 & r \le 0 \end{cases} \quad (9.14)$$

$$r = \frac{\frac{1}{2}(q_A - q_B)}{\vec{r} \bullet \nabla q_B}$$

to limit scaled differences

$r_s = r \frac{2\vec{r}}{\overrightarrow{r_{BA}}}$ where $\overrightarrow{r_{BA}}$ is the vector from the centre of cell B to the centre of cell A

or to limit the gradients directly - each component of the gradient is limited using

$$\Psi(r_x) = \max[0, \min(\beta r_x, 1), \min(r_x, \beta)] \quad (9.15)$$

$$r_x = \frac{\nabla q_{Ax}}{\nabla q_{Bx}}$$

The reconstructed solution is then given by

$$q_{Fr} = q_B + \Psi(r_x)\vec{r_x}\nabla q_{Bx} + \Psi(r_y)\vec{r_y}\nabla q_{By} + \Psi(r_z)\vec{r_z}\nabla q_{Bz} \quad (9.16)$$

and a check on the monotonicity condition is then carried out such that

For $q_A - q_B > 0$ and $q_{Fr} - q_B > 0$

$$If \quad \Psi(r_x)\vec{r_x}\nabla q_{Bx} + \Psi(r_y)\vec{r_y}\nabla q_{By} + \Psi(r_z)\vec{r_z}\nabla q_{Bz} > q_A - q_B \quad (9.17)$$

$$q_{Fr} = q_A$$

For $q_A - q_B < 0$ and $q_{Fr} - q_B < 0$

$$If \quad \Psi(r_x)\vec{r_x}\nabla q_{Bx} + \Psi(r_y)\vec{r_y}\nabla q_{By} + \Psi(r_z)\vec{r_z}\nabla q_{Bz} < q_A - q_B \quad (9.18)$$

$$q_{Fr} = q_A$$

If $q_A - q_B$ and $q_{Fr} - q_B$ have differing signs

$$q_{Fr} = q_B \quad (9.19)$$

Unlike limiting the gradients directly, when limiting with scaled differences no account is taken of the effects of mesh skewing. In order to take some account of skewing this scaled difference limiting is combined with a directional approach, as in Aftosmis[40], in which only the component normal to the face is limited.

One of the issues highlighted as influencing the convergence characteristic of a code is the choice of type of limiters, in particular the use of limiters that employ the Min and Max function as in Superbee and Minmod. The use of the Superbee limiter for characteristic decomposition is necessary as it is the compressive nature of the Superbee limiter which is needed to conserve vorticity. In figure 55 slope limiter functions providing monotone second order solutions are bounded by Minmod at the bottom and Superbee at the top all passing through the point of second order accuracy $\Psi(1)=1$.

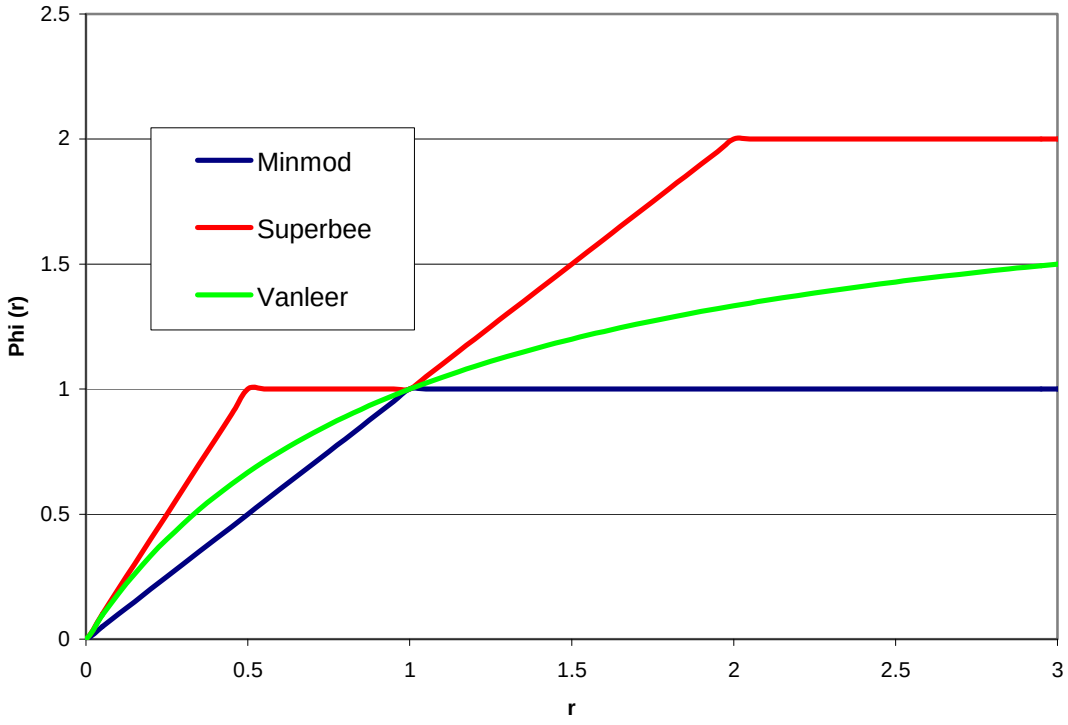

Figure 55 – Plots of limiter values Phi(r) against ratio of differences r for Minmod, Suoerbee and Vanleer limiters.. Superbee and Minmod bound the region in which functions provide second order monotone solutions

There are a number of diffusive differentiable limiters that can be used instead of Minmod for application to the genuinely nonlinear fields in characteristic decomposition.

The Van Leer limiter given by

$$\Psi(r)_{VL} = \frac{2r}{r+1} \tag{9.20}$$

is a differentiable limiter which is more compressive than the Minmod limiter but may improve convergence characteristic due to its smooth nature. There are no differentiable limiters which come close enough to the upper monotonicity bounds to make them suitable candidates to replace Superbee. The use of the non-differentiable Superbee limiter is therefore a necessary evil in the application of characteristic decomposition.

In summary there are three different formulations of Characteristic Decomposition that are investigated in the next section

The first – referred to as 'Characteristic Decomposition – New' limits only the face normal component of the gradient and uses scaling factors to take account of mesh stretching.

The second – referred to as 'Characteristic Decomposition – New 2' limits the gradients directly.

The third – referred to as 'Characteristic Decomposition – New 2V' limits the gradients directly and also replaces the Minmod limiter with the Van Leer limiter.

The issue of the accuracy of the gradient calculation used in the reconstruction on vorticity conservation has been investigated by comparison of results obtained using a constrained least squares employing nearest neighbour and results obtained using

nearest neighbours and neighbours of neighbours. The increased vorticity conservation in the incompressible convecting vortex case was found to be less than 2% improvement in conservation of peak vorticity whilst the additional computational cost per iteration was found to be approximately 30%. It is likely that the effect of varying the accuracy of the gradient calculation on the accuracy of the results would be more marked for grids containing greater levels of distortion than those considered in the current study. This issue has not been investigated any further here.

10. Results for New Limiting Schemes on Unstructured Grids.

Slotted Flap Aerofoil Case

Compressible Solver –

Figure 56 shows the effect of the application of the new methods of Characteristic Decomposition in the compressible flow solver on the slotted flap aerofoil test case compared to the baseline Characteristic Decomposition scheme.

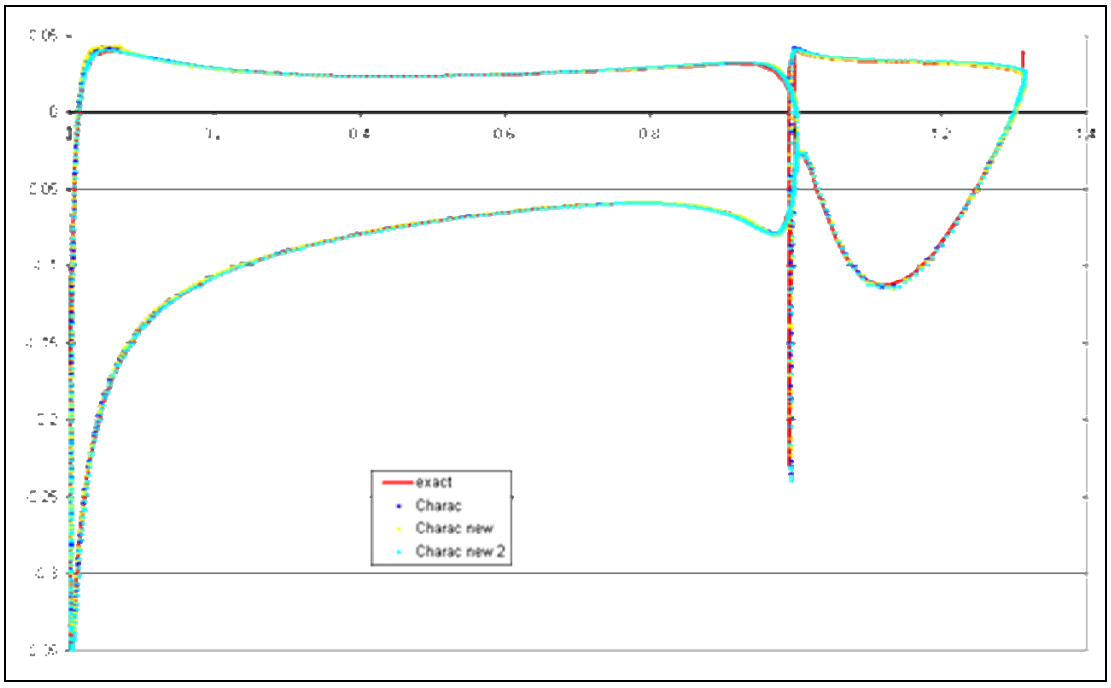

Figure 56 – Pressure Distribution for the Characteristic, Charteristic New and Characteristic New 2 schemes

The Characteristic Decomposition - New 2V scheme failed to achieve a converged solution as did the Superbee scheme in earlier tests. The reason for this failure is thought to be that the additional compression provided by the substitution of the Van Leer limiter for the Minmod limiter causes the calculation to become unstable and diverge. Both the Characteristic Decomposition – New and New 2 seem to provide similar level of accuracy to the original characteristic decomposition for this test case. Figure 57 shows the pressure distribution around the leading edge of the aerofoil at a closer scale.

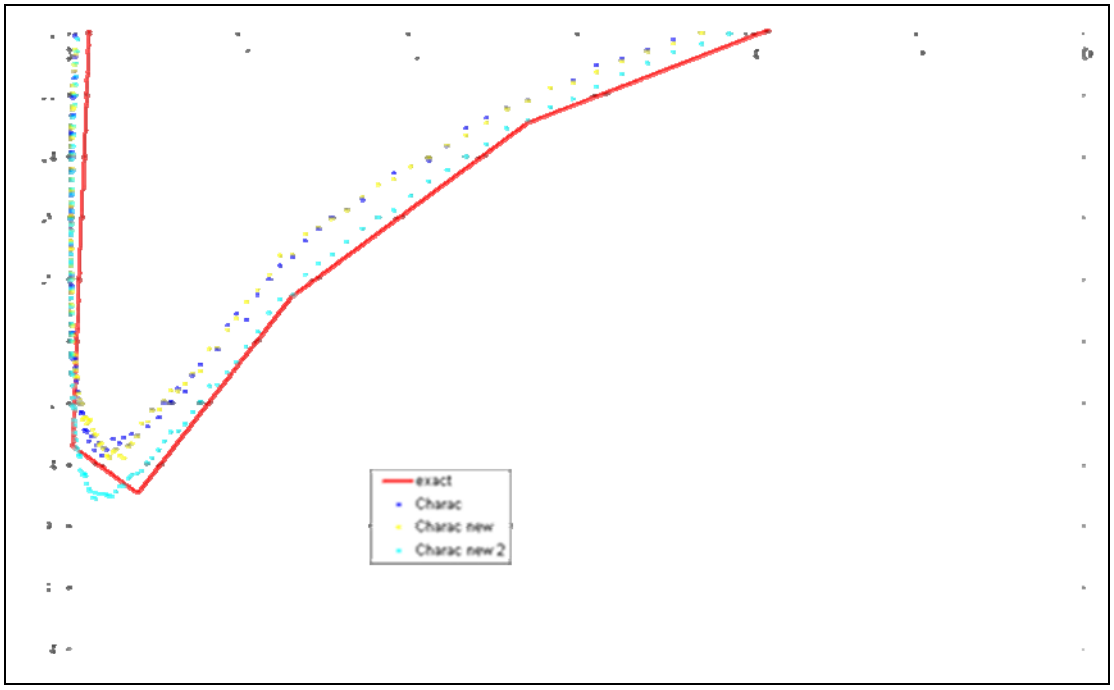

Figure 57 – Close up of the leading edge from Figure 56 – it can be seen that all the schemes come close to the analytic solution with the Characteristic New 2 providing the best result

It can be seen that Characteristic Decomposition new 2 provides a more accurate solution for the pressure distribution in this area than the other two schemes which provide similar results. The convergence histories of these schemes are compared in Figure 58.

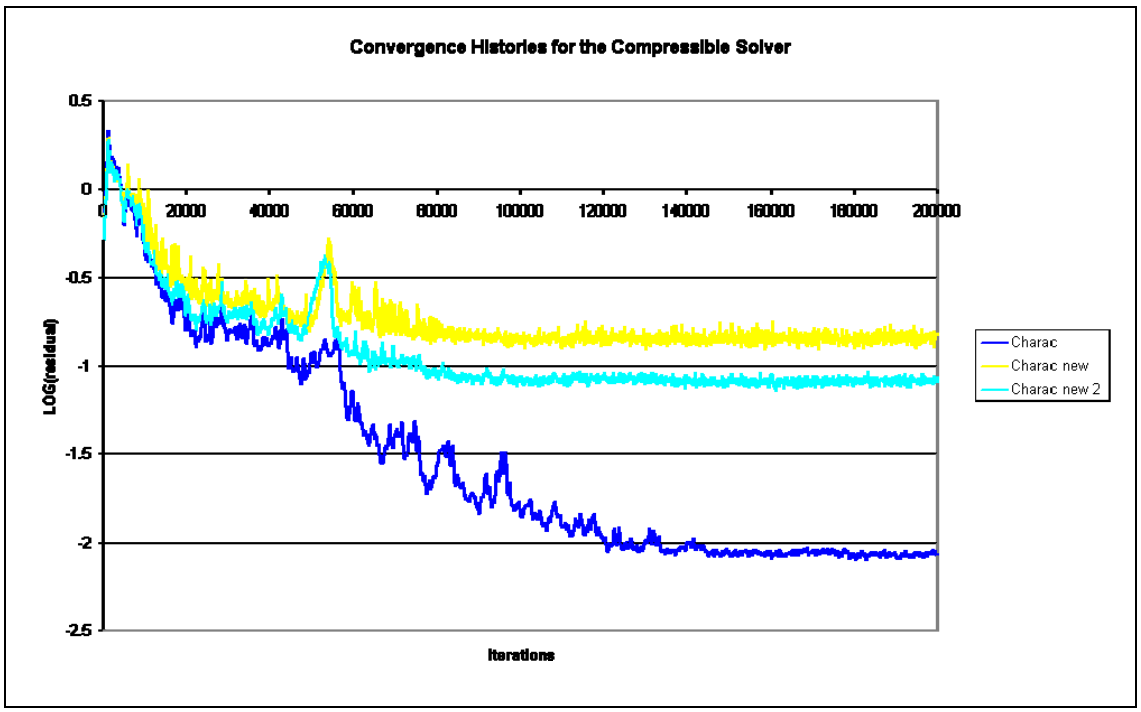

Figure 58 – Convergence Histories for the Characteristic, characteristic New and Characteristic New2 schemes. It can be seen that all schemes suffer from convergence stall which is most pronounced in the Characteristic New scheme.

Both of the new versions of Characteristic Decomposition suffer from convergence stall at a higher level of the residual than the original Characteristic Decomposition for this test case.

Artificial Compressibility Solver –

Figure 59 shows the effect of the application of the new methods of Characteristic Decomposition in the artificial compressibility flow solver on the slotted flap aerofoil test case compared to the baseline Characteristic Decomposition scheme.

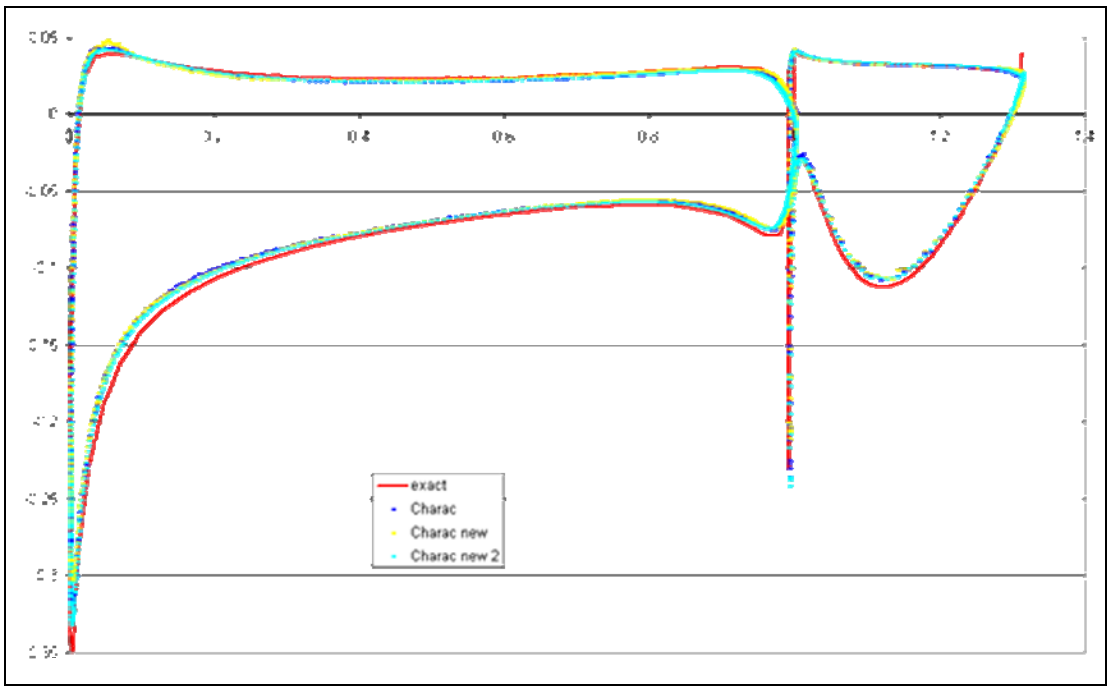

Figure 59 – Pressure Distribution for the Characteristic, Charteristic New and Characteristic New 2 schemes

Again the Characteristic Decomposition - New 2V scheme failed to achieve a converged solution. The performance of the other new formulations appears to be similar to that of the original characteristic decomposition over the majority of the aerofoil pressure distribution. Figure 60 shows the pressure distribution around the leading edge of the aerofoil at a closer scale.

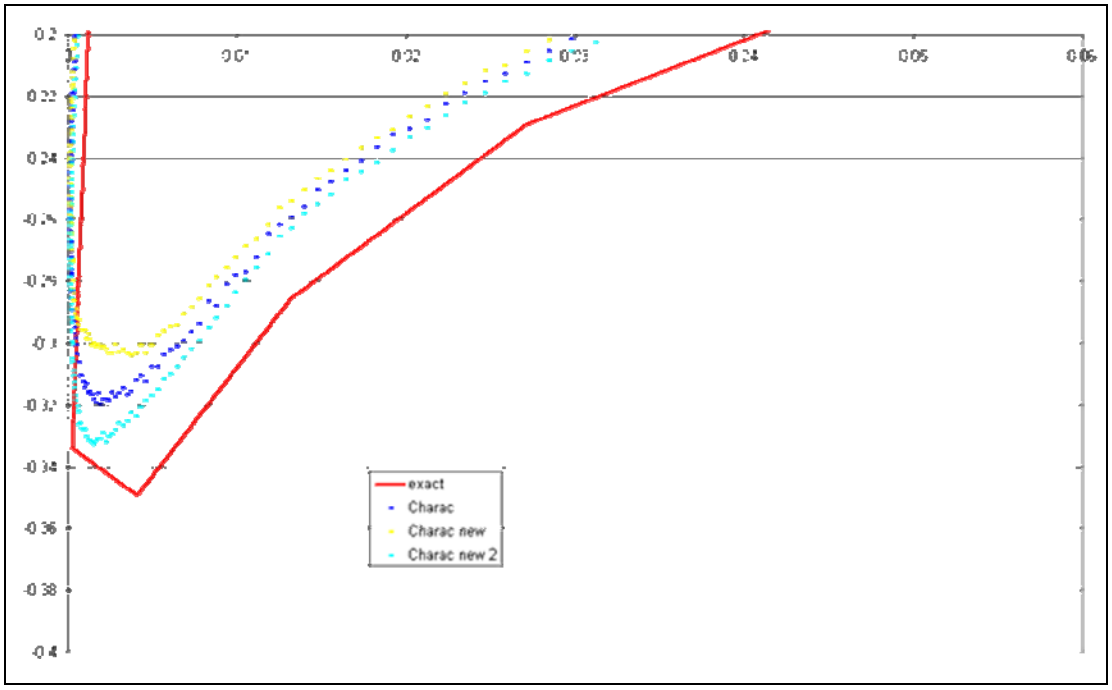

Figure 60 – Close up of the leading edge from Figure 59 – it can be seen that the Characteristic New 2 provides the best result

In the artificial compressibility solver the Characteristic Decomposition – New 2 scheme is again providing the most accurate solution in this region but differently in this solver the Characteristic Decomposition – New scheme does not resolve this region of the pressure distribution as well as the original Characteristic Decomposition scheme. The convergence histories for these calculations are shown in figure 61.

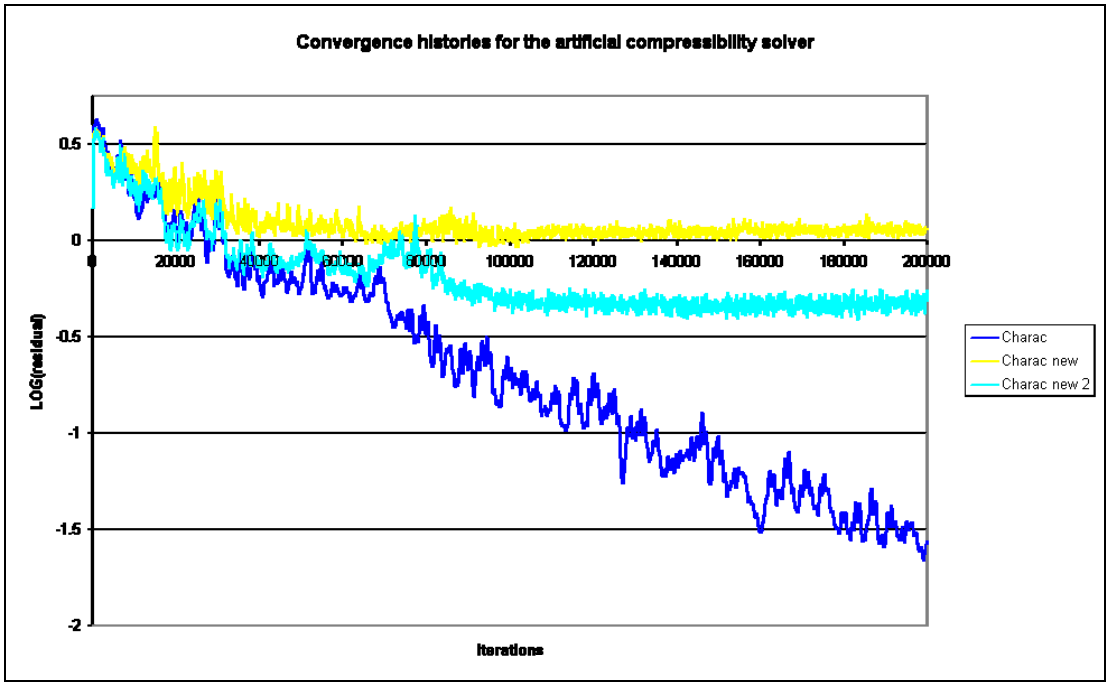

Figure 61– Convergence Histories for the Characteristic, characteristic New and Characteristic New2 schemes. It can be seen that both the Characteristic New and New2 schemes suffer from convergence stall which is most pronounced in the Characteristic New scheme.

The convergence behaviour of the new Characteristic Decomposition schemes in the artificial compressibility solver is much worse than the original baseline Characteristic Decomposition scheme. The Characteristic Decomposition – new scheme fails to converge to a value of the residual below unity. The Characteristic Decomposition – New 2 scheme stalls at approximately half an order of magnitude reduction in the residual.

The solutions of the schemes for both the compressible and artificial compressibility schemes for three levels of grid density are shown in Appendix D. There is little effect on the convergence of the solutions towards the exact solution for the differing schemes and in increases in accuracy found on the finest grid above seem to be duplicated on the coarser grids as expected.

Unsteady Laminar Flow over a Circular Cylinder –

For the calculation of the laminar flow over a circular cylinder calculated with the unstructured grid the Strouhal number calculated from the solutions using the three variations of Characteristic Decomposition remained at S_t=0.146 as in the baseline incompressible scheme indicating that the differing formulations have not substantially altered the effective viscosity of the code. The following figures show the vorticity shed from the laminar cylinder at 300 time steps for Characteristic Decomposition and the three altered Characteristic Decomposition schemes.

a.

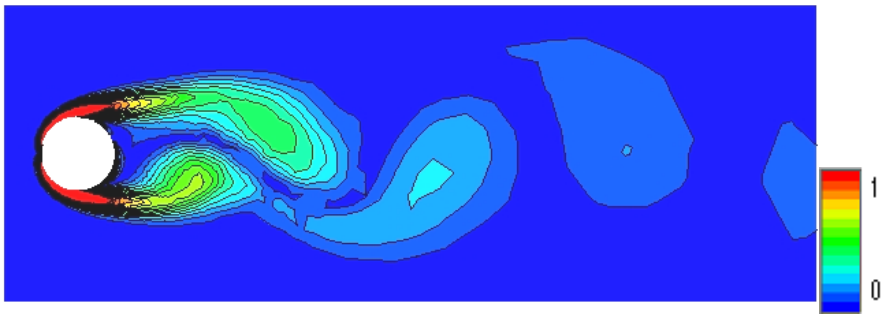

b.

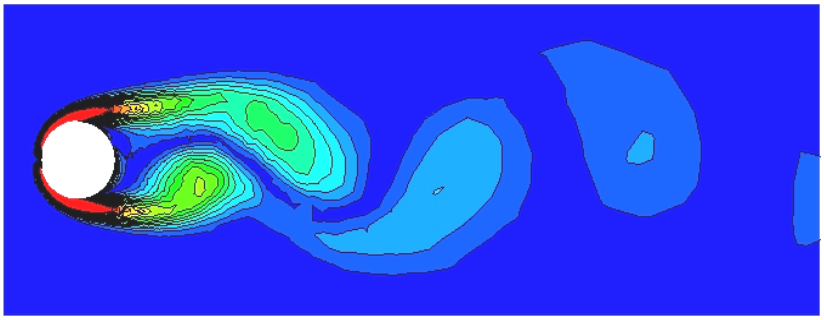

c.

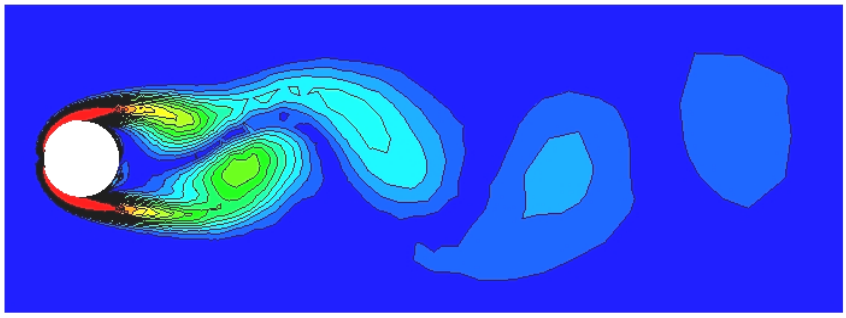

d

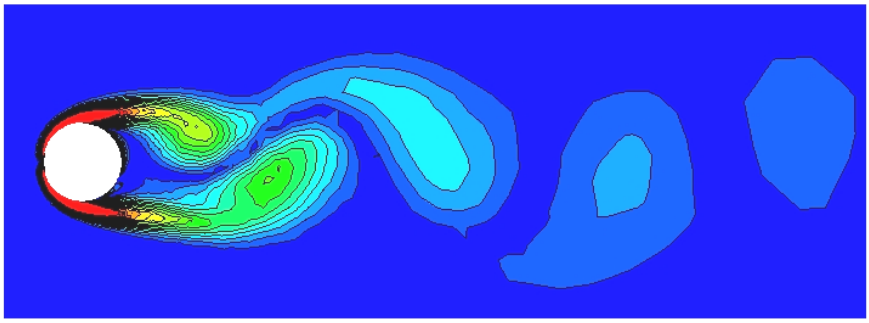

Figure 62 - Plot for Unstructured Grids of vorticity magnitude calculated from the velocity field non-dimensionalised by the physical freestream speed of sound a=Charac Decomp, b=Charac Decomp New, c=Charac Decomp New 2, d= Charac Decomp New 2V

Again it is hard to make a meaningful comparison in terms or downstream vorticity conservation characteristics of the different implementations due to the fact that the onset of vortex shedding happens at different times in the physical timesteps of the calculations for different cases and so the positions of the shed vortices at any one physical time are not in synch across the different calculations.

Results for the compressible convecting vortex case.

Unstructured Grid –

The decline in peak vorticity for the unstructured vortex case for Characteristic Decomposition and the three variations of Characteristic decomposition are shown in Figure 63 and change in enstrophy with time in Figure 64

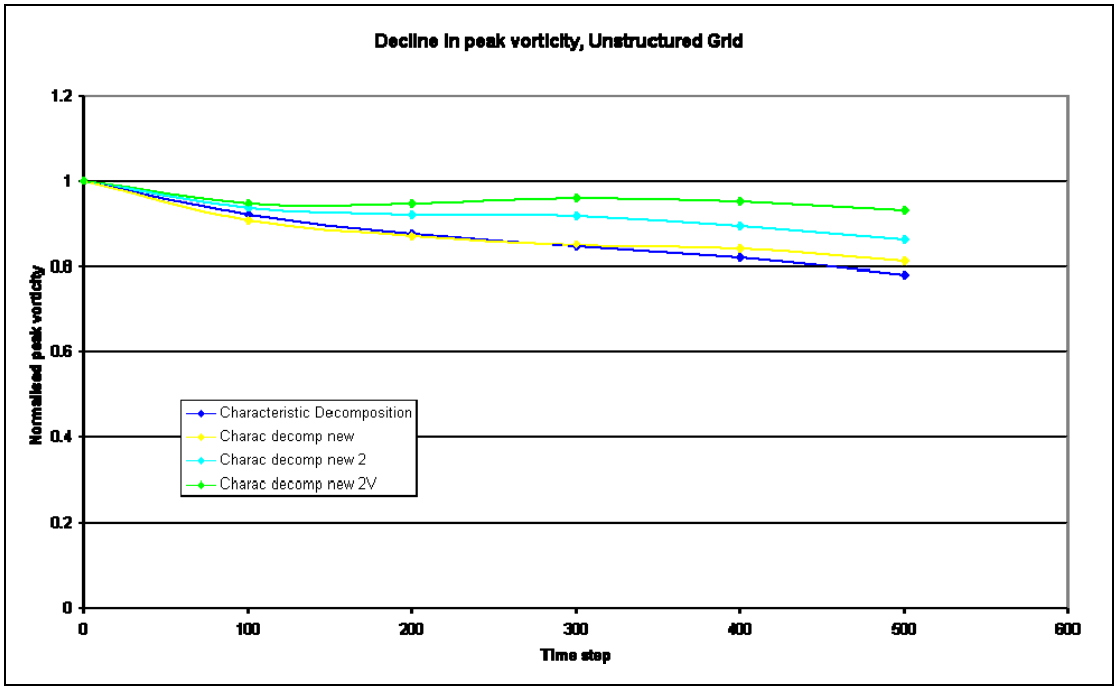

Figure 63– Decline in Peak Vorticity for Unstructured Grid calculation. All the new schemes show an improvement in peak vorticity conservation over the Characteristic Decomposition scheme with Charac Decomp new 2V showing the greatest conservation of peak vorticity

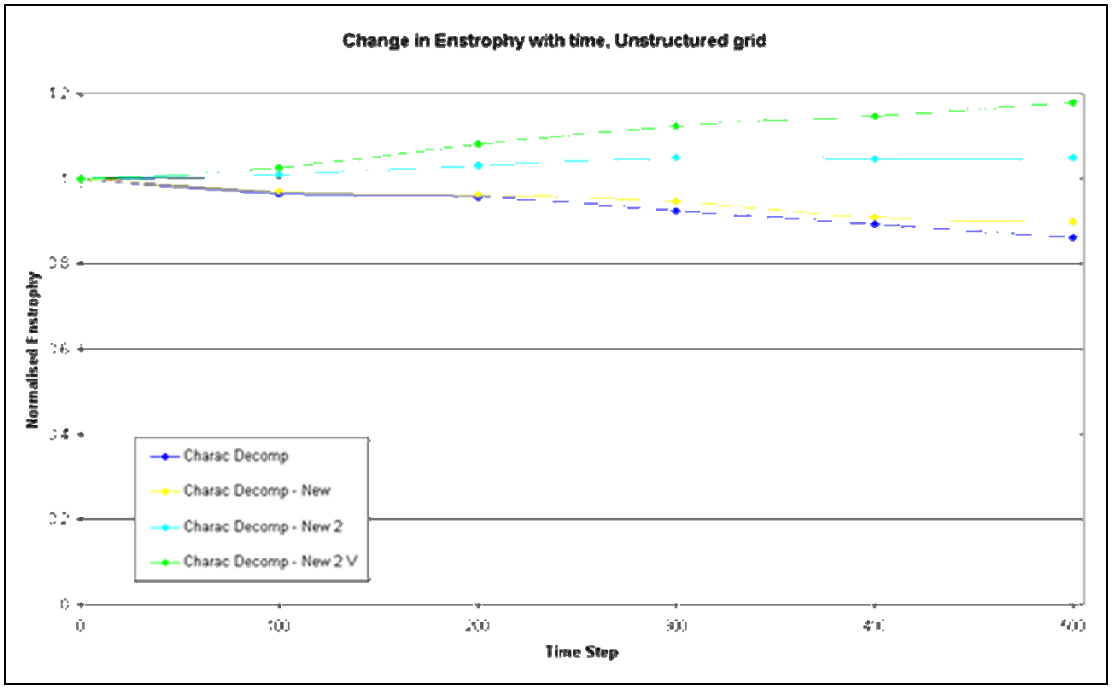

Figure 64 - Change in Enstrophy for Unstructured Grid calculation. Characteristic Decomp New shows a small improvement over the Charac Decomp scheme when maintaining Enstrophy. Charac Decomp New 2 and New 2V generate spurious enstrophy with the value rising above unity.

The following figure 65 depicts vorticity magnitude at 500 time steps for each of the adapted characteristic decomposition schemes compared to the baseline Characteristic Decomposition scheme.

Although all the schemes tried show an improvement over the initial implementation of Characteristic Decomposition there is a problem, as found with the use of the Superbee limiter, with a gain in enstrophy throughout the computational domain with time.

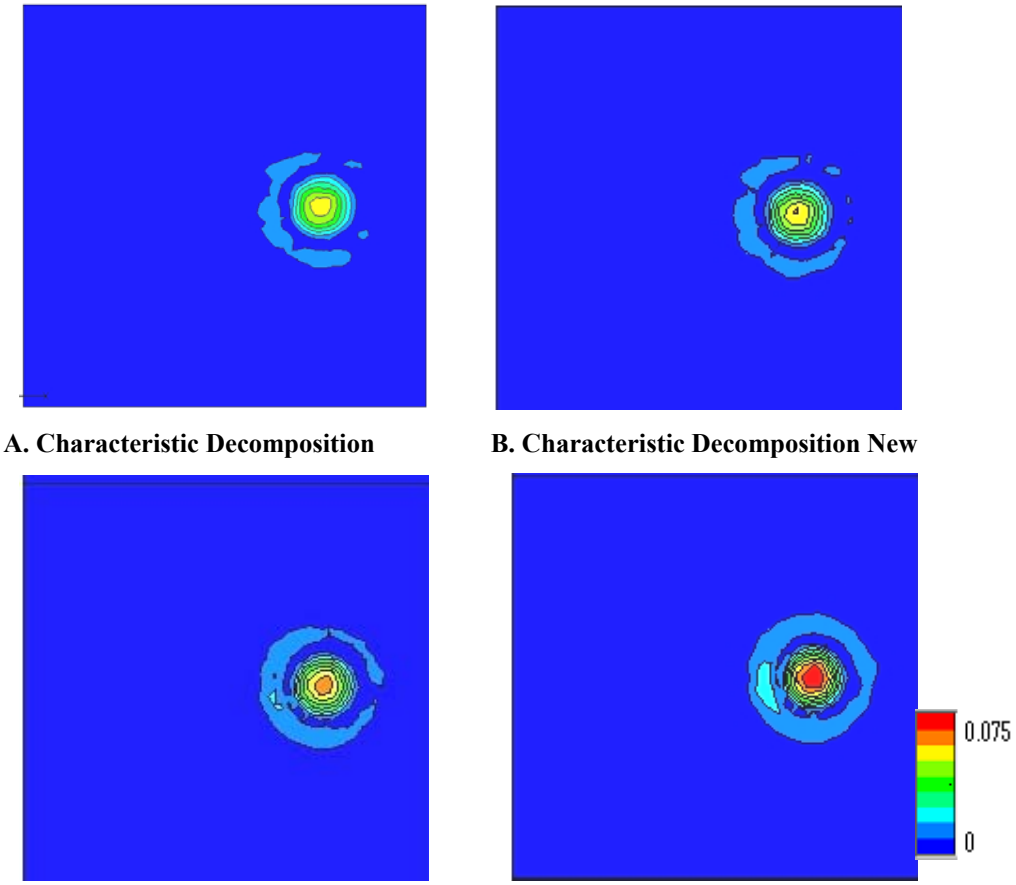

A. Characteristic Decomposition **B. Characteristic Decomposition New**

C. Characteristic Decomposition New 2 **D. Characteristic Decomposition New 2V**

Figure 65 - Plots of vorticity magnitude calculated from nondimensionalised velocity distribution for the unstructured grid calculation. The generation of spurious vorticity by the Characteristic Decomposition New 2 and New 2V schemes is evident whilst both the Charateristic Decomposition and Charateristic Decomposition New schemes improve vorticity conservation without suffering from this problem.

Results for the artificial compressibility convecting vortex case.

Unstructured Grid –

The decline in peak vorticity for the unstructured vortex case for Characteristic Decomposition and the three variations of Characteristic Decomposition are shown in Figure 66 and change in enstrophy with time in Figure 67. For this test case all the methods applied show a similar level of vorticity decline apart from Characteristic Decomposition New 2V which shows some improvement over the initial formulation of Characteristic decomposition. All of the test cases show a decline in enstrophy with time indicating dissipation of energy occurring within the calculations.

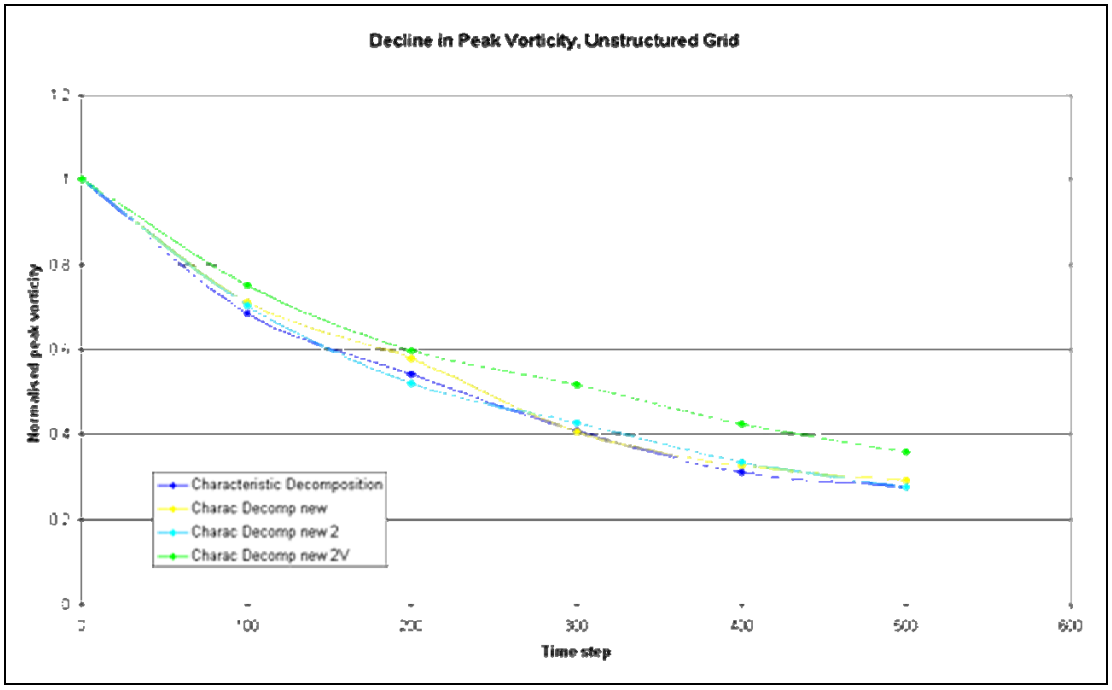

Figure 66 – Decline in Peak Vorticity for Untructured Grid calculation. The Charac Decomp new 2V shows a greater conservation of peak vorticity than all the other schemes

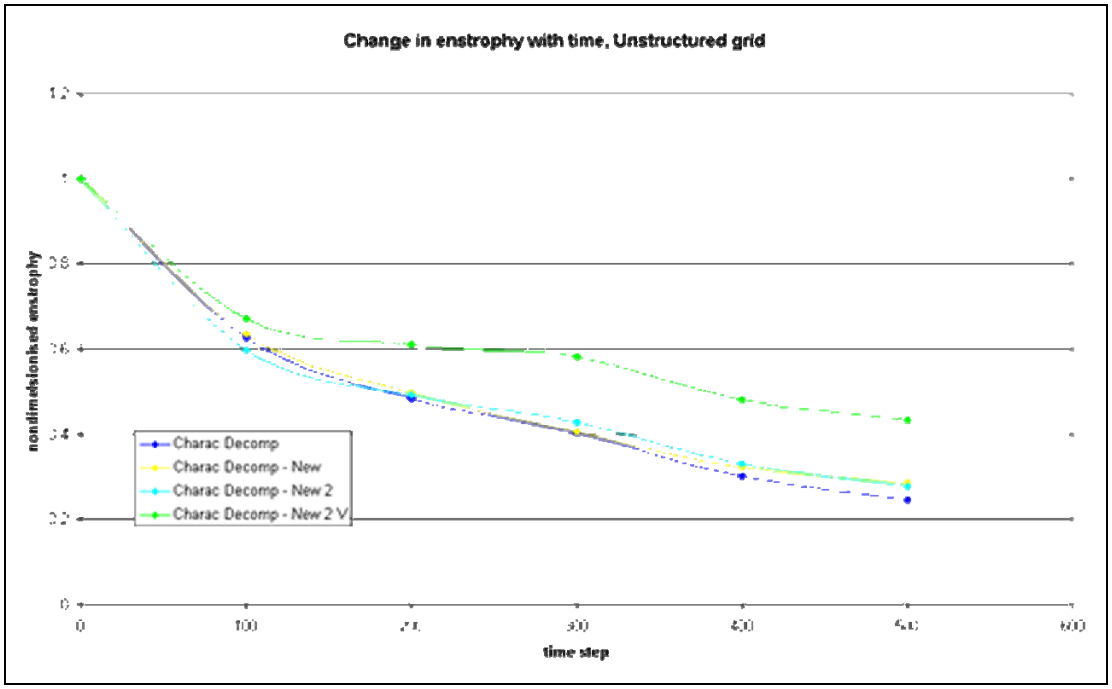

Figure 67- Change in Enstrophy for Unstructured Grid calculation. Characteristic Decomp New and New 2 show a small improvement over the Charac Decomp scheme when maintaining Enstrophy. The improvement for Charac Decomp New 2V is the largest.

The following figure 68 depicts vorticity magnitude at 500 time steps for each of the adapted Characteristic Decomposition schemes compared to the baseline Characteristic Decomposition scheme. Figure 68 shows little difference between the distributions of vorticity magnitude for each of the Characteristic Decomposition schemes.

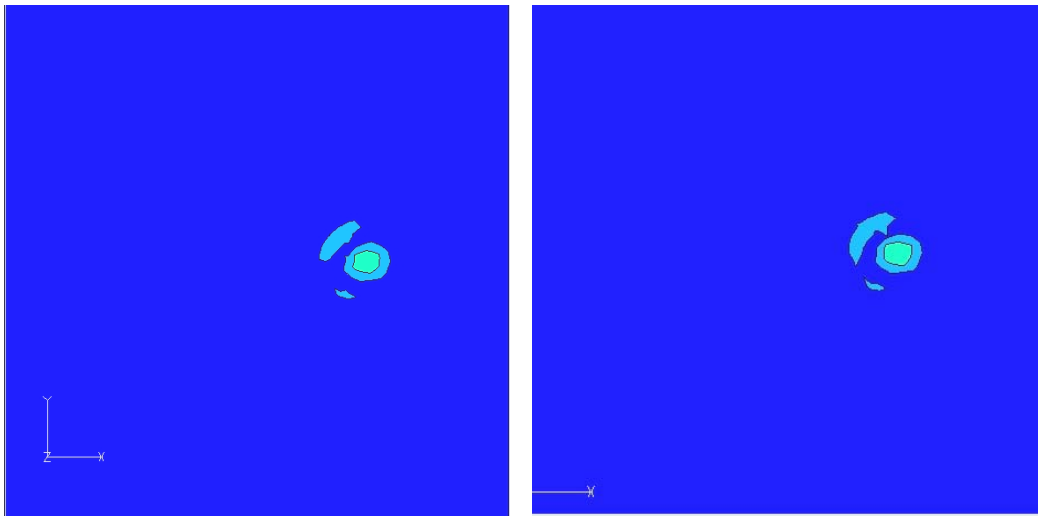

A. Characteristic Decomposition B. Characteristic Decomposition New

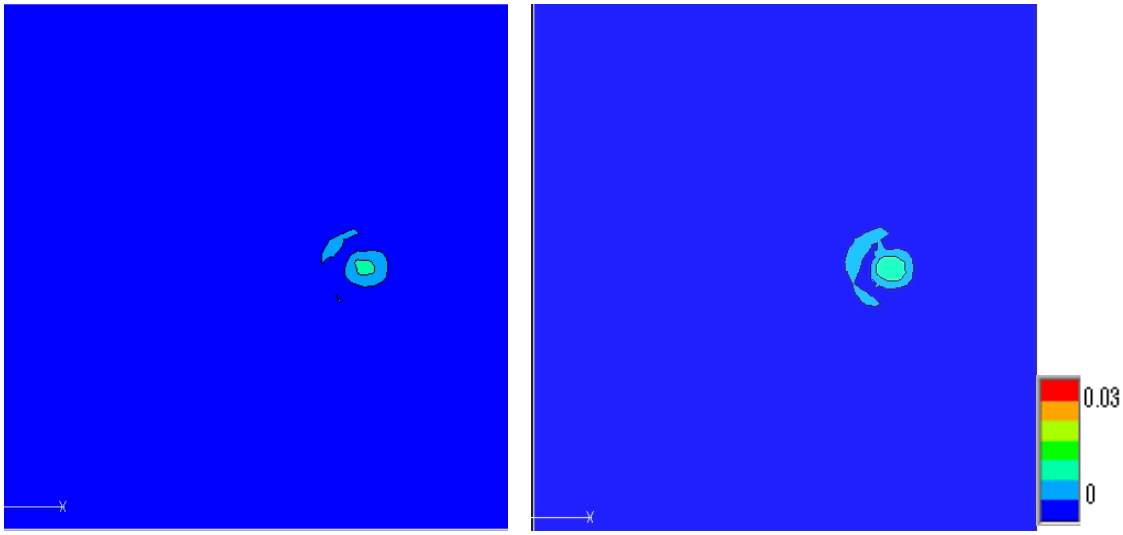

C. Characteristic Decomposition New 2 D. Characteristic Decomposition New 2V

Figure 68 - Plots of vorticity magnitude calculated from nondimensionalised velocity distribution for the unstructured grid calculation. There is no generation of spurious vorticity for any of the schemes in this case.

11. Assessment of the improvements in vorticity conservation for Characteristic Decomposition.

For the compressible structured convecting vortex case, carried out on an 80x80 grid implementation of Characteristic Decomposition provided an increase in normalised final peak vorticity from 0.439 for the Barth and Jespersen scheme to 0.806 which is an improvement of 83.6% with an increased computational cost of approx 25% per iteration. The implementation of the Characteristic scheme in this case did not suffer from increasing enstrophy with time in the computational domain as the calculation carried out with the Superbee limiter did.

A calculation carried out on a 160x160 structured grid, corresponding to a four fold increased computational cost over the 80x80 grid, with the Barth and Jespersen limiter provided a final normalised peak vorticity of 0.67 which is a 23% increase which is less than that obtained with the coarser grid employing Characteristic Decomposition which only cost an additional 25% computational cost.

For the compressible unstructured convecting vortex case, carried out on a grid with 3000 cells implementation of Characteristic Decomposition and Characteristic Decomposition New provided an increase in normalised final peak vorticity from 0.59 for the Barth and Jespersen scheme to 0.78 and 0.81 respectively which is an improvement of 32% and 33% respectively with an increased computational cost of approx 25% per iteration. The implementation of the Characteristic schemes in this cases did not suffer from increasing enstrophy with time in the computational domain as the calculations carried out with the Superbee limiter and the Characteristic Decomposition New 2 and New2V did.

A calculation carried out on a 12000 cell unstructured grid, corresponding to a four fold increase in computational cost over the 3000 cell grid, with the Barth and Jespersen limiter provided a final normalised peak vorticity of 0.79 which is approximately the same as the improvement obtained by the Characteristic Decomposition and Characteristic Decomposition New which only provided an additional 25% computational cost per iteration.

For the artificial compressibility structured convecting vortex case, carried out on an 80x80 grid implementation of Characteristic Decomposition provided an increase in normalised final peak vorticity from 0.088 for the Barth and Jespersen scheme to 0.225 which is an improvement of 155.7% with an increased computational cost of approx 25% per iteration. The implementation of the Characteristic scheme in this case did not suffer from increasing enstrophy with time in the computational domain as the calculation carried out with the Superbee limiter did.

A calculation carried out on a 160x160 structured grid, corresponding to a four fold increased computational cost over the 80x80 grid, with the Barth and Jespersen limiter provided a final normalised peak vorticity of 0.164 which is an 86% increase which is less than that obtained with the coarser grid employing Characteristic Decomposition which only cost an additional 25% computational cost.

For the artificial compressibility unstructured convecting vortex case, carried out on a grid with 3000 cells implementation of Characteristic Decomposition, Characteristic Decomposition New, New 2 and New 2V provided an increase in normalised final peak vorticity from 0.121 for the Barth and Jespersen scheme to 0.28, 0.29, 0.28 and 0.36 respectively which is an improvement of 131%, 140%, 131% and 198% respectively with an increased computational cost of approx 25% per iteration. All implementations of Characteristic decomposition schemes in this case did not suffer from increasing enstrophy with time in the computational domain.

A calculation carried out on a 12000 cell unstructured grid, corresponding to a four fold increase in computational cost over the 3000 cell grid, with the Barth and Jespersen limiter provided a final normalised peak vorticity of 0.234 which is an improvement of 93% which is less than all the improvements obtained by the Characteristic Decomposition schemes which only provided an additional 25% computational cost per iteration.

For all the differing applications of Characteristic Decomposition to steady calculations there were clear issues with convergence stall compared to the Barth and Jespersen Limiter, the worst of these was the Characteristic Decomposition – New 2V scheme which failed to converge for the slotted flap aerofoil case. However in all

these cases the convergence issues were not as severe as those associated with the Superbee limiter.

12. Conclusions

It can be concluded that the method of characteristic decomposition provides an effective method of improving the vorticity conservation in a calculation at less computational cost than would be required to gain the same level of vorticity conservation by grid refinement on both structured and unstructured grids.

It has been confirmed that implementation of Characteristic Decomposition is an effective method of vorticity conservation when applied to an artificial compressibility scheme.

It has been confirmed that the method of Characteristic Decomposition is effective in a second order scheme and not just in higher order schemes – where testing of this method for vorticity conservation has been concentrated.

Three adapted methods for Characteristic Decomposition on unstructured grids were proposed and tested. All methods provided an improvement in vorticity conservation over the original Characteristic Decomposition scheme in the compressible solver applied to a convecting vortex. For this test case the Characteristic Decomposition – New scheme was the only one that did not suffer from the problem of increasing enstrophy in the computational domain. For the artificial compressibility solver the Characteristic Decomposition – New 2V provided the best improvement in vorticity conservation for the convecting vortex case and none of the Characteristic Decomposition schemes suffered from increasing enstrophy.

There are greater convergence problems associated with all the vorticity conserving schemes tested in this work than for the baseline Barth and Jespersen limiter.

13. Recommendations for Further Work

Further investigation of the issue of generation of spurious vorticity and increasing enstrophy in Characteristic Decomposition is warranted. There may be a relationship between vorticity strength and generation of spurious enstrophy in a calculation as the problems of increasing enstrophy were much more apparent in the compressible solver convecting vortex test case.

There are obvious convergence issues for the method of characteristic decomposition - likely to be associated with the triggering of the non-differentiable limiters in smooth regions of the flow. Further work to look at ways of improving the convergence of Characteristic Decomposition schemes would be valuable. It may be possible to take an approach similar to that of[45] where thresholds are set so that limiters are switched off in smooth regions of the flow. Careful consideration of how to apply thresholds in order not to deactivate the limiters in the region of vorticity would need to be taken.

APPENDIX A

Derivation of Osher's Flux for the Artificial Compressibility Equations

Governing System of Equations

The left hand side of the unsteady x split three dimensional artificial compressibility equations employing dual time stepping follows. At each physical time step the solution is marched to a steady state in pseudo-time, where the pseudo-time derivative $\partial Q_\tau / \partial \tau$ tends to zero, and the unsteady incompressible equations are recovered.

$$\frac{\partial \overline{Q}_t}{\partial t} + \frac{\partial \overline{Q}_\tau}{\partial \tau} + \frac{\partial H}{\partial x} = 0 \qquad (1)$$

where

$$\overline{Q}_t = \begin{pmatrix} 0 \\ \overline{u} \\ \overline{v} \\ \overline{w} \end{pmatrix} \qquad \overline{Q}_\tau = \begin{pmatrix} P \\ \overline{u} \\ \overline{v} \\ \overline{w} \end{pmatrix} \qquad H = \begin{pmatrix} \overline{u}c^2 \\ \overline{u^2} + P \\ \overline{vu} \\ \overline{wu} \end{pmatrix}$$

$\overline{u} = V \cdot n \qquad V = \begin{pmatrix} u \\ v \\ w \end{pmatrix} \qquad n = \begin{pmatrix} n_x \\ n_y \\ n_z \end{pmatrix}$ is the local surface normal, outward pointing, unit vector

c is the artificial compressibility coefficient

Derivation of the Riemann Solver of Osher for the Artificial Compressibility Equations

The derivation of Osher's flux depends on integration in phase space. The integration paths are integral curves associated with the set of right eigenvectors of the system. For the artificial compressibility equations these curves along with their intersection

points need to be determined. The generalised Riemann invariants are used to determine the intersection points. The Osher flux is defined by equation (2).

$$F_{i+1/2} = F(U_0) + \int_{U_0}^{U_1} A^{-}(U)\,dU \qquad (2)$$

where the integral *is taken in phase space along*

$$I(U) = I_1(U) \cup I_{2,3}(U) \cup I_4(U)$$

giving

$$F_{i+1/2} = F_0 + \int_{U_0}^{U_{1/3}} A^{-}(U)dU + \int_{U_{1/3}}^{U_{2/3}} A^{-}(U)dU + \int_{U_{2/3}}^{U_1} A^{-}(U)dU \qquad (3)$$

the eigenvalues of the system are calculated from equation (1)

$$\begin{aligned} \lambda_1 &= \bar{u} - a \\ \lambda_2 &= \lambda_3 = \bar{u} \\ \lambda_4 &= \bar{u} + a \end{aligned} \qquad (4)$$

where

$a = artificial\ speed\ of\ sound = \sqrt{\bar{u}^2 + c^2}$

It is noted that the artificial speed of sound will always be greater than the flow velocity and so there will be no need to consider sonic points in the determination of Osher's flux.

The vector of right eigenvectors is given by

$$R = \begin{bmatrix} -(a+\bar{u}) & 0 & 0 & (a-\bar{u}) \\ 1 & 0 & 0 & 1 \\ -\dfrac{\bar{v}}{a} & 1 & 1 & \dfrac{\bar{v}}{a} \\ -\dfrac{\bar{w}}{a} & 1 & -1 & \dfrac{\bar{w}}{a} \end{bmatrix} \qquad (5)$$

The Riemann invariants are determined from the right eigenvectors given by (5).

Across wave 1

$$\frac{dP}{-(\bar{u}+a)} = \frac{d\bar{u}}{1} = \frac{d\bar{v}}{\bar{v}/-a} = \frac{d\bar{w}}{\bar{w}/-a} \tag{6}$$

giving

$$\int dP + \int (\bar{u}+a)d\bar{u} = constant$$

$$I_1(P,\bar{u}) = P + \frac{\bar{u}^2}{2} + \frac{c^2}{2}\ln(\bar{u}+a) + \frac{\bar{u}a}{2} \tag{7}$$

and

$$\int \frac{1}{a} d\bar{u} + \int \frac{1}{\bar{v}} d\bar{v} = \text{constant}$$

$$\mathrm{I}_1(\bar{u},\bar{v}) = In(\bar{u} + \sqrt{\bar{u}^2 + c^2}) + In\left(\bar{v}\right) \tag{8}$$

and

$$\int \frac{1}{a} d\bar{w} + \int \frac{1}{\bar{w}} d\bar{w} = \text{constant}$$

$$\mathrm{I}_1(\bar{u},\bar{w}) = In(\bar{u} + \sqrt{\bar{u}^2 + c^2}) + In\left(\bar{w}\right) \tag{9}$$

Across wave 2 P = constant and $\bar{u}$ = constant

Across wave 3

$$\frac{dP}{-(\bar{u}-a)} = \frac{d\bar{u}}{1} = \frac{d\bar{v}}{\bar{v}/a} = \frac{d\bar{w}}{\bar{w}/a} \tag{10}$$

Giving

$$\int dP + \int (\bar{u} - a) d\bar{u} = constant$$

$$I_2(P, \bar{u}) = P + \frac{\bar{u}^2}{2} - \frac{c^2}{2} \ln(\bar{u} + a) - \frac{\bar{u}a}{2} \tag{11}$$

and

$$\int \frac{1}{a} d\bar{u} - \int \frac{1}{v} d\bar{v} = \text{constant}$$

$$\mathrm{I}_2(\bar{u}, \bar{v}) = In(\bar{u} + \sqrt{\bar{u}^2 + c^2}) - In\left(\bar{v}\right) \tag{12}$$

and

$$\int \frac{1}{a} d\bar{u} - \int \frac{1}{w} d\bar{w} = \text{constant}$$

$$\mathrm{I}_2(u, \bar{w}) = In(\bar{u} + \sqrt{\bar{u}^2 + c^2}) - In\left(\bar{w}\right) \tag{13}$$

collecting all relationships given by the Riemann invariants (7),(8),(9),(11),(12),(13) together gives

$$\bar{u}_{1/3} = \bar{u}_{2/3} = \bar{u}_*$$

$$a_{1/3} = a_{2/3} = a_* = \sqrt{\bar{u}_*^2 + c^2}$$

$$P_{1/3} = P_{2/3} = P_*$$

$$\Psi_0 = P_0 + \frac{\bar{u}_0^{\,2}}{2} + \frac{c^2}{2}\ln(\bar{u}_0 + a_0) + \frac{\bar{u}_0 a_0}{2} = P_* + \frac{\bar{u}_*^{\,2}}{2} + \frac{c^2}{2}\ln(\bar{u}_* + a_*) + \frac{\bar{u}_* a_*}{2}$$

$$\Phi_{0\bar{v}} = In(\bar{u}_0 + \sqrt{\bar{u}_0^{\,2} + c^2}) + In(\bar{v}_0) = In(\bar{u}_* + \sqrt{\bar{u}_*^{\,2} + c^2}) + In(\bar{v}_{1/3})$$

$$\Phi_{0\bar{w}} = In(\bar{u}_0 + \sqrt{\bar{u}_0^{\,2} + c^2}) + In(\bar{w}_0) = In(\bar{u}_* + \sqrt{\bar{u}_*^{\,2} + c^2}) + In(\bar{w}_{1/3})$$

$$\Psi_1 = P_1 + \frac{\bar{u}_1^{\,2}}{2} - \frac{c^2}{2}\ln(\bar{u}_1 + a_1) - \frac{\bar{u}_1 a_1}{2} = P_* + \frac{\bar{u}_*^{\,2}}{2} - \frac{c^2}{2}\ln(\bar{u}_* + a_*) - \frac{\bar{u}_* a_*}{2}$$

$$\Phi_{1\bar{v}} = In(\bar{u}_1 + \sqrt{\bar{u}_1^{\,2} + c^2}) - In(\bar{v}_1) = In(\bar{u}_* + \sqrt{\bar{u}_*^{\,2} + c^2}) - In(\bar{v}_{2/3})$$

$$\Phi_{1\bar{w}} = In(\bar{u}_1 + \sqrt{\bar{u}_1^{\,2} + c^2}) - In(\bar{w}_1) = In(\bar{u}_* + \sqrt{\bar{u}_*^{\,2} + c^2}) - In(\bar{w}_{2/3})$$

(14)

Equations (14) can be used to give an expression for $\bar{u}^*$ in terms of known values.

$$c^2 \ln(\bar{u}_* + \sqrt{\bar{u}_*^2 + c^2}) + \bar{u}_* \sqrt{\bar{u}_*^2 + c^2} - (\Psi_0 - \Psi_1) = 0 \qquad (15)$$

This function has only one zero so the Newton-Raphson method can be used to determine $\bar{u}^*$. Taking $\bar{u}^* = \bar{u}_0$ as an initial estimate for $\bar{u}^*$ the Newton-Raphson method is given by.

$$u^*_{n+1} = u^*_n - \frac{f(u^*_n)}{f'(u^*_n)} \qquad n = 0,1,2,3..... \tag{16}$$

where

$$f(u^*) = c^2 \ln(u^* + \sqrt{u^{*2} + c^2}) + u^* \sqrt{u^{*2} + c^2} - (\Psi_0 - \Psi_1)$$

and

$$f'(u^*) = 2\sqrt{u^{*2} + c^2}$$

Determination of the Osher flux

The value of each of the terms in the Osher Flux can now be determined by inspection of the signs of the eigenvalues along each of the integration paths.

Along $I_1(U)$ –

$\lambda_1 = \bar{u} - a \qquad a = \sqrt{\bar{u}^2 + c^2} \rangle 0$ and $\sqrt{\bar{u}^2 + c^2} \rangle \bar{u}$ for all $\bar{u}$

so $\lambda_1 \langle 0$ for all $\bar{u}$ and

$$\int_{U_0}^{U_{1/3}} A^-(U)dU = F(U_{1/3}) - F(U_0) \tag{17}$$

Along $I_2(U)$ –

$\lambda_2 = \bar{u}_* =$ constant along I_2

if $\bar{u}_* \geq 0 \qquad \lambda_2^-(\bar{u}) = 0 \qquad$ so $\qquad \int_{U_{1/3}}^{U_{2/3}} A^-(U)dU = 0 \tag{18}$

if $\bar{u}_* \langle 0 \qquad \int_{U_{1/3}}^{U_{2/3}} A^-(U)dU = F(U_{2/3}) - F(U_{1/3}) \tag{19}$

Along $I_3(U)$ –

$\lambda_3 = \bar{u} + a \qquad$ so $\qquad \bar{u} \quad \lambda_3 \rangle 0$ for all $\bar{u}$ and

$$\int_{U_{2/3}}^{U_1} A^-(U)dU = 0 \tag{20}$$

This means there are only two alternatives to consider for the flux formula.

$$
\begin{aligned}
&If \quad \bar{u}_* < 0 \\
&F_{i+1/2} = F_0 + F_{1/3} - F_0 + F_{2/3} - F_{1/3} = F_{2/3} \\
&If \quad \bar{u}_* \geq 0 \\
&F_{i+1/2} = F_0 + F_{1/3} - F_0 = F_{1/3}
\end{aligned}
\tag{21}
$$

Once the value of $\bar{u}^*$ has been determined the value of all the other variables can be calculated from the Riemann invariants.

APPENDIX B

Applying Characteristic Decomposition in an Artificial Compressibility Solver.

Characteristic decomposition is applied in the interpolation algorithm. The limited differences of the local conservative variables, limited by both a compressive and diffusive limiter, are calculated. These values, along with the matrix of left eigenvectors, are used to transform to characteristic variables for the interpolation to be carried out with the compressive limiter applied to the linear degenerate fields and the diffusive limiter to the genuinely non-linear fields.

The relations used in the method of characteristic decomposition are as follows

$$W = L\overline{Q} \qquad (1)$$

In the method of characteristic decomposition it is also assumed that

$$\Delta W = L\,\Delta\overline{Q} \qquad (2)$$

Giving

$$W_{i+1/2} = L\overline{Q} + L\Delta\overline{Q} \qquad (3)$$

Here the linearly degenerate fields are calculated with the $\Delta\overline{Q}$ values limited with the compressive limiter and the genuinely non-linear fields with the difussive limiter

The reverse transformation to local conservative variables is given by

$$\overline{Q} = RW \qquad (4)$$

In order to apply characteristic decomposition it is first necessary to transform from Primitive variables to the local Conserved variables, of the split three dimensional Euler equations, in the interpolation algorithm. These are given below.

$$q = \begin{bmatrix} P \\ u \\ v \\ w \end{bmatrix} \quad \Rightarrow \quad \overline{Q} = \begin{bmatrix} P \\ \overline{u} \\ \overline{v} \\ \overline{w} \end{bmatrix} \qquad (4)$$

Where

$\overline{u}, \overline{v}, \overline{w}$ *are the components of velocity transformed so that* $\overline{u}$ *is normal to the face in question*

Where

$$\begin{aligned} \overline{u} &= a(1,1)u + a(1,2)v + a(1,3)w \\ \overline{v} &= a(2,1)u + a(2,2)v + a(2,3)w \\ \overline{w} &= a(3,1)u + a(3,2)v + a(3,3)w \end{aligned} \qquad (5)$$

where a is the coordinate transformation matrix from global to local coordinates

The limited gradients of the conserved variables are then calculated for both the compressive and diffusive limiters. In order to do this it is necessary to have the values of

$$\nabla \overline{Q}$$

These can be obtained by applying the chain rule as the gradient of the primitive variable are already available.

$$\frac{\partial \overline{Q}_l}{\partial x_i} = \sum_j \frac{\partial \overline{Q}_l}{\partial q_j} \frac{\partial q_j}{\partial x_i} \qquad (6)$$

Application of the chain rule gives the following relations

For $\overline{Q}_1 = P$

$$\frac{\partial \overline{Q}_1}{\partial q_1} = 1 \qquad (7)$$
$$\frac{\partial \overline{Q}_1}{\partial q_{2\to 5}} = 0$$

For $\overline{Q}_2 = \overline{u}$

$$\frac{\partial \overline{Q}_2}{\partial q_1} = 0$$
$$\frac{\partial \overline{Q}_2}{\partial q_2} = a(1,1) \qquad (8)$$
$$\frac{\partial \overline{Q}_2}{\partial q_3} = a(1,2)$$
$$\frac{\partial \overline{Q}_2}{\partial q_4} = a(1,3)$$

For $\overline{Q}3=\overline{v}$

$$\frac{\partial \overline{Q}_3}{\partial q_1} = 0$$
$$\frac{\partial \overline{Q}_3}{\partial q_2} = a(2,1) \qquad (9)$$
$$\frac{\partial \overline{Q}_3}{\partial q_3} = a(2,2)$$
$$\frac{\partial \overline{Q}_3}{\partial q_4} = a(2,3)$$

For $\overline{Q}4=\overline{w}$

$$\frac{\partial \overline{Q}_4}{\partial q_1} = 0$$
$$\frac{\partial \overline{Q}_4}{\partial q_2} = a(3,1) \qquad (10)$$
$$\frac{\partial \overline{Q}_4}{\partial q_3} = a(3,2)$$
$$\frac{\partial \overline{Q}_4}{\partial q_4} = a(3,3)$$

Once the limited gradients of the local conserved variables have been calculated and limited with both the diffusive and compressive limiters it is necessary to calculate the matrices of the right and left eigenvectors. For the split three-dimensional compressible Euler equations these are given by

$$R = \begin{bmatrix} -(\bar{u}+a) & 0 & 0 & -(\bar{u}-a) \\ 1 & 0 & 0 & 1 \\ \dfrac{\bar{v}}{-a} & 1 & 1 & \dfrac{\bar{v}}{a} \\ \dfrac{\bar{w}}{-a} & 1 & -1 & \dfrac{\bar{w}}{a} \end{bmatrix} \qquad (11)$$

$$L = \begin{bmatrix} \dfrac{-1}{2a} & \dfrac{-(\bar{u}-a)}{2a} & 0 & 0 \\ \dfrac{-(\bar{v}+\bar{w})}{2a^2} & \dfrac{-\bar{u}(\bar{v}+\bar{w})}{2a^2} & \dfrac{1}{2} & \dfrac{1}{2} \\ \dfrac{-(\bar{v}-\bar{w})}{2a^2} & \dfrac{-\bar{u}(\bar{v}-\bar{w})}{2a^2} & \dfrac{1}{2} & -\dfrac{1}{2} \\ \dfrac{1}{2a} & \dfrac{(\bar{u}+a)}{2a} & 0 & 0 \end{bmatrix} \qquad (12)$$

Where

$$a = artificial\ speed\ of\ sound = \sqrt{\bar{u}^2 + c^2} \qquad (13)$$

The first and last columns of R and first and last rows of L relate to the $\lambda=\bar{u}$ -a and $\lambda=\bar{u}$ +a genuinely non-linear characteristic fields. The second, third and fourth columns of R and second, third and fourth rows of L relate to the degenerate $\lambda=\bar{u}$ characteristic fields.

The L matrix can be split into two matrices one containing the information used to calculate the degenerate fields using the compressively limited $\bar{Q}$ gradient values, L1, and one containing the information used to calculate the genuinely nonlinear fields using the more diffusive limited $\bar{Q}$ gradient values, L2.

$$L1 = \begin{bmatrix} 0 & 0 & 0 & 0 \\ \frac{-(\bar{v}+\bar{w})}{2a^2} & \frac{-\bar{u}(\bar{v}+\bar{w})}{2a^2} & \frac{1}{2} & \frac{1}{2} \\ \frac{-(\bar{v}-\bar{w})}{2a^2} & \frac{-\bar{u}(\bar{v}-\bar{w})}{2a^2} & \frac{1}{2} & -\frac{1}{2} \\ 0 & 0 & 0 & 0 \end{bmatrix} \qquad (14)$$

$$L2 = \begin{bmatrix} \frac{-1}{2a} & \frac{-(\bar{u}-a)}{2a} & 0 & 0 \\ 0 & 0 & 0 & 0 \\ 0 & 0 & 0 & 0 \\ \frac{1}{2a} & \frac{(\bar{u}+a)}{2a} & 0 & 0 \end{bmatrix} \qquad (15)$$

The second order scheme with characteristic decomposition can be written in terms of the conserved variables and matrix of left eigenvectors as follows.

$$W_{i+1/2} = R^{-1}(\bar{Q}_i)\bar{Q}_i + L1(\bar{Q}_i)\overline{\nabla \bar{Q}_i \cdot \vec{r}_{i\to i+1/2}}^{Compressive} + L2(\bar{Q}_i)\overline{\nabla \bar{Q}_i \cdot \vec{r}_{i\to i+1/2}}^{Diffusive} \qquad (16)$$

the local conserved variables are then recovered via

$$\bar{Q}_i = R(\bar{Q}_i)W_{i+1/2} \qquad (17)$$

And the primitive variables q are then recovered from the local conserved variables.

APPENDIX C

Applying Characteristic Decomposition in a Compressible Solver.

Characteristic decomposition is applied in the interpolation algorithm. The limited differences of the local conservative variables, limited by both a compressive and diffusive limiter, are calculated. These values, along with the matrix of left eigenvectors, are used to transform to characteristic variables for the interpolation to be carried out with the compressive limiter applied to the linear degenerate fields and the diffusive limiter to the genuinely non-linear fields.

The relations used in the method of characteristic decomposition are as follows

$$W = L\overline{Q} \qquad (1)$$

In the method of characteristic decomposition it is also assumed that

$$\Delta W = L\,\Delta\overline{Q} \qquad (2)$$

Giving

$$W_{i+1/2} = L\overline{Q} + L\Delta\overline{Q} \qquad (3)$$

Here the linearly degenerate fields are calculated with the $\Delta\overline{Q}$ values limited with the compressive limiter and the genuinely non-linear fields with the difussive limiter

The reverse transformation to local conservative variables is given by

$$\overline{Q} = RW \qquad (4)$$

In order to apply characteristic decomposition it is first necessary to transform from Primitive variables to the local Conserved variables, of the split three dimensional Euler equations, in the interpolation algorithm. These are given below.

$$q=\begin{bmatrix}\rho\\ u\\ v\\ w\\ P\end{bmatrix} \quad \Rightarrow \quad \overline{Q}=\begin{bmatrix}\rho\\ \rho\overline{u}\\ \rho\overline{v}\\ \rho\overline{w}\\ E\end{bmatrix} \qquad (5)$$

Where

$\overline{u},\overline{v},\overline{w}$ *are the components of velocity transformed so that*
$\overline{u}$ *is normal to the face in question*

Where

$$\begin{aligned}\overline{u} &= a(1,1)u + a(1,2)v + a(1,3)w\\ \overline{v} &= a(2,1)u + a(2,2)v + a(2,3)w\\ \overline{w} &= a(3,1)u + a(3,2)v + a(3,3)w\end{aligned} \qquad (6)$$

where a is the coordinate transformation matrix from global to local coordinates

$$E = \rho(\frac{1}{2}V^2 + e) \qquad (7)$$

$$e = \frac{P}{(\gamma - 1)\rho} \qquad (8)$$

$$V = \sqrt{\overline{u}^2 + \overline{v}^2 + \overline{w}^2} \qquad (9)$$

The limited gradients of the conserved variables are then calculated for both the compressive and diffusive limiters. In order to do this it is necessary to have the values of

$$\nabla \overline{Q}$$

These can be obtained by applying the chain rule as the gradient of the primitive variable are already available.

$$\frac{\partial \overline{Q}_l}{\partial x_i} = \sum_j \frac{\partial \overline{Q}_l}{\partial q_j} \frac{\partial q_j}{\partial x_i} \qquad (10)$$

Application of the chain rule gives the following relations

For $\overline{Q}_1 = \rho$

$$\frac{\partial \overline{Q}_1}{\partial q_1} = 1 \qquad (11)$$
$$\frac{\partial \overline{Q}_1}{\partial q_{2\to 5}} = 0$$

For $\overline{Q}2 = \rho\overline{u}$

$$\frac{\partial \overline{Q}_2}{\partial q_1} = \overline{u}$$
$$\frac{\partial \overline{Q}_2}{\partial q_2} = \rho \times a(1,1)$$
$$\frac{\partial \overline{Q}_2}{\partial q_3} = \rho \times a(1,2)$$
$$\frac{\partial \overline{Q}_2}{\partial q_4} = \rho \times a(1,3)$$
$$\frac{\partial \overline{Q}_2}{\partial q_5} = 0 \qquad (12)$$

For $\overline{Q}3=\rho\bar{v}$

$$\frac{\partial\overline{Q}_3}{\partial q_1}=\bar{v}$$
$$\frac{\partial\overline{Q}_3}{\partial q_2}=\rho\times a(2,1)$$
$$\frac{\partial\overline{Q}_3}{\partial q_3}=\rho\times a(2,2)$$
$$\frac{\partial\overline{Q}_3}{\partial q_4}=\rho\times a(2,3)$$
$$\frac{\partial\overline{Q}_3}{\partial q_5}=0 \qquad (13)$$

For $\overline{Q}4=\rho\overline{w}$

$$\frac{\partial\overline{Q}_4}{\partial q_1}=\overline{w}$$
$$\frac{\partial\overline{Q}_4}{\partial q_2}=\rho\times a(3,1)$$
$$\frac{\partial\overline{Q}_4}{\partial q_3}=\rho\times a(3,2)$$
$$\frac{\partial\overline{Q}_4}{\partial q_4}=\rho\times a(3,3)$$
$$\frac{\partial\overline{Q}_4}{\partial q_5}=0 \qquad (14)$$

For $\overline{Q}_5 = E$

$$\frac{\partial \overline{Q}_5}{\partial q_1} = \frac{1}{2}V^2$$
$$\frac{\partial \overline{Q}_5}{\partial q_2} = 2\rho(a(1,1)\overline{u} + a(2,1)\overline{u} + a(3,1)\overline{u})$$
$$\frac{\partial \overline{Q}_5}{\partial q_3} = 2\rho(a(1,2)\overline{v} + a(2,2)\overline{v} + a(3,2)\overline{v}$$
$$\frac{\partial \overline{Q}_5}{\partial q_4} = 2\rho(a(1,3)\overline{w} + a(2,3)\overline{w} + a(3,3)\overline{w}$$
$$\frac{\partial \overline{Q}_5}{\partial q_5} = \frac{1}{\gamma - 1} \qquad (15)$$

Once the limited gradients of the local conserved variables have been calculated and limited with both the diffusive and compressive limiters it is necessary to calculate the matrices of the right and left eigenvectors. For the split three-dimensional compressible Euler equations these are given by

$$R = \begin{bmatrix} 1 & 1 & 0 & 0 & 1 \\ \overline{u} - a & \overline{u} & 0 & 0 & \overline{u} + a \\ \overline{v} & \overline{v} & 1 & 0 & \overline{v} \\ \overline{w} & \overline{w} & 0 & 1 & \overline{w} \\ H - \overline{u}a & \frac{1}{2}V^2 & \overline{v} & \overline{w} & H + \overline{u}a \end{bmatrix} \qquad (16)$$

$$L = \frac{\gamma - 1.0}{2a^2}\begin{bmatrix} H + \frac{a}{\bar{\gamma}}\left(\bar{u} - a\right) & -\left(\bar{u} + \frac{a}{\bar{\gamma}}\right) & -\bar{v} & -\bar{w} & 1 \\ -2H + \frac{4}{\bar{\gamma}}a^2 & 2\bar{u} & 2\bar{v} & 2\bar{w} & -2 \\ -\frac{2\bar{v}a^2}{\bar{\gamma}} & 0 & \frac{2a^2}{\bar{\gamma}} & 0 & 0 \\ -\frac{2\bar{w}a^2}{\bar{\gamma}} & 0 & 0 & \frac{2a^2}{\bar{\gamma}} & 0 \\ H - \frac{a}{\bar{\gamma}}\left(\bar{u} + a\right) & -\bar{u} + \frac{a}{\bar{\gamma}} & -\bar{v} & -\bar{w} & 1 \end{bmatrix} \quad (17)$$

Where

$$H = (E + P)/\rho \quad (18)$$

$$a = \sqrt{\frac{\gamma P}{\rho}} \quad (19)$$

$$\bar{\gamma} = \gamma - 1 \quad (20)$$

The first and last columns of R and first and last rows of L relate to the λ=u-a and λ=u+a genuinely non-linear characteristic fields. The second, third and fourth columns of R and second, third and fourth rows of L relate to the degenerate λ=u characteristic fields.

The L matrix can be split into two matrices one containing the information used to calculate the degenerate fields using the compressively limited $\overline{Q}$ gradient values, L1, and one containing the information used to calculate the genuinely nonlinear fields using the more diffusive limited $\overline{Q}$ gradient values, L2.

$$L1=\begin{bmatrix} 0 & 0 & 0 & 0 & 0 \\ -2H+\frac{4}{\bar{\gamma}}a^2 & 2\bar{u} & 2\bar{v} & 2\bar{w} & -2 \\ -\frac{2\bar{v}a^2}{\bar{\gamma}} & 0 & \frac{2a^2}{\bar{\gamma}} & 0 & 0 \\ -\frac{2\bar{w}a^2}{\bar{\gamma}} & 0 & 0 & \frac{2a^2}{\bar{\gamma}} & 0 \\ 0 & 0 & 0 & 0 & 0 \end{bmatrix} \qquad (21)$$

$$L2=\begin{bmatrix} H+\frac{a}{\bar{\gamma}}\left(\bar{u}-a\right) & -\left(\bar{u}+\frac{a}{\bar{\gamma}}\right) & -\bar{v} & -\bar{w} & 1 \\ 0 & 0 & 0 & 0 & 0 \\ 0 & 0 & 0 & 0 & 0 \\ 0 & 0 & 0 & 0 & 0 \\ H-\frac{a}{\bar{\gamma}}\left(\bar{u}+a\right) & -\bar{u}+\frac{a}{\bar{\gamma}} & -\bar{v} & -\bar{w} & 1 \end{bmatrix} \qquad (22)$$

The second order scheme with characteristic decomposition can be written in terms of the conserved variables and matrix of left eigenvectors as follows.

$$W_{i+1/2}=R^{-1}(\overline{Q}_i)\overline{Q}_i+\overbrace{L1(\overline{Q}_i)\overline{\nabla Q}_i\cdot\vec{r}_{i\to i+1/2}}^{Compressive}+\overbrace{L2(\overline{Q}_i)\overline{\nabla Q}_i\cdot\vec{r}_{i\to i+1/2}}^{Diffusive} \qquad (23)$$

the local conserved variables are then recovered via

$$\overline{Q}_i=R(\overline{Q}_i)W_{i+1/2} \qquad (24)$$

And the primitive variables q are then recovered from the local conserved variables.

Appendix D

Grid convergence results for all slotted flap aerofoil cases.

Compressible Cases -

Figure 69 – Pressure distribution for the baseline Barth and Jespersen scheme for three grid densities.

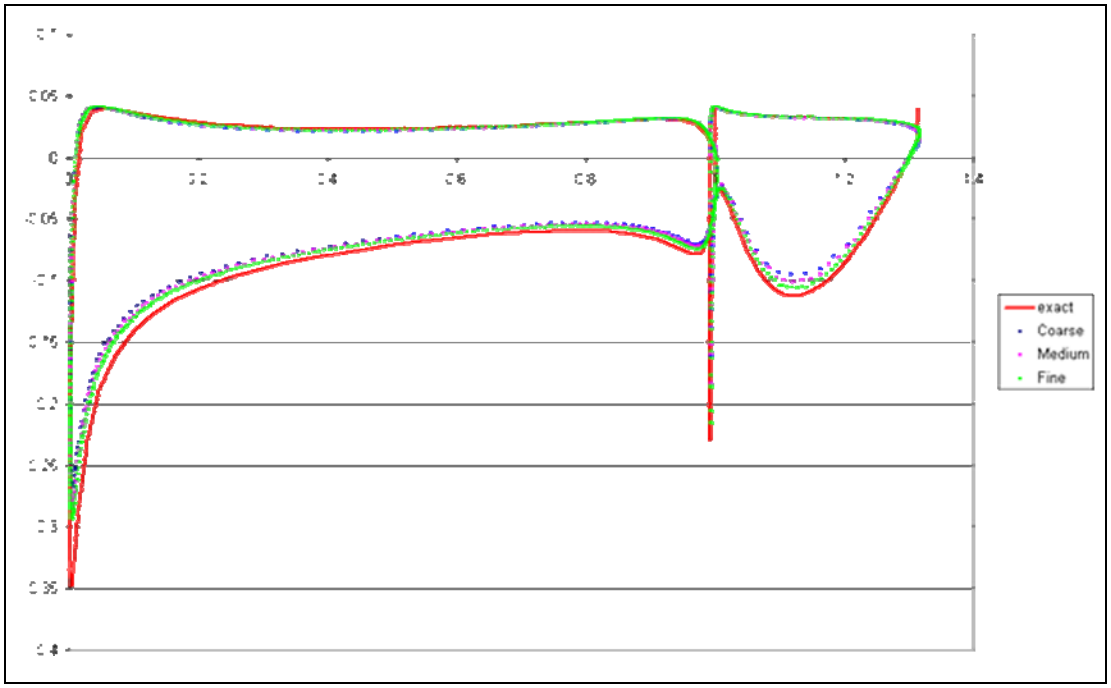

Figure 70 - Pressure distribution for the Characteristic Decomposition scheme for three grid densities.

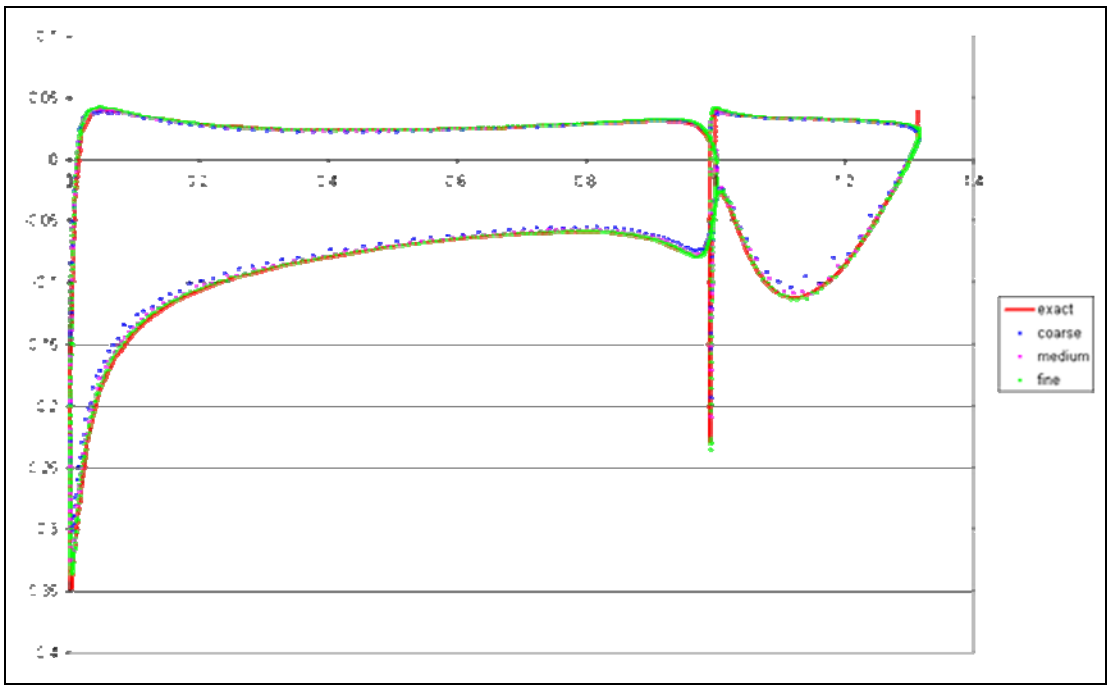

Figure 71 - Pressure distribution for the Characteristic Decomposition New scheme for three grid densities.

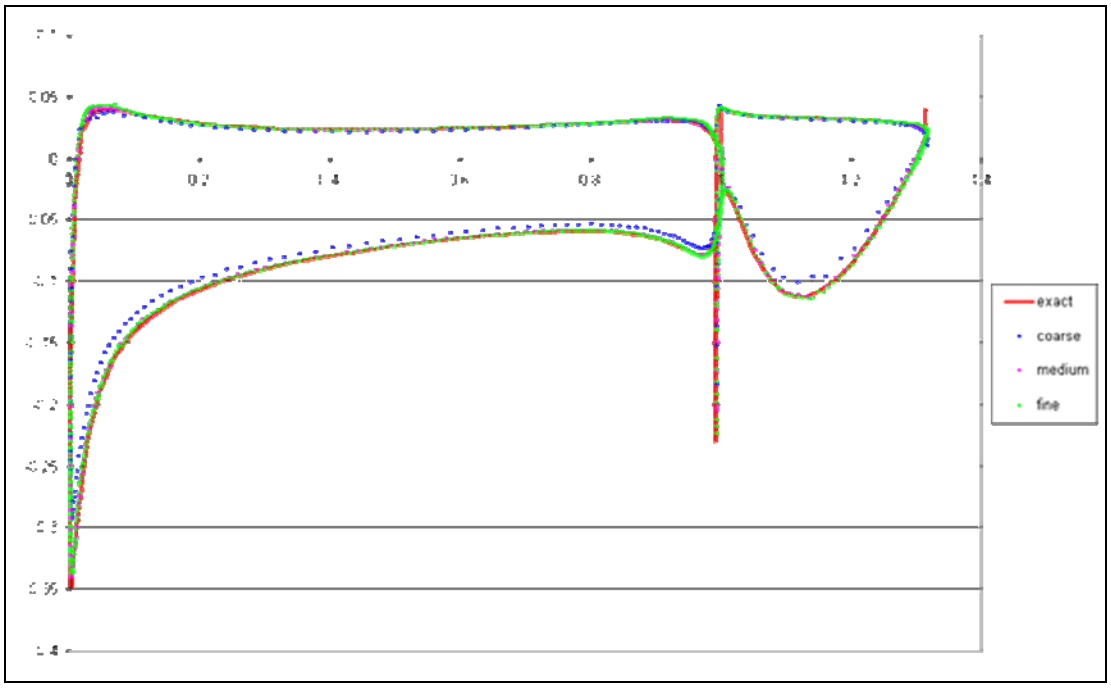

Figure 72 - Pressure distribution for the Characteristic Decomposition New 2 scheme for three grid densities.

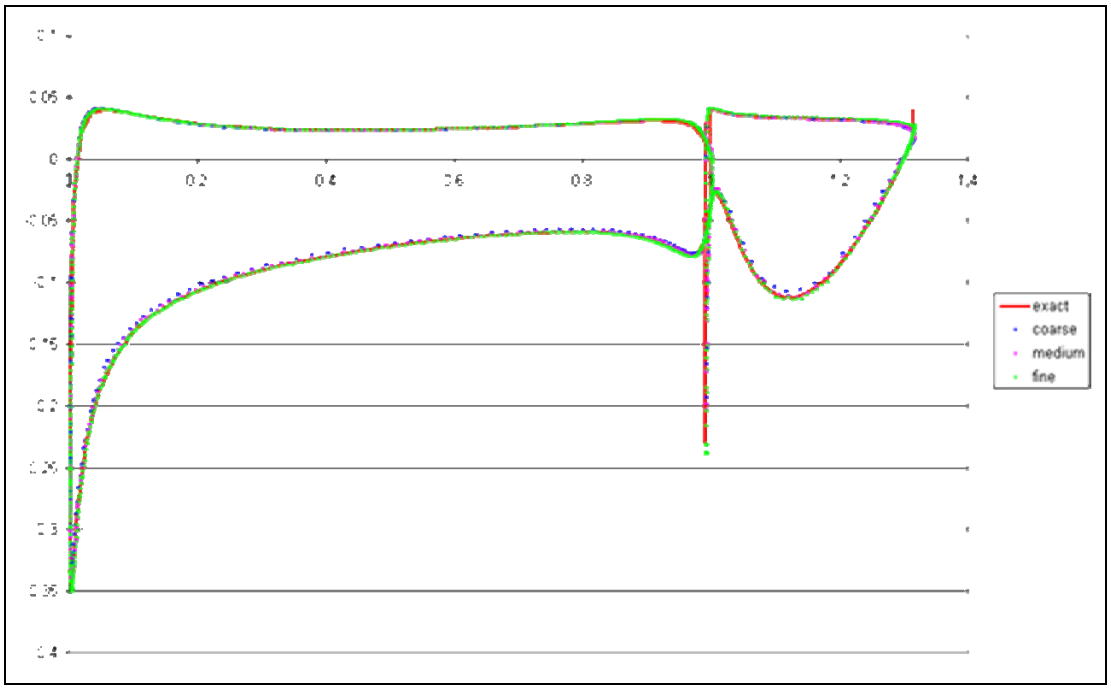

Artificial Compressibility Cases -

Figure 73 - Pressure distribution for the baseline Barth and Jespersen scheme for three grid densities.

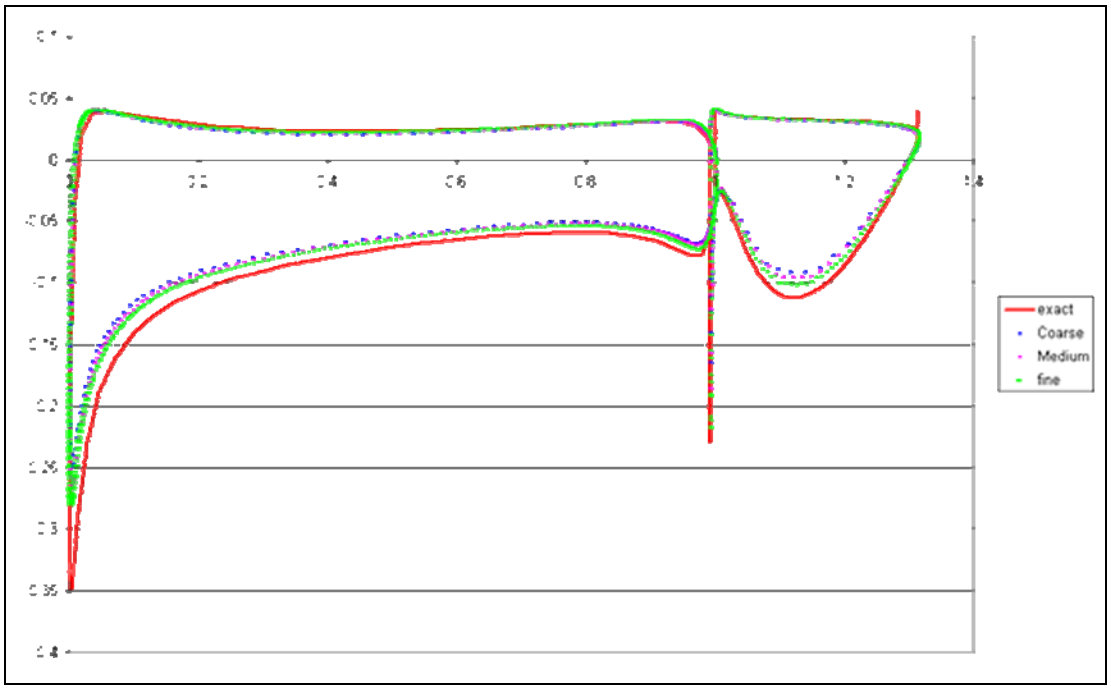

Figure 74 - Pressure distribution for the Characteristic Decomposition scheme for three grid densities.

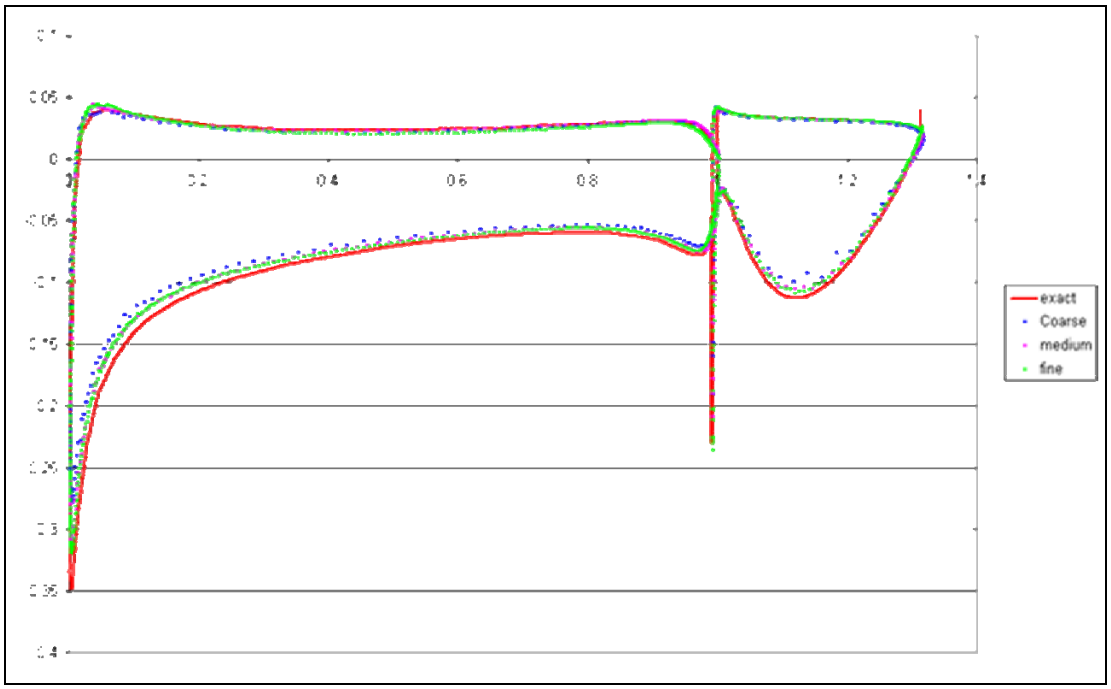

Figure 75 - Pressure distribution for the Characteristic Decomposition New scheme for three grid densities.

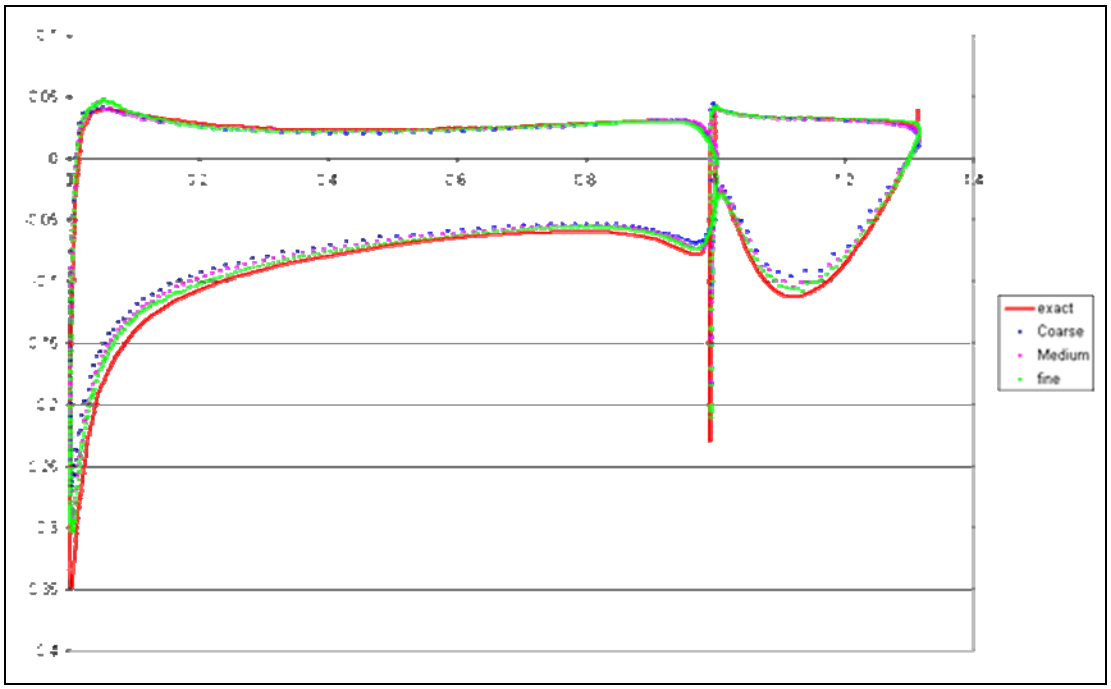

Figure 76 - Pressure distribution for the Characteristic Decomposition New 2 scheme for three grid densities.

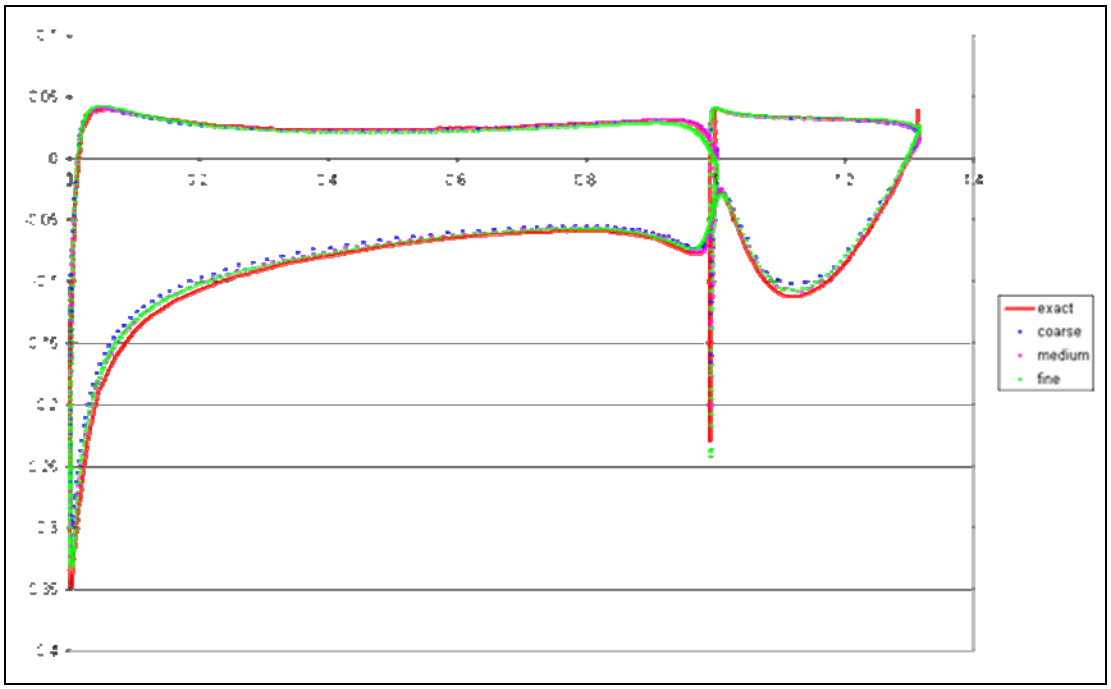

References

1. Hirsch, Numerical Computation of Internal and External Flows, Volume 1. Wiley, New York 1987
2. Hirsch, Numerical Computation of Internal and External Flows, Volume 2. Wiley, New York 1987
3. E.F Toro. Riemann Solvers and Numerical Methods for Fluid Dynamics. A Practical Introduction. Springer-Verlag. Second Edition, June 1999
4. Roe. Vorticity Capturing. AIAA 01-31130
5. Roe and Morton, Vorticity Preserving Lax-Wendroff-Type Schemes for the System Wave Equation. SIAM Journal of Scientific Computing, Vol. 23, No 1, 2001 170-192
6. Lax. Hyperbolic systems of Conservation Laws II. Communications on Pure and Applied Mathematics, Vol. 10, No 4, 1957
7. E. Wik, E. Numerical investigation of micro vortex generators, MSc Thesis, Cranfield University, 2003
8. Wake and Choi, Investigation of High-Order Upwinded Differencing for Vortex Convection. AIAA Journal. Vol. 34, No 2, 1996, 332-337
9. Hariharan. Rotary-Wing Wake Capturing: High-Order Schemes Toward Minimizing Numerical Vortex Dissipation. Journal of Aircraft, Vol. 39, No 5, 2002, 822-829
10. Hariharan and Sankar. High-Order Essentially Nonoscillatory Schemes for Rotary-Wing Wake Computations. Journal of Aircraft, Vol 41, No 2, 2004, 258-267
11. Steinhoff, Wenren and Wang. Numerical Vorticity Capturing For Vortex Solid Body Interaction Problems. AIAA 93-3343
12. Steinhoff, Hu and Grossman. Numerical Method for Vorticity Confinement in Compressible Flow. AIAA Journal, Vol. 40, 2002, 1945-1953
13. Hyman and Shashkov. Natural Discretizations for the Divergence, Gradient and Curl on Logically Rectangular Grids. Computers Mathematics Applications. Vol. 33, No 4, 1997, 81-104

14. Hyman and Shashkov. Adjoint Operators for the Natural Discretizations of the Divergence, Gradient and Curl on Logically Rectangular Grids. Applied Numerical Mathematics, Vol. 25, 1997, 413-442
15. Ismail and Roe, Towards a Vorticity Preserving Second Order Finite Volume Scheme Solving the Euler Equations, AIAA 2005-5235
16. Tam and Web. Dispersion-Relation-Preserving Finite Difference Schemes for Computational Acoustics. Journal of Computational Physics, Vol. 107, 1993, 262-281
17. Nance, Viswanathan and Sankar. Low-Dispersion Finite Volume Scheme for Aeroacoustic Applications. AIAA Journal, Vol. 35, No 2, 1997, 255-262
18. Wang, Sankar and Tadghighi. Prediction of Rotorcraft Noise with a Low-Dispersion Finite Volume Scheme. AIAA 99-0480
19. Brown, Rotor Wake Modelling for Flight Dynamic Simulation of Helicopters. AIAA Journal, Vol. 38, No 1, 2000, 57-63
20. Billet and Toro, On WAF-Type Schemes for Multidimensional Hyperbolic Conservation Laws. Journal of Computational Physics, Vol. 130, 1997, 1-24
21. Kim, Williams and Lyrintzis. Improved Method for Rotor Wake Capturing. Journal of Aircraft, Vol. 39, No 5, 2002, 794-803
22. Sweby. High resolution Schemes Using Flux Limiters for Hyperbolic Conservation Laws. SIAM Journal of Numerical Analysis, Vol. 21, No 5, 1984, 995-1011
23. LeVeque, Randall J, Finite-volume methods for hyperbolic problems, Cambridge University Press, 2002
24. A.J. Chorin. A Numerical method for solving incompressible viscous flow problems. J. of Computational Physics. 2:12-26, 1967
25. C.L. Merkle and M. Athavale, Time accurate unsteady incompressible flow algorithms based on artificial compressibility. AIAA paper 87-1137
26. M. Breuer and D Hanel. Dual time stepping method for 3-D viscous incompressible vortex flows, Computers & Fluids Vol 22 No 4/5 pp 467-484, 1993
27 B. Engquist and S. Osher. One sided difference approximation for Nonlinear conservation laws. Math Comp 36(154):321-351, 1981

28.S.Osher and F. Solomon. Upwind difference schemes for hyperbolic conservation laws. Math Comp, 38(158):339-374, 1982

29 E. Turkel, Preconditioned methods for solving the incompressible and low speed compressible equations, J. of Computational Physics, 72:227-298, 1987

30. E. Turkel and Arnone, Pseudo-compressibility methods for the incompressible flow equations. AIAA paper 93-3329

31 Y.P. Marx, Evaluation of the artificial compressibility method for the solution of the incompressible navier stokes equations. 9th GAMM Conference of Numerical Methods in Fluid Mechanics, Lausanne, Sept 1991

32. A. Rizzi, Hyperbolic preconditioning to solve the incompressible euler equations for vortex flow. In Numerical Methods for Fluid Dynamics II. The institute of mathematics and its applications conference series. Clarendon Press. 1986

33. D.T Elsworth and E.F. Toro. A numerical investigation of the artificial compressibility method for the solution of the navier-stokes equations. Cranfield College of Aeronautics Report No 9213, Nov 1992

34. Barth and Jespersen, The Design and Application of Upwind Schemes on Unstructured Meshes, AIAA 89-0366

35. Williams, A Comparison of the Surface-Source Solution with an Exact Solution for the Two Dimensional Inviscid Flow about a Slotted-Flap Aerofoil, Aeronautical Research Council Current Papers, 1214, 1972

36 F.White, Viscous Fluid Flow, McGraw Hill International Editions, 1991

37 Anderson, J.D., Modern Compressible Flow , McGraw Hill Inc., New York, 1982.

38. Van Leer, Towards the Ultimate Conservative Difference Scheme. Journal of Computational Physics, Vol. 32, 1979, 101-136

39 Venkatakrishnan. Convergence to Steady State Solutions of the Euler Equations on Unstructured Grids with Limiters. Journal of Computational Physics. Vol. 118, 1995, 120-130

40 Aftosmis, Gaitoned and Taveres, On the Accuracy Stability and Accuracy of various reconstruction Schemes on Unstructured Meshes, AIAA 94-0415

41 Berger, Aftosmis and Murman. Analysis of Slope Limiters on Irregular Grids. AIAA 2005-0490

42 Batten, Lambert and Causon. Positively Conservative High-Resolution Convection Schemes for Unstructured Elements. International Journal for Numerical Methods in Engineering. Vol. 39, 1996, 1821-1838

43 Hubbard. Multidimensional Slope Limiters for MUSCL-Type Finite Volume Schemes on Unstructured Grids. Journal of Computational Physics, Vol. 155, 1999, 54-74

44 Jawahar and Kamath. A High-Resolution Procedure for Euler and Navier-Stokes Computations on Unstructured Grids. Journal of Computational Physics, Vol. 164, 2000, 165-203

45 Venkatakrishnan. Convergence to Steady State Solutions of the Euler Equations on Unstructured Grids with Limiters. Journal of Computational Physics. Vol. 118, 1995, 120-130